

Properties of Magnetic Switchbacks in the Near-Sun Solar Wind

Samuel T. Badman ^{1†}, Naïs Fargette ^{2, 3†}, Lorenzo Matteini ^{3*†}, Oleksiy V. Agapitov ^{4, 5}, Mojtaba Akhavan-Tafti ⁶, Stuart D. Bale ⁴, Srijan Bharati Das ¹, Nina Bizien ⁷, Trevor A. Bowen ⁴, Thierry Dudok de Wit ^{7, 8}, Clara Froment ⁷, Timothy Horbury ³, Jia Huang ⁴, Vamsee Krishna Jagarlamudi ⁹, Andrea Larosa ^{10, 11}, Maria S. Madjarska ^{12, 13, 14}, Olga Panasenco ¹⁵, Etienne Pariat ^{16, 17}, Nour E. Raouafi ⁹, Alexis P. Rouillard ^{2, 18}, David Ruffolo ¹⁹, Nikos Sioulas ^{20, 4}, Shirsh Lata Soni ²¹, Luca Sorriso-Valvo ^{11, 22}, Gabriel Ho Hin Suen ^{23, 7}, Marco Velli ²⁰, Jaye Verniero ²⁴

¹Center for Astrophysics, Harvard & Smithsonian, Cambridge, Massachusetts, 02138, USA.

²Institut de Recherche en Astrophysique et Planétologie, CNES, CNRS, Université de Toulouse, Toulouse, 31400, France.

³Department of Physics, Imperial College London, London, UK.

⁴Space Sciences Laboratory, University of California, Berkeley, California, 94720, USA.

⁵Astronomy and Space Physics Department, National Taras Shevchenko University of Kyiv, Kyiv, 01601, Ukraine.

⁶Department of Climate and Space Sciences and Engineering, University of Michigan, Ann Arbor, Michigan, 48109, USA.

⁷LPC2E, OSUC, Univ Orleans, CNRS, CNES, F-45071, Orleans, France.

⁸International Space Science Institute, Bern, 3012, Switzerland.

⁹John Hopkins University Applied Physics Laboratory, Laurel, Maryland, 20723, USA.

¹⁰School of Physical and Chemical Sciences, Queen Mary University of London, London, UK.

¹¹Institute for Plasma Science and Technology (ISTP), CNR, 70126, Bari, Italy.

¹²Max Planck Institute for Solar System Research, Gottingen, 37077, Germany.

¹³Korea Astronomy and Space Science Institute, Daejeon, 34055, South Korea.

¹⁴Space Research and Technology Institute, Bulgarian Academy of Sciences, Sofia, 1113, Bulgaria.

¹⁵Advanced Heliophysics, Pasadena, California, 91106, USA.

¹⁶French-Spanish Laboratory for Astrophysics in Canarias, CNRS, Instituto de Astrofísica de Canarias, 38205, La Laguna, Tenerife, Spain.

¹⁷Sorbonne Université, École polytechnique, Institut Polytechnique de Paris, Université Paris Saclay, Observatoire de Paris-PSL, CNRS, Laboratoire de Physique des Plasmas, 75005, Paris, France.

¹⁸Leibniz-Institut für Astrophysik Potsdam (AIP), Potsdam, 11482, Germany.

¹⁹Department of Physics, Faculty of Science, Mahidol University, Bangkok, 10400, Thailand.

²⁰Department of Earth, Planetary, and Space Sciences, University of California, Los Angeles, California, 90095, USA.

²¹Department of Physics and Astronomy, University of Iowa, IA 52242-1479, Iowa City, USA.

²²School of Electrical Engineering and Computer Science, Department of Electromagnetics and Plasma Physics, KTH Royal Institute of Technology, SE-11428, Stockholm, Sweden.

²³Department of Space and Climate Physics, University College London, London, UK.

²⁴Heliophysics Science Division, NASA Goddard Space Flight Center, Greenbelt, Maryland, 20771, USA.

*Corresponding author(s). E-mail(s): l.matteini@imperial.ac.uk ;

†These authors contributed equally to this work.

Abstract

Magnetic switchbacks are fluctuations in the solar wind in which the interplanetary magnetic field sharply deflects away from its background direction so as to create folds in magnetic field lines while remaining of roughly constant magnitude. The magnetic field and velocity fluctuations are extremely well correlated in a way corresponding to Alfvénic fluctuations propagating away from the Sun. For a background field which is nearly radial this causes an outwardly propagating jet to form. Switchbacks and their characteristic velocity jets have recently been observed to be nearly ubiquitous by Parker Solar Probe with *in situ* measurements in the inner heliosphere within 0.3 AU. Their prevalence, substantial energy content, and potentially fundamental role in the dynamics of the outer corona and solar wind motivate the significant research efforts into their understanding. Here we review the *in situ* measurements of these structures (primarily by Parker Solar Probe). We discuss how they are identified and measured, and present an overview of the primary observational properties of these structures, both in terms of individual switchbacks and their collective arrangement into “patches”. We identify both properties for which there is a strong consensus and those that have limited or qualified support and require further investigation. We identify and collate several open questions and recommendations for future studies.

Keywords: Solar Corona, Solar Wind, Solar Magnetic Fields, Alfvén Waves

Contents

1	On the Striking Nature of Switchbacks	3
1.1	First Observations in the Young Solar Wind	3
1.2	A Brief Historical Overview	4
1.3	Parker Solar Probe Instrumentation	5
1.4	Key Questions Associated with Switchbacks	5
1.5	Outline	6
2	Switchback Definition	6
2.1	Prototypical Example	7
2.2	Link to Velocity Spikes	7
3	Review of Methodologies	9
3.1	Identification using Deflection from a Background Field	9
3.1.1	Impact of the Magnetic Field Background Choice	9
3.1.2	Deflection Angle Thresholds	10
3.2	Manual Identification of Switchbacks	11
3.3	Alternative Methods and Takeaways	13
4	Switchback Properties and Structure	14
4.1	Plasma Population Inside Switchbacks	14
4.1.1	Steady Plasma Properties Overview	14
4.1.2	Switchback Proton and Alpha Temperatures	16
4.1.3	Steady Plasma Properties Takeaways	18
4.2	Switchback Occurrence, Geometry, and Boundaries	18
4.2.1	Deflection Angle and Duration Statistics	19
4.2.2	Size, Shape, and Orientation	20
4.2.3	Non-Alfvénic Boundary Features	21
4.2.4	Discontinuity Classification	22
4.2.5	Switchbacks and Magnetic Reconnection	23
4.2.6	Waves at Switchback Boundaries	26
4.2.7	Geometry and Boundary Takeaways	27
4.3	Switchbacks, Turbulence, and Ion-scale waves	29
4.3.1	Background on Alfvénic Turbulence	29

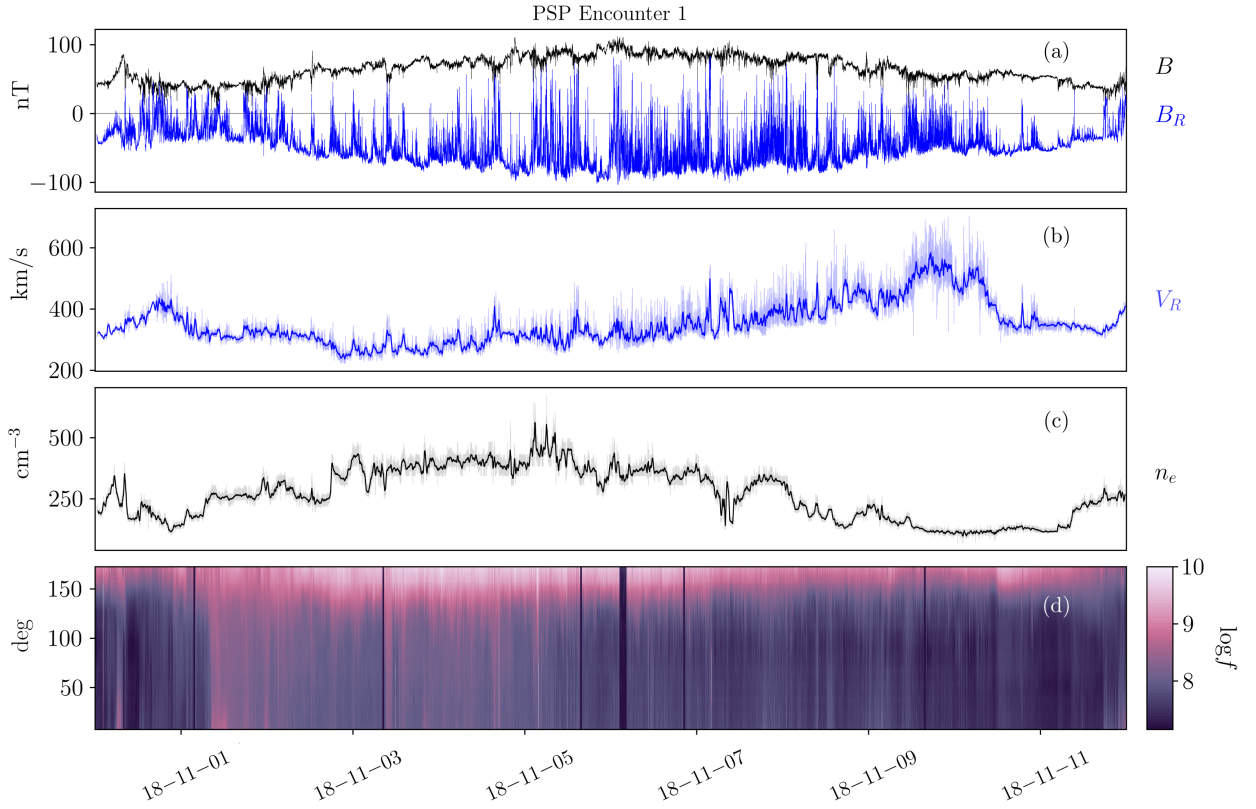


Fig. 1 Parker measurements of the young solar wind during the mission’s first orbit, showing (a) the magnetic field amplitude and radial component as the spacecraft goes from 60 to 35 R_{\odot} on November 6; (b) the radial solar wind speed together with a 20-minute average; (c) the electron density inferred using quasi-thermal noise spectroscopy (see Sect. 1.3) with a 20-minute average; (d) the pitch angle distribution of suprathermal electrons (314 eV).

4.3.2	Approach to Turbulence Studies	30
4.3.3	Turbulent Spectra	31
4.3.4	Intermittency and Dissipation	31
4.3.5	Cross-helicity, Residual energy and Alfvénicity of the fluctuations	31
4.3.6	Interaction with Ion Scale Waves	33
4.3.7	Switchbacks & Turbulence Takeaways	35
5	The Underlying Structure of the Solar Wind	35
5.1	Switchback patches	35
5.2	Switchback Occurrence in Different Solar Wind Streams	37
5.3	Switchbacks in Low Alfvén Mach Number Wind	39
5.4	Switchbacks Collective Behavior Takeaways	40
6	Summary and Open Questions	41
6.1	Knowledge Gaps	42
6.2	Final Remarks	43

1 On the Striking Nature of Switchbacks

1.1 First Observations in the Young Solar Wind

From the very first orbit of the Parker Solar Probe (Parker; [Fox et al, 2016](#); [Raouafi et al, 2023](#)) mission with the Sun, *in situ* data revealed surprising and notable features: the solar wind exhibited frequent magnetic deflections, accompanied by velocity enhancements (“spikes”) and significant changes in the radial magnetic field component ([Bale et al, 2019](#); [Kasper et al, 2019](#)). These structures, of Alfvénic nature – i.e., implying high correlation between magnetic field and velocity variations – are commonly referred to as *magnetic switchbacks* as the magnetic field fluctuations, especially in the early Parker orbits, lead to

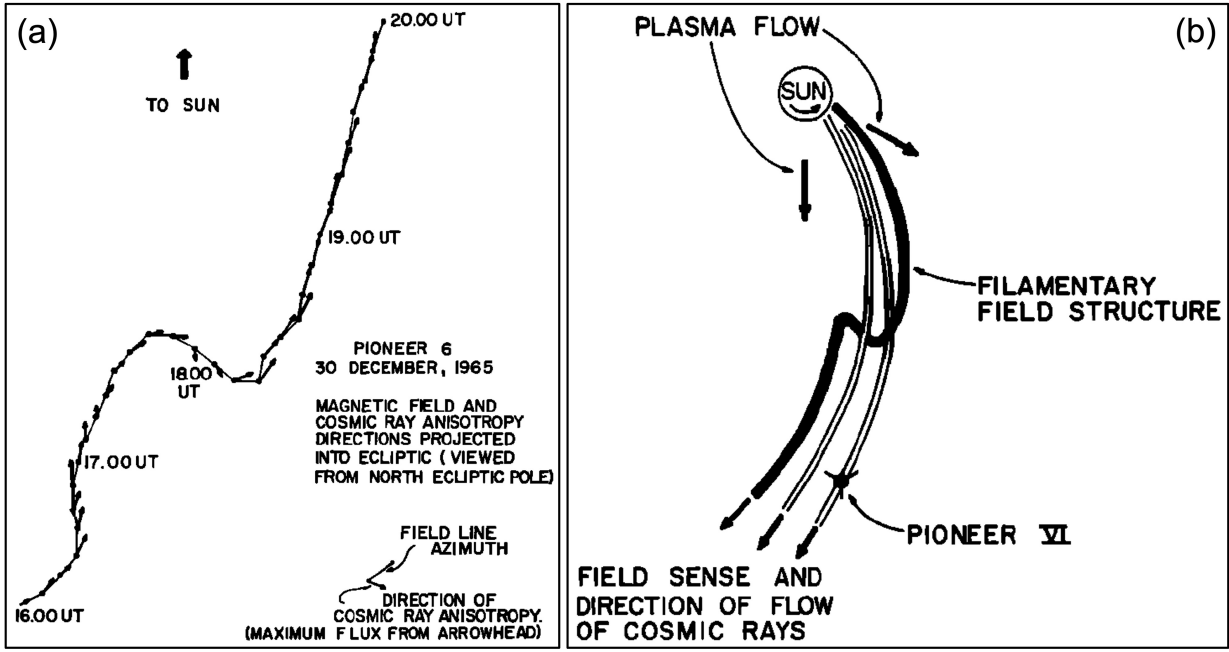


Fig. 2 Observation from Mariner-II showcasing abrupt changes in the direction of the interplanetary magnetic field. Left panel: magnetic field and cosmic ray anisotropy; right panel: derived field line and (solar) cosmic ray flow. Reproduced from [McCracken and Ness \(1966\)](#).

local reversals of the radial magnetic field component. A more comprehensive description of the properties defining switchbacks is provided in Sect. 2.

Figure 1 highlights the prevalence of magnetic switchbacks in the young solar wind. As Parker approaches perihelion (November 6, 2018), its radial distance from the Sun decreasing from 60 solar radii (R_\odot) down to 35 R_\odot , rapid reversals in the radial component of the magnetic field B_R are observed to pervade the solar wind (top panel). Though the mean radial field is negative, innumerable rapid oscillations to positive are observed while the pitch angle distribution (PAD) of suprathermal electrons (bottom panel) remains concentrated around 180° . This means that the faster electrons, that are channelled along the field, are actually propagating backwards during the reversals (see figure 10 of [Owens and Forsyth, 2013](#)), implying that the reversals are only local folds in magnetic field lines ([Balogh et al, 1999](#); [Kasper et al, 2019](#); [Bale et al, 2019](#)), while the spacecraft remains magnetically connected to the same polarity region on the Sun, here a region of inward field.

Although switchbacks are commonly depicted as 2D kinks in magnetic field lines (Fig. 2), their internal structure is probably more complex (see e.g., [Shi et al, 2024](#)).

1.2 A Brief Historical Overview

Measurements from various spacecraft have reported the occurrence of abrupt changes in the interplanetary magnetic field direction. In historical observations conducted at distances beyond 0.3 AU, such occurrences were relatively infrequent. These events were subject to different interpretations, only some of which align with our current understanding of magnetic switchbacks. The initial indication of the potential existence of magnetic field switchbacks was reported by [McCracken and Ness \(1966\)](#) through the analysis of magnetic field and cosmic ray measurements obtained from Mariner-II. Their interpretation, based on the close alignment between cosmic ray anisotropy and magnetic field lines, led them to conclude that filamentary structures existed within the interplanetary magnetic field (Fig. 2). [Michel \(1967\)](#) provided one of the first suggestions that a velocity modulation (jet-like enhancement) is associated with the folding of the interplanetary field in switchbacks, although we now understand that this is due to their Alfvénic nature, rather than background velocity shears ([Matteini et al, 2014](#)). [Horbury et al \(2018\)](#) established clear evidence for the occurrence of these plasma jets in measurements obtained from the Helios solar wind, particularly in proximity to 0.3 AU. Observations made by the Ulysses mission beyond 1 AU further contributed to our understanding, revealing magnetic field rotations exceeding 90° in relation to the Parker spiral (as documented by [Balogh et al, 1999](#); [Yamauchi et al, 2004](#)). Additional evidence supporting the existence of magnetic switchbacks was identified through observations made by the ISEE-3 mission ([Kahler et al, 1996](#))

and the ACE mission (Gosling et al, 2009; Li et al, 2016). A more detailed historical overview is available in Velli and Owens (2026, this collection).

1.3 Parker Solar Probe Instrumentation

In this review, we primarily examine magnetic switchback properties as measured by the Parker mission (Fox et al, 2016). As some discussions require an understanding of the instrumentation limitations on board, we briefly discuss the *in situ* instrumentation on board the Parker spacecraft.

Parker carries three *in situ* instrument suites whose data are shown throughout this work:

- The Electromagnetic Fields Investigation suite (FIELDS; Bale et al, 2016; Malaspina et al, 2016; Pulupa et al, 2017) measures AC and DC electric and magnetic fields, radio waves, and quasi-thermal noise spectroscopy (QTN) plasma electron diagnostics.
- The Solar Wind Alphas, Electrons and Protons suite (SWEAP; Kasper et al, 2016; Case et al, 2020; Whittlesey et al, 2020; Livi et al, 2022) measures particle velocity distribution functions up to 30 keV and derives bulk properties of electrons, protons, and alpha particles.
- The Integrated Science Investigation of the Sun suite (IS \odot IS; McComas et al, 2016) measures the direction-resolved fluxes and energy distributions of energetic electrons, protons, and heavy ions (from 25 keV to 6 MeV for electrons, and 20 keV/nucleon to 200 MeV/nucleon for ions).

The key *in situ* signatures of switchbacks are shown in Fig. 1 during E1, i.e., the first encounter of the Parker mission with the Sun (in the remainder of the paper, E_x stands for Encounter number x and where encounter formally refers to continuous intervals where Parker was within 0.25 au of the Sun (although it can be used somewhat more loosely in the literature to index perihelia). Data is shown in the RTN frame of reference, where \mathbf{R} (radial) is the Sun to spacecraft unit vector, \mathbf{T} (tangential) is the cross product between the Sun's spin axis and \mathbf{R} , and \mathbf{N} (normal) completes the direct orthogonal frame.

The FIELDS DC magnetic field 3D vector (whose radial component is shown in panel 1a) provides one of the primary signatures of switchbacks (Bale et al, 2019) is measured by a pair of fluxgate magnetometers located on a boom trailing the spacecraft. FIELDS also provides a robust measurement of the electron density (Fig. 1c) via QTN from the FIELDS Radio Frequency Spectrometer (FIELDS/RFS; Pulupa et al, 2017; Moncuquet et al, 2020), but the measurement is only available when the spacecraft is sufficiently close to the Sun for the effective length of the antennae to be longer than the Debye length and therefore for the plasma frequency to be well inside the frequency range of the instrument (typically within a heliocentric distance of around $70 R_{\odot}$).

The proton bulk properties (including velocity, Fig. 1b) are measured by the Solar Probe Cup (SPC; Case et al, 2020) and the Solar Probe Analyzer for ions (SPAN-i; Livi et al, 2022). SPC is a Faraday cup with a narrow field of view oriented towards the Sun. SPAN-i is an electrostatic analyzer with a wider field of view oriented on the ram side of the spacecraft. Both SPC and Span-i give partial coverage of the velocity distribution functions (VDFs). SPAN-i further has a time-of-flight chamber which allows it to discriminate different mass per charge ratios and therefore provide separate data products for protons and alpha particles. No matter the species, the quality of the determination, particularly in density and temperature, depends on the location of the peak of the VDF in these two fields of view. This can change strongly during different parts of the orbit, due to the combined effects of aberration (changing speed of the plasma relative to the spacecraft throughout the orbit) as well as to intrinsic variations in solar wind speed (which occur throughout the orbit but also especially during switchbacks).

The last panel of Fig. 1 shows the pitch angle distributions (PAD) of suprathermal electrons as measured by the Solar Probe Analyzer for electrons (SPAN-e; Whittlesey et al, 2020), which is an electrostatic analyzer with two sensors oriented on the spacecraft on the ram and anti-ram sides (thereby providing nearly 4π steradians coverage of electron VDFs). The pitch angles show the relative orientation between the flow direction of suprathermal electrons (or strahl) and the magnetic field.

1.4 Key Questions Associated with Switchbacks

The ubiquity of switchbacks in Parker measurements below 0.3 AU (e.g., Bale et al, 2019; Kasper et al, 2019), their substantial energy content (e.g., Halekas et al, 2023; Rivera et al, 2024a), and their diagnostic potential for coronal processes and solar wind basic physics, have made their understanding a focal point of heliophysics research. They have been widely studied in the early phases of the Parker mission, and formed a large segment of early results reviewed previously in Raouafi et al (2023). Their existence raises the following key questions:

1. **Are switchbacks dynamically important in the initial acceleration of the solar wind and potentially in magnetized astrophysical winds in general?** Are switchbacks actively contributing to the acceleration of the flow in the corona and below the Alfvén radius?
2. **Are switchbacks a significant source of heating for non-adiabatic expansion of the plasma in interplanetary space?** Switchbacks carry away a considerable extra amount of Poynting flux and bulk kinetic energy from the Corona; this energy excess can be converted into thermal energy during expansion and could be a potential main contribution to solar wind heating farther from the Sun. Recent works suggest they are significant for both the acceleration and heating of the fast wind beyond the Alfvén point (Rivera et al, 2024a), injecting energy directly into the turbulent cascade (Hernández et al, 2021) but with decreasing importance for slower wind types (Halekas et al, 2023).
3. **Are switchbacks direct signatures of the processes responsible for solar wind acceleration in the lower corona?** Even if switchbacks are not directly responsible for the acceleration of the plasma, they could be produced by the same mechanisms that cause the plasma acceleration, e.g., interchange reconnection. Therefore, understanding switchbacks may shed light on the acceleration processes. Different models for switchback generation and their link to solar dynamics and sources are reviewed in Tripathi et al (2026, this collection) and Wyper et al (2026, this collection).
4. **Are switchbacks passive tracers of solar dynamics?** Switchbacks are nearly ubiquitous in the near-Sun solar wind. This presence makes them an indirect probe of solar dynamics imprinted in the solar wind. By studying switchback modulation and properties, we can probe properties of source regions that cannot be explored *in situ*. An example of this is discussed in Sect. 5 of this paper.

1.5 Outline

This review is structured as follows:

- In Sect. 2, we present the defining features of magnetic switchbacks and illustrate these features with real examples. (See also section 4.1 of Raouafi et al, 2023)
- In Sect. 3, we discuss the diverse methodologies used throughout the literature to detect switchbacks and build statistics on them.
- In Sect. 4 we review investigations into different types of properties of individual switchback spikes, focusing on their plasma populations (Sect. 4.1), their geometry and boundary properties (Sect. 4.2) and their relationship to more general solar wind turbulence and electromagnetic wave activity (Sect. 4.3). (See also section 4.2 of Raouafi et al, 2023, which this section updates and expands on)
- In Sect. 5, we zoom out to examine the collective behavior of switchbacks, including their arrangement into patches and differences in their properties in different types of solar wind streams.
- Finally, in Sect. 6, we close by summarizing the main elements of this review and presenting some key open questions for which further study is required to reach definitive conclusions.

2 Switchback Definition

To study magnetic switchback properties in the solar wind, it is particularly important that the scientific community agrees on a common definition for these structures (see Sect. 3 for a review of how definitions and methodologies may impact statistical studies). Here, we propose a consensus definition as a list of expected switchback features.

- A switchback is a sharp deflection of the magnetic field vector away from the ambient direction and back; “sharp” meaning that their boundaries have a short timescale compared to the switchback duration. The deviation should be significant with respect to the local level of fluctuations, typically at least a few tens of degrees. While most switchbacks deflect less than 90°, some do lead to changes in the polarity of the magnetic field. We refer to these more than 90° deflections as local “polarity reversals” throughout the paper.
- Switchbacks have an approximately constant magnetic field magnitude B , meaning that, geometrically, the magnetic field vector \mathbf{B} evolves on a sphere throughout the structure. The switchback boundaries are thus 1D arcs on the sphere surface.
- Switchbacks are local folds in the magnetic field and are not associated with a change of polarity at the source. They thus exhibit the same electron strahl pitch angle direction throughout the switchback.
- Switchbacks are Alfvénic, displaying the high correlation between magnetic field and velocity variations that corresponds to fluctuations propagating away from the Sun in the background field. As a consequence, kinks in the magnetic field, leading to changes in the radial magnetic field (B_R), are usually associated

with enhancements in the radial bulk proton velocity (V_R), with the peak in velocity occurring at the maximum field deflection. We note that this spike in V_R is in fact a 1D projection of the velocity vector also moving on a sphere centered on the reference frame in which the motional electric field goes to zero (Matteini et al, 2015), sometimes referred to as the DeHoffman Teller frame (Horbury et al, 2020, see also Sect. 2.2).

It is important to note that while our definition of switchbacks allows for a spectrum of deflection angles relative to some choice of background field, there are distinct lower thresholds applied to this spectrum throughout the literature (see Sect. 3). The most restrictive of these is a 90° threshold from which the term “switchback” originates. This additional criterion is often applied to assess whether models are sufficient to explain these largest switchbacks (see Wyper et al, 2026, this collection, for a review).

Finally, note that, because of their typical MHD scale (duration of minutes/tens of seconds), switchbacks can be considered at first order an ideal-MHD solution, therefore their magnetic-velocity structure is solely supported by the self-consistent motional electric field $\mathbf{E} = -\mathbf{V} \times \mathbf{B}$ (see e.g., Matteini et al, 2015). However, if deflections are particularly sharp, non-ideal effect can play a role at boundaries, see Sect. 4.2.3.

2.1 Prototypical Example

We illustrate these defining features in a realistic context in Fig. 3, where we show observations from Parker during its 5th perihelion (June, 2020). During the selected time interval, several typical signatures of magnetic switchbacks are observed. Sharp deflections from the background field are present at different scales, including two impressive large, close-to 180° reversals in the first half of the interval (between 15:50 and 16:20 UT) and multiple smaller deflections that sometimes reverse the radial magnetic field in the second half between (17:20 and 18:40 UT). The solar wind is mostly Alfvénic during this interval, with the radial velocity V_R positively correlated to B_R , exhibiting radial velocity spikes coincident with the switchbacks. The electron strahl orientation with respect to the magnetic field remains constant around 180° throughout the interval, meaning that at maximum deflection, the strahl is briefly moving sunward. The density fluctuates between 450 and 800 cm⁻³, with some compression potentially associated with the switchbacks considered here. Note that, as switchbacks observed in the inner Heliosphere are typically embedded in low-beta plasma, the relative jump in density is often larger than in B , as expected for pressure balance. The magnetic field deflections occur at roughly constant B , as further illustrated by the hodograms of \mathbf{B} shown in the bottom panels (3e, 3f). There, the two large deflections (15:55–16:20 UT) are associated with red points ($B_R \in [50, 100]$ nT, B_T negative) and closely follow the constant $B = 117$ nT sphere.

This time interval also illustrates that the exact distinction between switchbacks and background solar wind turbulence is not easily captured. Often, potential switchback structures are ambiguous in the solar wind, due to smaller deflection angles (15:10–15:45 UT), internal fluctuations inside a larger deflection (18:00–18:10 UT), or imperfect B conservation, for instance. The choice of whether to label such structures as switchbacks varies between studies, and some features like constant B or Alfvénicity are discussed in Sect. 4.

2.2 Link to Velocity Spikes

Fig. 3 shows that velocity spikes associated with switchbacks are always positive. An explanation for this apparent one-sidedness of solar wind velocity fluctuations, first noticed by Gosling et al (2009), was provided by Matteini et al (2014). Large amplitude Alfvénic fluctuations in the MHD regime display the following correlation between magnetic field and velocity fluctuation vectors:

$$\frac{\delta \mathbf{V}}{V_A} = \pm \frac{\delta \mathbf{B}}{B}, \quad (1)$$

where $V_A = B/\sqrt{\mu_0 \rho}$ is the Alfvén speed, with ρ the mass density, and μ_0 the vacuum permeability constant. The positive (negative) correlation corresponds to waves propagating along the negative (positive) direction of the magnetic field. As a consequence, the expected radial velocity change in a switchback is:

$$|\delta V_R| = \frac{|\delta B_R|}{B} V_{ph}, \quad (2)$$

where we have introduced an effective “phase speed” V_{ph} that is different and smaller than V_A because the ratio of kinetic to magnetic energies r_A in the fluctuations is always somewhat smaller than 1. In other words, the effective velocity is $V_{ph} = V_A$ when there is equal content in magnetic and kinetic energy fluctuations (no residual energy), i.e. in intervals of high correlation between $\delta \mathbf{B} - \delta \mathbf{V}$ (high cross-helicity

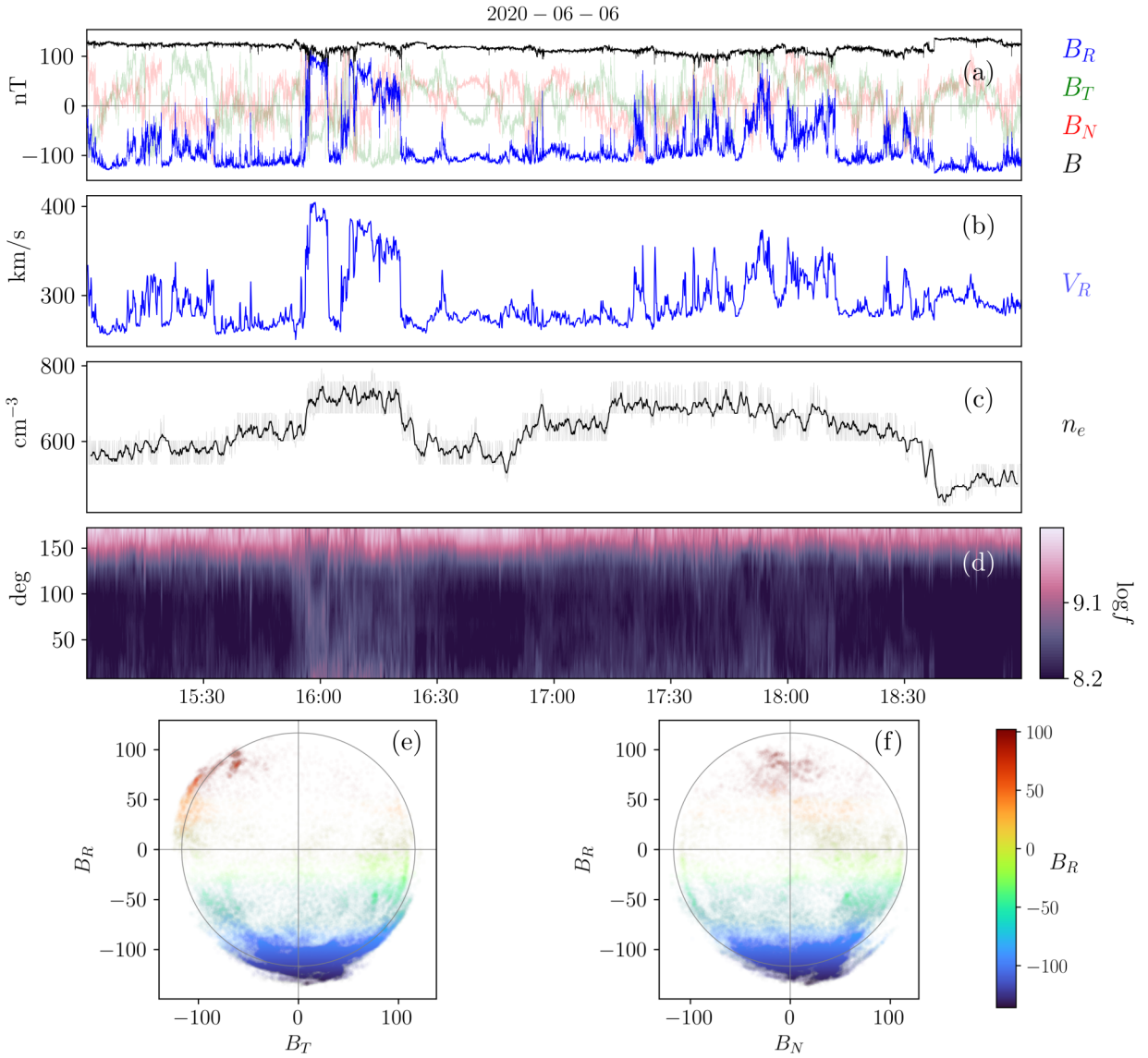


Fig. 3 Magnetic switchbacks observed by Parker at $28 R_{\odot}$ during E5. The top panels display timeseries of (a) the magnetic field vector, (b) the radial solar wind velocity from SPAN, (c) the 1-minute average of the electron density from QTN, and (d) the PAD of suprathermal electrons (314 eV). The bottom panels show scatter plots of B_R vs B_T (e) and B_R vs B_N (f) colored by B_R during the considered time interval.

– see Sect. 4.3.1 for definitions), while typically the relation $V_{ph} < V_A$ is observed in intervals with lower cross-helicity. Alfvénicity in switchbacks and observed deviations are discussed in Sect. 4.2.3.

Since fluctuations in solar wind streams with high Alfvénicity correspond to waves that predominantly propagate away from the Sun, the positive or negative sign in Eq. (1) holds for the correlation in a background magnetic field pointing back towards the Sun or away from the Sun, respectively. In a switchback that changes the sign of the field, the result will always be an outward jet, $\delta V_R > 0$, as long as the background field is predominantly radial (Matteini et al, 2014). Assuming a radial solar wind flow V_0 , it is then possible to express variations of the local speed V associated with switchbacks in the inner Heliosphere, as:

$$V = V_0 + V_{ph} [1 - \cos(\theta_{BR})], \quad (3)$$

where V_0 is the minimum speed of the background, associated here with a positive radial magnetic field (Matteini et al, 2014). Under the assumption of little magnetic field compression, the magnitude of the magnetic field ($|\mathbf{B}|$) is approximately constant, implying that the maximum magnetic field variation is $|\delta\mathbf{B}| = 2B$. The maximum speed enhancement in a switchback is therefore $|\delta\mathbf{V}| = 2V_A$, associated with a full reversal of the background magnetic field. For switchbacks at 90° , $V \sim V_0 + V_A$.

3 Review of Methodologies

The definition of switchbacks provided in Sect. 2 is abstracted from observations collected by spacecraft *in situ* over a great range of distances and throughout the solar cycle. However, as exhibited in Fig. 3, any individual event observed *in situ* more often than not presents departures in some features from the ideal definition. Some switchback characteristics are easier to quantify and detect algorithmically using thresholds in some quantity (such as the deflection angle in the magnetic field), whereas others present subjective aspects or are more difficult to quantify (such as rotation abruptness or required Alfvénicity). For example, although measuring the deflection of the magnetic field vector does not automatically test for Alfvénicity or reject current sheet crossings, it allows for comprehensive statistical event collection. Stricter methods tend to require manual input, leading to more subjectivity and smaller event numbers in statistics. In this section, we review the range of different methodologies used to identify switchbacks in the present literature and discuss their relative assumptions. It is important to keep track of the method chosen to identify switchbacks, as it may affect the inferred properties of switchbacks discussed in the later sections of the paper.

3.1 Identification using Deflection from a Background Field

Since switchbacks are partly defined as sudden magnetic field rotations (Sect. 2), it is common to study them as a simple deflection from a background field. Such a treatment requires two parts: first, a choice of background orientation from which the switchback deflects, and second, a method to characterize and separate the deflection relative to the background. Here, we first highlight the impact the choice of the background field may have on switchback analyses and results (Sect. 3.1.1). Next, we examine the effects of the varying deflection thresholds used by various authors and show that no clear consensus exists on *how small* a deflection should be categorized as a switchback (Sect. 3.1.2).

3.1.1 Impact of the Magnetic Field Background Choice

Various background magnetic field definitions have been used to identify switchbacks, and two kinds of approaches are typically used. One is to compute the background field from the data, using different statistical parameters like the mean, median (Dudok de Wit et al, 2020) or mode values (Bale et al, 2019). The other consists of modeling the expected background field independently, either assuming a radial nominal magnetic field (e.g., Horbury et al, 2018; Larosa et al, 2021; Akhavan-Tafti et al, 2021; Woolley et al, 2020) or using the Parker spiral model (e.g., Horbury et al, 2020; Laker et al, 2021; Fargette et al, 2021). The time interval over which the background is computed should exceed the timescale of magnetic switchbacks, and is typically chosen to be a few hours. All methods have certain limitations: mean, median, and mode values might be biased by the switchbacks themselves (see e.g., Badman et al, 2021), while model accuracy may vary.

In Fig. 4, we illustrate how different background choices will affect a given analysis. Three different background fields computed over 6h are compared: a purely radial magnetic field, the Parker spiral field, and a 6h-mode magnetic field. By definition, both the B_N component of the Parker spiral in the ecliptic and the B_T and B_N components of the radial field are equal to zero throughout the interval. While all methods converge to a similar B_R background, the differences in the B_T and B_N backgrounds are particularly striking. In the bottom panels, we illustrate how these different backgrounds lead to the selection of different solar wind structures. The 2D histograms show the distribution of points deflected more than 60° away from each background field, while the white contour tracks the nominal distribution of the magnetic field components. These distributions of the deflected magnetic field differ significantly between the three methods. The radial background field neglects the B_T component of the expected Parker spiral and, consequently, the detected deviations are strongly biased toward a positive B_T . By contrast, the distributions 60° away from both the Parker spiral model and the sliding mode are more isotropic in B_T . All distributions of B_R are different. Overall, structures labeled as “switchbacks deflected by more than 60° ” will be different across the three methods.

From this example, it seems clear that the switchback definition cannot be solely based on the radial direction, as the tangential component of the Parker spiral remains significant in portions of Parker’s orbit. This is especially important in continuing to identify these structures in other spacecraft datasets farther from the Sun, where, because the background magnetic field may be at large angles to the radial, the velocity signature is no longer apparent as a one-sided spike (Gosling et al, 2009; Bourouaine et al, 2022). The Parker spiral model or the ambient background field (median or mode) produces more accurate references to define magnetic switchbacks. While each will call for a different interpretation of the results (deflection

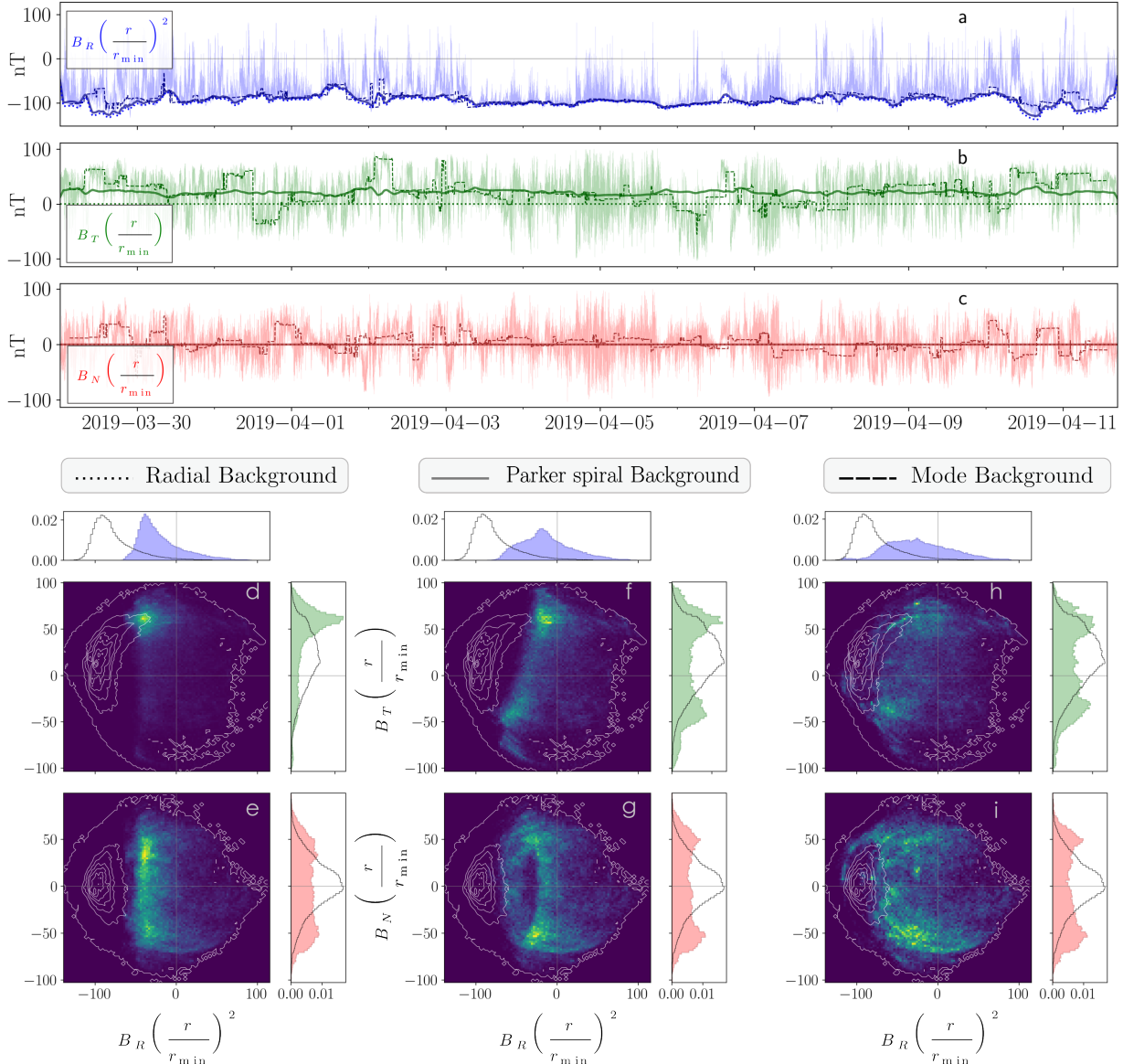


Fig. 4 Impact of switchback definition. In panels *a* to *c*, we show the magnetic field components in the RTN frame during E2, normalized by the closest approach radial distance of $35 R_{\odot}$. We overplot the radial field (dotted lines), the Parker spiral field (full lines), and a 6h-mode field (dashed lines). In panels *d* to *i*, we plot in white the 2D distribution contours of the normalized magnetic field components (B_R , B_T in panels *d*, *f*, *h*, and B_R , B_N in panels *e*, *g*, *i*). Superimposed in color are the 2D histograms of the points that are located more than 60° away from the computed background fields, i.e., the radial direction (*d*, *e*), the Parker spiral (*f*, *g*), and the 6h-mode vector (*h*, *i*). We also add the normalized projected distributions on the side, as a black line for the full 2D distribution and color-shaded for the “more than 60° away” points. Reproduced from Fargette (2022), copyright by the author

from an expected physical model or an ambient field), we advise choosing one of these two methods in future statistical studies.

3.1.2 Deflection Angle Thresholds

Figure 5 shows a histogram of observed switchback deflection angles in terms of the normalized deflection parameter $z = (1 - \cos \alpha)/2$, where α is the deviation angle from the identified background field (a median over 6 hour intervals, Dudok de Wit et al, 2020). These switchbacks, compiled from Parker E1 through E13, show a largely featureless distribution in z , confirming the initial result of Dudok de Wit et al (2020). This hints towards a continuum of nearly self-affine deflections, preventing a quantitative threshold for deflection angle that categorizes a switchback. Demarcating some common choices of z values in Fig. 5 reveals that studies that do not impose a strong reversal in the magnetic field direction ($\alpha < 90^\circ$) have all demanded a rather low z threshold.

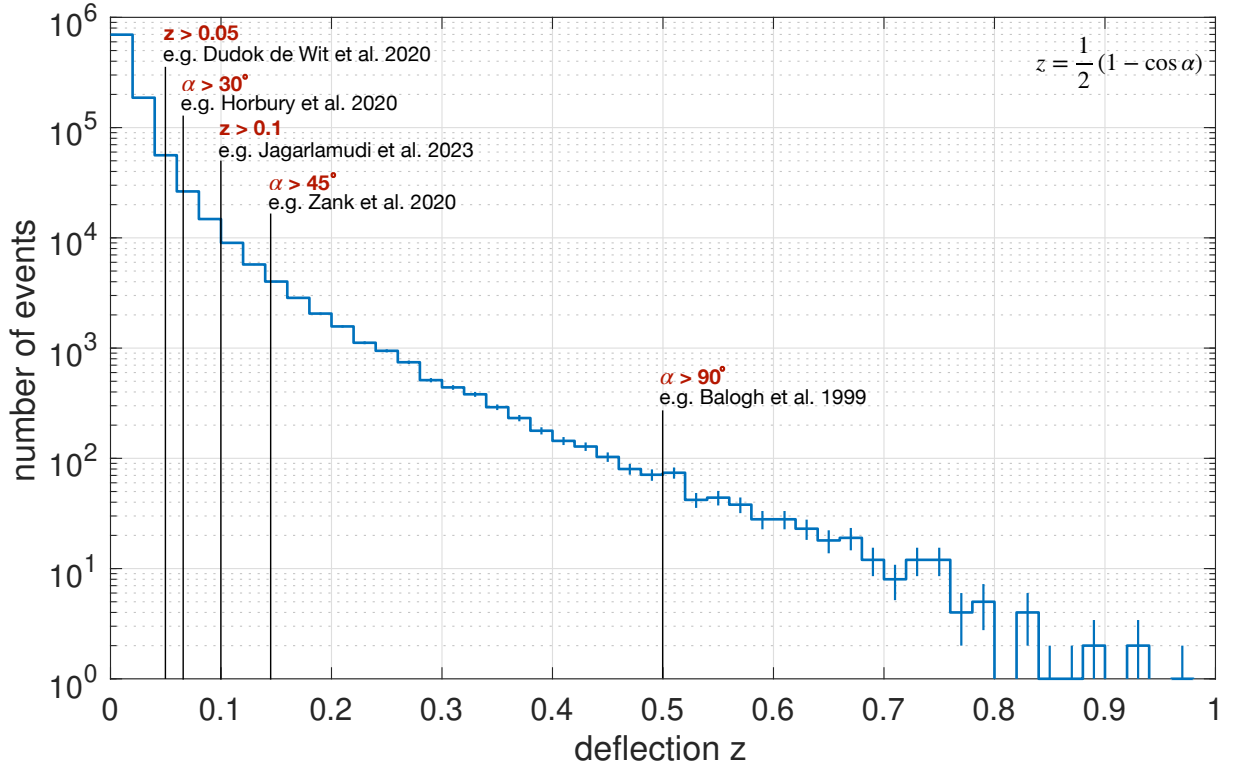


Fig. 5 Histogram showing the distribution of *normalized deflection z*, as defined by [Dudok de Wit et al \(2020\)](#), for individual switchback events during the E1–E13. Some common choices of thresholds in magnetic field deflections are indicated with a mention of the first study that made that choice to define a switchback.

The radial magnetic field reversal as a requirement to identify switchbacks has been used in the analysis of both Ulysses ([Balogh et al, 1999](#)) and Parker data ([Macneil et al, 2020](#); [Mozer et al, 2021](#); [Tenerani et al, 2021](#); [Pecora et al, 2022](#)). These authors use the $\alpha > 90^\circ (z > 0.5)$ criterion on the basis that switchbacks were first reported as field reversals in Parker data ([Bale et al, 2019](#)). However, such fluctuations lie on a continuum of deflection angles, and there is no clear departure from self-similarity at $z = 0.5$, although the statistical significance of larger fluctuations, especially for near-one z values is quite poor.

Several studies have relaxed the deflection threshold to intermediate angles, such as 25° ($z = 0.05$, [Dudok de Wit et al, 2020](#)), 30° ([Horbury et al, 2020](#)), 37° ([Jagarlamudi et al, 2023](#)) and 45° ([Zank et al, 2020](#); [Laker et al, 2021](#); [Woolley et al, 2020](#); [Laker et al, 2022](#)). Such choices, highlighted in Fig. 5, also appear somewhat arbitrary in the context of the featureless spectrum of deflection angles, although for very low deflection angles, such fluctuations are not meaningfully distinct from general stochastic variation in the *in situ* data (see Sect. 4.2.1). Further, it has been shown that quiet solar wind intervals (devoid of switchbacks) present a standard deflection of around 15° around the Parker spiral, while larger amplitudes tend to have a systematic offset compared to this direction ([Farglette et al, 2022](#)). Therefore, this value may be viewed as a reasonable minimum threshold value.

The choice of lower deflection Alfvénic fluctuations to qualify as switchbacks is further bolstered by the distribution of deflection angle α with regards to the Alfvén Mach number M_A (defined as v_{sw}/v_A , where v_{sw} is the magnitude of the proton velocity vector defined by plasma moments). It displays a “herringbone” structure where individual striations (conjectured to arise from flows of similar origin) show a systematic increase in deflection angle with an increase in M_A ([Bandyopadhyay et al, 2022](#); [Liu et al, 2023b](#)). Since an increase in M_A is expected due to solar wind acceleration, switchback deflection angles are thus expected to increase with distance from the Sun. With an abundance of deflections being below 90° , the renaming of “switchbacks” to “Alfvénic deflections” has been suggested, but has not yet been adopted ([Liu et al, 2023b](#)). The connection between switchbacks and sub-Alfvénic wind is discussed further in Sect. 5.3.

3.2 Manual Identification of Switchbacks

In several studies, the selection of switchbacks to perform statistical studies has been the result of a manual identification by the authors. A two-step process is usually involved, where the raw time-series of observations

Method	References	Method Summary	Assumptions
Deflection thresholds	$\alpha \geq 25^\circ$ Dudok de Wit et al (2020)^{E1} $\alpha \geq 30^\circ$ Horbury et al (2020)^{E1} $\alpha \geq 37^\circ$ Jagaramudi et al (2023)^{E1,2,4-10} $\alpha \geq 45^\circ$ Zank et al (2020)^{E1} Woolley et al (2020)^{E1,2} Laker et al (2021)^{E1,2} Laker et al (2022)^{E1-8} $\alpha \geq 90^\circ$ Balogh et al (1999)^U Macneil et al (2020)^H Badman et al (2021)^{E1-5} Mozer et al (2021)^{E3-7} Tenerani et al (2021)^{H,U,E1-6} Pecora et al (2022)^{E1-8}	Local, instantaneous deflections (z -angle) of the magnetic field are computed with respect to a chosen background model. Time periods with z -angle larger than a prescribed threshold are labeled as a switchback.	Ad-hoc choices of z -angles that are not consistent across studies. Generally, the method does not impose a lower limit of window length for switchback patches and/or strength of magnetic field deflections.
Manual “by-eye”	Burlaga (1969)^P Tsurutani and Smith (1979)^P Horbury et al (2001)^{G,W,I} Knetter et al (2003)^C Knetter et al (2004)^C Borovsky (2016)^{H,A,W,U} Kasper et al (2019)^{E1,2} Woolley et al (2020)^{E1,2} Martinović et al (2021)^{E1,2} Hernández et al (2021)^{E1} Larosa et al (2021)^{E1} Fedorov et al (2021)^S McManus et al (2022)^{E3,4} Huang et al (2023a)^{E1,2,4-8} Huang et al (2023b)^{E1,2,4-8} Akhavan-Tafti and Soni (2024)^{E1-14}	Generally involves a two-step process with an initial automated timeseries picking followed by a manual or visual screening of events. Step 1 may be based on criteria such as a minimum z -angle or strength of magnetic field deflection or a minimum number of data points constituting the spike.	Short-lived switchback patches and/or weaker amplitude field deflections might be overlooked due to subjective bias. Choice of Step 1 criteria may lead to variable switchback identification across different studies.
Velocity spike	Horbury et al (2018)^H	Velocity threshold is used to pick out Alfvénic deflections over a smoothed background velocity obtained from a running average using a boxcar function.	No threshold for magnetic field deflection. Mandates a specific ad-hoc choice for velocity spike threshold and length of background averaging window.
Velocity spike and deflection combination	Farrell et al (2020)^{E1} Farrell et al (2021)^{E1} Rasca et al (2021)^{E1,2} Rasca et al (2022)^{E1,2} Rasca et al (2023)^{E8,12}	“Switchback index” defined as the product of velocity and magnetic fluctuations, $\delta B_r \cdot \delta V_r$.	The approach prioritizes identifying sharp boundaries. Assumes an averaging timescale (usually 30 s) to define fluctuation quantities.
MCMC optimization of Gaussian populations	Fargette et al (2022)^{E1,2,4-9}	Continuous timeseries of magnetic field is converted from RTN coordinates to spherical polar coordinates aligned with the Parker spiral to find remnant deflections. Involves Bayesian fitting of these deflections under two Gaussian populations — quiet solar wind and SBs.	Only one dominant population of SBs is assumed to be present in the solar wind. No lower limit for the minimum angle of deflection.
Individual events	Telloni et al (2022)Sm	Isolated switchback structures analyzed with specialized tools on a case-by-case basis.	Observed an S-shaped kink structure in white light coronagraph observations, requiring a very large structure with a density enhancement.

Table 1 Summary of a few major methods of switchback identification. Superscripts on the references indicate ‘A’ for ACE, ‘C’ for Cluster, ‘EX’ for the Xth Parker encounter, ‘G’ for Geotail, ‘H’ for Helios, ‘P’ for Pioneer, ‘S’ for Solar Orbiter, ‘Sm’ for Metis coronagraph onboard Solar Orbiter, ‘U’ for Ulysses, and ‘W’ for Wind.

is first processed using some criteria from Sect. 2 definition (field deflection and Alfvénic bulk velocity enhancements) and is followed by data visual inspection to build a catalog of switchbacks. While visual inspection necessarily introduces a bias in switchback selection and requires a large workload, it remains an efficient and robust way of identifying switchbacks. Here, we review how some switchback catalogs were built, based partly or totally on visual inspection.

Visual inspection has been extensively used on past mission data to identify solar wind discontinuities. Deflections of the interplanetary magnetic field were visually identified and studied with Pioneer (Tsurutani and Smith, 1979; Burlaga, 1969), the Geotail, Wind, and IMP 8 satellites at 1 AU (Horbury et al, 2001), as well as the Cluster mission (Knetter et al, 2003, 2004). Strong deviations from the Parker spiral direction were also manually identified consistently across four satellites at different radial distances (Helios 1 at 0.3 AU, Wind and ACE at 1 AU, and Ulysses at 2.3 AU, Borovsky, 2016). More recently, several papers released switchback catalogs in Parker data based on visual inspection, examples of which follow: A list of 1074 events from E1 and E2 was assembled by Martinović et al (2021). Through multiple independent visual inspections of the magnetic field rotations coincident with bulk velocity enhancements, they further confirmed 921 events with five regions for each switchback: (1) the leading quiet region (LQR) with stable velocities and magnetic fields before the switchback; (2) the leading transition region (LTR), where the magnetic field rotates from LQR toward its switchback orientation; (3) the switchback itself with stable field orientation; (4) the trailing transition region (TTR); and (5) the trailing quiet region (TQR). This method was later used to identify 92 additional switchbacks from E3 and E4 (McManus et al, 2022). In parallel, 70 switchbacks were identified during the first encounter by Larosa et al (2021) based on several signatures, namely a deflection of the magnetic field, an increase in magnetic fluctuation accompanied by an increase in proton bulk velocity and radial temperature. Another catalog of 1748 switchback candidates was produced by Huang et al (2023a) and Huang et al (2023b) using data spanning E1–E8 (excluding E3). The thresholds were first set in terms of B_R/B and a minimum number of points constituting the switchback spike. This was followed by manual screening of better switchback candidates based on the requirements that suprathermal electrons do not change their main distributions, and that the magnetic and velocity fluctuations are dominantly Alfvénic. Finally, visual inspection has also been used to identify periods of quiet solar wind and periods of high switchback occurrence (Hernández et al, 2021; Fargette et al, 2022).

All these catalogs have been used to perform statistical analysis of the properties of switchbacks, such as kinetic properties (Martinović et al, 2021; Larosa et al, 2021) and variation of plasma parameters inside and outside switchbacks (McManus et al, 2022; Huang et al, 2023b). These different lists of switchbacks may not be mutually consistent, as the criteria used to identify each structure vary between references. One may also note from table 3.1.2 that many “by-eye” catalogs in the Parker era only examined the first 1–2 encounters. The extent to which existing catalogs are consistent remains to be systematically examined and separated by identification method. However, as will be shown in table 2, it is already apparent that the differing identification methods result in very different number statistics, with more strict or laborious definitions necessarily resulting in sparser numbers of events.

3.3 Alternative Methods and Takeaways

In addition to magnetic field deflections and visual identification of individual structures, other methods and criteria have been used to detect switchbacks. For example, some studies have implemented thresholds on the amplitude of “velocity spikes” (Horbury et al, 2018; Kasper et al, 2019). The amplitude of the velocity increase, however, depends on the background Alfvén speed, so this velocity threshold is bound to change with radial distance for similar deflection angles.

A more probabilistic approach has also been proposed by Fargette et al (2022): rather than setting arbitrary thresholds on the magnetic field deflection angle, they assume that two populations of solar wind co-exist and calculate the probability for a given data point to belong to a quiet solar wind interval or to a switchback.

Finally, Telloni et al (2022) reported the first possible observation of a switchback in the solar corona. They reported a single large propagating S-shaped structure observed by the Metis coronagraph onboard Solar Orbiter, possibly the signature of a large solar jet. They argued that the switchback structure was generated via interchange reconnection between the coronal loops above an active region and nearby open-field regions. However, by virtue of being observed in white light (implying a global density enhancement of the structure), such a switchback may not be typical since most *in situ* events are not typically elevated in plasma density (see Sect. 4). Further, this remote sensing method necessarily involves line of sight integration which may permit non-unique solutions to the apparent magnetic topology consistent with the observation.

More robust inferences would require more information than apparent morphology such as using multiple independent lines of sight or polarization-based 3D localization.

We have seen in this section that several methods exist in the literature to define and identify magnetic switchbacks, each with its own assets and drawbacks. Scientific results on switchbacks may vary significantly depending on the choice of background solar wind, the choice of threshold, and the choice of switchback definition. We therefore advise caution when interpreting results, depending on the method used. Additionally, the criteria for switchback identification may change as they evolve in the solar wind, and we refer to [Mallet et al \(2026, this collection\)](#) for a deeper understanding of switchback evolution. In the remainder of this review, we present results obtained studying the properties of magnetic switchbacks, highlighting where the methodologies used can explain differences in results between studies.

4 Switchback Properties and Structure

We move now to a discussion of the major properties inferred about switchbacks and their implication in terms of origin and impact. We separate these studies into three broad categories: 1) Investigations pertaining to whether switchbacks contain distinct steady plasma populations from the general solar wind (Sect. 4.1); 2) Studies on switchback geometry and boundaries (Sect. 4.2) and 3) Studies that determine whether switchbacks contain distinct fluctuation characteristics compared to general Alfvénic turbulence in the solar wind (Sect. 4.3).

4.1 Plasma Population Inside Switchbacks

Exploring the plasma characteristics inside a switchback is important to the question of switchback formation. The processes leading to the origin of switchbacks are still a matter of open debate (see [Wyper et al, 2026, this collection](#)). Three broad categories include the generation and injection at coronal heights, e.g. by interchange reconnection ([Fisk and Kasper, 2020](#); [Drake et al, 2021](#); [Bale et al, 2021](#)), large-scale velocity shear due to coronal jets or motion of the magnetic footpoint between source regions of fast and slow streams ([Landi et al, 2006](#); [Schwadron and McComas, 2021](#); [Toth et al, 2023](#)), and the continuous *in situ* formation by expansion and nonlinear processes, e.g. turbulence ([Squire et al, 2020](#); [Ruffolo et al, 2020](#); [Mallet et al, 2021](#); [Shoda et al, 2021](#); [Johnston et al, 2022](#); [Matteini et al, 2024](#)).

The presence of a distinct plasma population inside switchbacks, different from the surrounding solar wind, would be a clear indication that switchbacks are the result of direct injection via impulsive processes. If the switchback plasma is indistinguishable from its background, it suggests either switchbacks are formed in the accelerating solar wind, or that the switchback plasma has been able to mix significantly with the background during its transport from the sun. Another reason for the absence of specific plasma signatures might be that an originating impulsive event does not involve direct injection of plasma, for example, a pulse in the magnetic field only. Here, we review investigations pertaining to this overarching question. In the following subsections, two different types of investigations are discussed: studies that compare individual switchback spikes to their immediate surroundings, and studies that consider entire macroscopic streams in which switchbacks occur, and compare them with streams that lack significant switchback signatures, i.e., are “switchback quiet”. The results often differ between these two classes of studies but in instances when the results agree, the results may be considered more reliable.

4.1.1 Steady Plasma Properties Overview

We begin by collating recent results that compare typical steady plasma properties inside and outside switchbacks. These are presented in Table 2, where quantities such as magnetic field magnitude, the proton and alpha density, proton velocity, plasma β , pressure and electron strahl intensity and anisotropy inside and outside switchbacks are contrasted.. The parameters are drawn from several statistical studies, and the methodology used to identify switchbacks is noted in the table. For each entry, the property inside individual switchbacks is compared to its typical value immediately outside. As shown in the third column, these studies draw from different encounters (and phases of encounters therein) and so it should be noted that differing solar wind conditions, distances from the sun and direction of motion of the spacecraft are generally not differentiated in such studies.

Surveying this table, almost all plasma properties remain unchanged. This includes the magnetic field magnitude, electron and proton number density, alpha-to-proton abundance ratio, and differential alpha streaming (normalized by the Alfvén speed). This implies switchbacks are mostly Alfvénic fluctuations for which protons and alpha velocities rotate in rigid rotation in a frame co-moving with the switchback ([Neugebauer and Goldstein, 2013](#); [Matteini et al, 2015](#); [McManus et al, 2022](#)). The latter paper points out

Parameter	Interior/Exterior	Encounters	Switchback Definition and Number	Reference
$ B $	$\simeq 1$ Median=0.98 $\simeq 1$ Median = 1	Six days in E1 E1-E2 E1-E2, E4-E10	Manual “by-eye”, 70 Manual “by-eye”, 1074 Thresholding	Larosa et al (2021) Martinović et al (2021) Fig. 6 and Jagarlamudi et al (2023)
$N_e(QTN)$	$\simeq 1$ Median=0.98	E1-E2, E4-E10	Thresholding	Fig. 6 and Jagarlamudi et al (2023)
N_p	$\simeq 1$ Median=1.00 $\simeq 1$	Six days in E1 E1-E2	Manual “by-eye”, 70 Manual “by-eye”, 1074	Larosa et al (2021) Martinović et al (2021)
N_α/N_p	$\simeq 1$ Similar distribution	E3-E4 E1-E8 (no E3)	Manual “by-eye”, 92 Manual “by-eye”, 1748	McManus et al (2022) Huang et al (2023b)
V_p	> 1 Median=1.18 increment of $V_A/2$ > 1 Median=1.1	Six days in E1 E1-E2 E1-E2 & E4-E10	Manual “by-eye”, 70 Manual “by-eye”, 1074 Thresholding	Larosa et al (2021) Martinović et al (2021) Fig. 6 and Jagarlamudi et al (2023)
$V_{\alpha p}/V_A$	Similar distribution	E1-E8 (no E3)	Manual “by-eye”, 1748	Huang et al (2023b)
β	> 1 Median=1.45	Six days in E1	Manual “by-eye”, 70	Larosa et al (2021)
P_K	Slightly larger ≥ 1 Median= 1.12 ± 0.21	E1-E8 (no E3)	Manual “by-eye”, 1748	Huang et al (2023a)
P_B	Slightly smaller ≤ 1 Median= 0.90 ± 0.73	E1-E8 (no E3)	Manual “by-eye”, 1748	Huang et al (2023a)
P_{total}	$\simeq 1$ Median= 1.05 ± 0.12	E1-E8 (no E3)	Manual “by-eye”, 1748	Huang et al (2023a)
e-PADs A_E	> 1 Median= 1.30 ± 0.45	E1-E8 (no E3)	Manual “by-eye”, 1748	Huang et al (2023a)
e-PADs F_E	$\simeq 1$ Median= 1.00 ± 0.01	E1-E8 (no E3)	Manual “by-eye”, 1748	Huang et al (2023a)

Table 2 Comparison of general plasma properties between the interior and exterior of switchbacks. From left to right, the columns present the parameters, Inside-to-Outside comparisons, encounters of the data, the switchback definition in Table 3.1.2, switchback numbers, and the references. From top to bottom, the parameters include magnetic field strength $|B|$, electron number density N_e , proton number density N_p , alpha-to-proton abundance N_α/N_p , proton bulk speed V_p , alpha-to-proton differential speed normalized by local Alfvén speed $V_{\alpha p}/V_A$, plasma beta β , kinetic pressure P_K , magnetic pressure P_B , total pressure P_{total} , anisotropy (A_E) and integral intensity (F_E) of suprathermal electron pitch angle distributions (e-PADs).

that, while a lack of compositional difference implies *in situ* generation, a clear compositional signature could be hidden by differential velocity between the switchback wave speed and background solar wind.

The sum of kinetic (proton, alpha, and electron) pressure and magnetic pressure also remains constant during typical switchback fluctuations, implying the structures are in pressure balance with their surroundings. Lastly, while the suprathermal electron pitch angle distribution remains strongly peaked in a consistent direction either parallel or antiparallel to the magnetic field throughout each switchback (a key marker identifying switchbacks as topological folds rather than current sheets or loops, [Kasper et al, 2019](#)), the total distribution does exhibit signs of isotropization (the magnitude of the suprathermal electron pitch angle anisotropy, A_E , decreases, [Huang et al, 2023b](#)) suggesting switchbacks can scatter electrons to some extent. This finding, which comes from Parker/SPAN-e data, should be revisited to assess the potential impact of switchback-related Doppler shifts: the higher energy tail of the thermal population could appear in suprathermal energy ranges during the large velocity spikes comprising switchbacks.

The above results imply *individual* switchback’s plasma properties are largely not distinct from those of their surroundings. A different way to analyze these properties is to compare the plasma in intervals with many consecutive switchbacks with adjacent “quiet” intervals. Using this method, one finds that the plasma properties populate a finite width distribution whose peak generally matches the results presented in Table 2 for individual spikes. In Fig. 6, we present statistical distributions of the electron density, velocity, and magnetic field magnitude ratios between switchback and non-switchback regions (selected regions from [Jagarlamudi et al, 2023](#)). Non-switchback intervals are defined by requiring that the deflection parameter (see Sect. 3.1.2) satisfy $z < 0.1$ at least 60% of the time or the mean of z values inside the region is less than 0.1. The minimum duration of a non-switchback interval used is 20s. Intervals are chosen so that switchback and non-switchback intervals are adjacent to each other in time to avoid comparison of plasmas with very different background solar wind conditions.

We observe that the in-out ratio of magnetic field magnitudes and densities is nearly one for the majority of the intervals. However, there are a non-negligible number of intervals for which the ratios are sometimes higher and sometimes lower (see also [Larosa et al, 2021](#)).

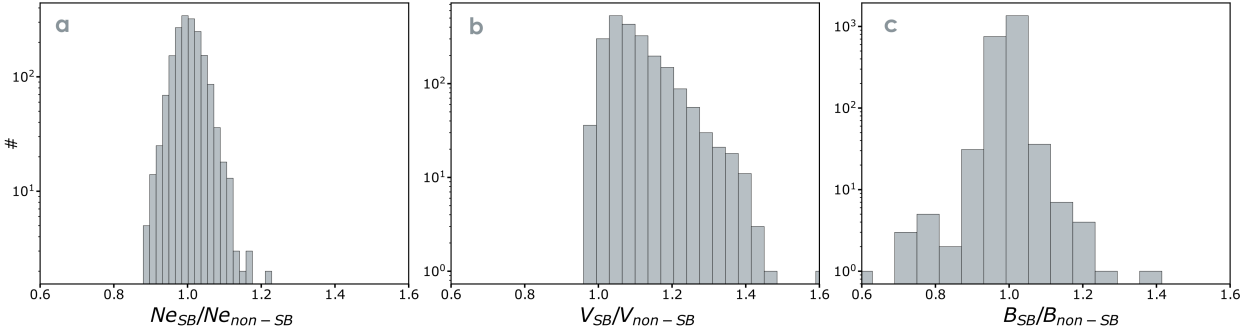


Fig. 6 Histogram of plasma parameter ratios between the switchback to non-switchback regions. Panel (a) electron density ratios, Panel (b) Bulk velocity ratios, and Panel (c) magnetic field magnitude ratios. (selected regions from [Jagarlamudi et al, 2023](#))

Moreover, while usually the magnitude field magnitude, pressure, and energy density are approximately constant in, i.e., fractional changes are much less than 1 (as shown above), it is often the case that switchbacks cause more of a disruption to magnetic pressure balance (and conservation of $|B|$) than the surrounding plasma. [Ruffolo et al \(2021\)](#) examined domains of nearly constant $|B|$ using Parker observations, and concluded that many (but not all) transitions between different regions of uniform $|B|$ were associated with switchbacks. In this sense, these constant- $|B|$ domains often represent regions of space in between the switchbacks or in between the boundaries of switchback patches, as will be discussed further in Sect. 5. As for the bulk velocity, a clear one-sided distribution in velocity is observed for switchbacks ([Gosling et al, 2009](#)). This is consistent with their identification as Alfvénic velocity spikes and readily explained in terms of outwardly propagating Alfvénic fluctuations (see Sect. 2).

4.1.2 Switchback Proton and Alpha Temperatures

The previous subsection did not discuss any thermodynamic properties of the plasma and in particular proton and alpha particle temperatures and anisotropies. The reason is that obtaining such quantities is complicated by instrumental effects arising from the finite portion of velocity space observable at a given instant by the SWEAP instrument (see Sect. 1.3). The observed velocity distribution functions (VDFs) can systematically move out of the instrument field of view during a switchback due to the velocity perturbation of the structure, distorting the measured temperature. The way such instrumental effects are modeled can easily affect the trends reported in the Parker Solar Probe literature. Nevertheless, it is an area of high interest, since it determines whether the switchback plasma may be considered to be in thermal equilibrium with its surroundings. The comparison of proton and alpha particle parallel and perpendicular temperatures and their ratios inside and outside switchbacks, together with the methodology used to obtain them, are summarized in Table 3.

As shown in the table, the results are generally mixed, but with a preponderance of results suggesting the proton temperature inside switchbacks is generally higher than in their surroundings. Results are also mixed when considering temperature anisotropy, with some studies concluding that the parallel and perpendicular temperatures are individually enhanced or unchanged. No studies report examples of lower proton temperature (parallel, perpendicular, or scalar).

On the other hand, Table 3 shows that the alpha temperature in switchbacks is typically lower with respect to their surroundings, both in absolute terms and with respect to the ratio to proton temperatures. These results remain somewhat controversial, and future studies are needed that carefully follow the systematic evolution of the VDFs during switchbacks. Close to the Sun, such studies when possible would ideally use both plasma instruments together on Parker (SPAN-i and SPC) to reduce field of view issues, while **further** from the Sun, the excellent angular coverage of the Proton-Alpha sensor in the Solar Orbiter's Solar Wind Analyser suite (SWA/PAS; [Owen et al, 2020](#)) instrument should be capitalized on. To highlight the importance of instrumental considerations, Table 4 presents a few studies that use temperature measurements by Parker/SWEAP in differing ways and from different periods of the mission with careful attention to systematic measurement effects. We go into some detail to highlight that this is a non-trivial task.

[Woolley et al \(2020\)](#) used proton core fits from SPC, which captures the 1D reduced VDF best along the radial direction, meaning only switchbacks with a near-full B_R reversal were considered. SPC data show clear temperature enhancements in lockstep with the magnetic field vector (see also [Rasca et al, 2021](#)). However, these were compared to the artificial dependence of the temperature on magnetic field orientation dependence common to Faraday Cups ([Kasper et al, 2002](#); [Huang et al, 2020a](#)). Plotting the radial component of the proton temperature tensor as a function of the instantaneous angle between the magnetic field and radial

Table 3 Comparison of various plasma temperatures between inside and outside switchbacks where the subscripts (p , α , \perp and \parallel) refer respectively to protons, alphas, and perpendicular or parallel components of the temperature tensor with respect to the orientation of the magnetic field. From left to right, the columns present the parameters, Inside-to-Outside results, encounters of the data, the selection methods of the switchbacks, and the related notes and references.

Parameters	Inside/Outside	Encounters	Switchback Definition and Number Statistics	Reference
T_p	$\simeq 1$	E1-E2	Manual “by-eye”, 1074	Martinović et al (2021)
	> 1	E1-E8 (no E3)	Manual “by-eye”, 1748	Huang et al (2023a)
	Median= 1.12 ± 0.20	E1-E2	“Switchback Index”, 25	Rasca et al (2021)
$T_{\parallel p}$	$\simeq 1$	E1-E2	Deflection thresholds, 5	Woolley et al (2020)
	> 1	six hours in E2	Manual “by-eye”, 6 patches	Woodham et al (2021)
	> 1 Median= 1.26 ± 0.50	E1-E8 (no E3)	Manual “by-eye”, 1748	Huang et al (2023a)
$T_{\perp p}$	$\simeq 1$	E1-E2	Deflection thresholds 2-4 days in each encounter	Laker et al (2024)
	> 1	E1-E8 (no E3)	Manual “by-eye”, 6 patches	Woodham et al (2021)
	Median= 1.06 ± 0.18	E5-E11 (no E9)	Manual “by-eye”, 1748	Huang et al (2023a)
T_{α}	$\simeq 1$	six hours in E2	Deflection thresholds 2-4 days in each encounter	Laker et al (2024)
	Median= 0.86 ± 0.44	E1-E8 (no E3)	Manual “by-eye”, 1748	Huang et al (2023a)
$T_{\parallel \alpha}$	< 1 Median= 0.82 ± 0.48	E1-E8 (no E3)	Manual “by-eye”, 1748	Huang et al (2023a)
$T_{\perp \alpha}$	< 1 Median= 0.85 ± 0.53	E1-E8 (no E3)	Manual “by-eye”, 1748	Huang et al (2023a)
T_{α}/T_p	< 1 Median= 0.75 ± 0.41	E1-E8 (no E3)	Manual “by-eye”, 1748	Huang et al (2023a)
$T_{\parallel \alpha}/T_{\parallel p}$	< 1 Median= 0.56 ± 0.40	E1-E8 (no E3)	Manual “by-eye”, 1748	Huang et al (2023a)
$T_{\perp \alpha}/T_{\perp p}$	< 1 Median= 0.79 ± 0.48	E1-E8 (no E3)	Manual “by-eye”, 1748	Huang et al (2023a)

Table 4 Comparison of results on proton temperature evolution during switchbacks (SBs) as observed on Parker Solar Probe. For each study, the dataset, the switchback definition used, the instrumental geometry effects considered, and the ultimate takeaways are listed.

	Woolley et al (2020)	Woodham et al (2021)	Laker et al (2024)
Data	SPC Proton Core Fits (1D) E01,E02	SPAN-i Proton Core Fits (3D) E02	SPAN-i Proton Core Fits (3D) E05-E11
SB Definition	Full reversal in B_R	Patches selected by eye.	No threshold deflection set, general quasi-periodic deflections
Geometrical Considerations	Measured deviation from theoretical instrument response.	Instances of large B field deflections ($> 10^\circ$) occurring faster than the SPAN-i integration time are rejected.	Data during large positive s/c frame tangential flow angle deflections ($< -5^\circ$) rejected.
Conclusions:	Individual SBs unchanged	SB patches hotter	Groups of neighboring SBs hotter

direction (see figure 4 of [Woolley et al, 2020](#)) showed little deviation from this geometrical prediction. [Woolley et al \(2020\)](#) therefore concludes that switchbacks do not appear hotter in SPC measurements, although they caution about the instrumental ambiguity and that SPC may therefore not be able to measure a temperature enhancement during large deflections. On the other hand, [Woodham et al \(2021\)](#) reported different conclusions but using SPAN-I 3D bi-Maxwellian proton core fits and expanding the switchback definition to general 3D field deflections superimposed on a larger scale “patch” (see Sect. 5), evoking a picture of individual switchbacks embedded in a larger 3D structure with systematic flow properties. They considered intervals with minimal artificial temperature broadening effects shared by electrostatic analyzers (ESAs) ([Verscharen and Marsch, 2011](#)) by rejecting time intervals where the field deflected significantly (as compared to the detector angular resolution) during intervals faster than a SPAN-ion integration time (see Table 4). They observed T_{\parallel} enhancements over large-scale patches of many switchbacks (see also Sect. 5) and argued similar enhancements could be observed in individual spikes. They interpreted this as evidence that patches of switchbacks may have a common solar origin. The competing conclusion found in [Woolley et al \(2020\)](#) was reconciled with a suggestion that the specific relationship between T_{\parallel} and the field orientation could be the same as the artificial SPC response ($T_{\parallel} \propto \sin \Theta_{RB}$ where Θ_{RB} is the angle between the magnetic field and the radial direction) such that an actual temperature enhancement signature may

be indistinguishable from the systematic instrumental signature observed with SPC data in [Woolley et al \(2020\)](#). They suggested that future work with later orbits, where SPAN-i field of view issues were less severe, would be necessary to resolve this.

[Laker et al \(2024\)](#) expanded upon the results of [Woodham et al \(2021\)](#) for later encounters E05-E11, using the same proton core bi-Maxwellian fitting methodology. They highlighted that in later Parker encounters, the systematic azimuthal motion of the spacecraft in the solar wind frame means VDFs are more completely sampled by the SPAN instrument. They loosened the switchback definition by not defining a threshold for deflection angle. By doing so, the switchback was then generalized to include quasi-periodic deflections (on a minute timescale) of the full magnetic field vector. They interpreted these Alfvénic quasi-periodic patterns as torsional Alfvén waves propagating from interchange reconnection sites in the corona. Associated with these quasi-periodic deflections, they found quasi-periodic variation in the proton core temperature (both T_{\perp} and T_{\parallel}). They additionally found a positive correlation between the change in perpendicular and parallel temperatures during the switchbacks and θ_{RB} , and argued that this does not rule out an *in situ* switchback generation mechanism. To ensure reliability of the SPAN-I measurements, they avoided intervals of large V_T flows that swung the proton core out of the SPAN-I field of view, defining a threshold angle that ensures the angle between the flow and spacecraft frame velocity does not deviate from radial in the +T direction.

By not applying a deflection threshold to the switchback definition, a less extreme underlying structure was identified in [Laker et al \(2024\)](#), defining individual switchbacks as sub-structures. This slightly differs from [Woodham et al \(2021\)](#), who defined the switchback based on deflection angle, and concluded increases of T_{\parallel} were linked to switchback patches. [Laker et al \(2024\)](#) instead identifies the deflection and T_{\parallel} increase as the bigger structure, with an embedded sub-structure of constant T_{\parallel} . To reconcile the conclusions in [Woolley et al \(2020\)](#), [Laker et al \(2021\)](#) also points out that in these later encounters, the switchbacks do not undergo a full deflection, and there is no SPC vs SPAN comparison available (due to data gaps and anti-coincident reliability).

4.1.3 Steady Plasma Properties Takeaways

Overall, switchback steady plasma properties are mostly consistent with that of steepened large amplitude Alfvén waves in which the magnetic field and velocity vector instantaneously vary together while most other plasma properties stay close to consistent with the surrounding wind. That is, they are largely incompressible in terms of the magnitude of the magnetic field and the plasma density (see Figure 6).

The notable exception to this picture is the temperature for which there are indications of potential enhancements and also modulation in anisotropy. Instrumental considerations and limited statistics mean that further work is needed to establish this concretely. Similarly, limited by instrumental capabilities, the presence of proton and alpha beams, alpha abundance and any evidence of heavier species modulation in and outside switchbacks remains an open question. Strategies including detailed velocity distribution function reconstruction at Parker, full VDF measurements at Solar Orbiter **farther** from the Sun, and combining multi-spacecraft instruments during conjunctions, are needed to make progress here. Further, the sources for these findings generally only span up to E11 and need updating with more recent encounters which have taken Parker even closer to the Sun, potentially swinging the VDF more favorably into the SPAN-I field of view.

4.2 Switchback Occurrence, Geometry, and Boundaries

Switchback structure, occurrence rate, boundary evolution may provide fundamental clues both into the origin of switchbacks, their growth and decay, as well as to the question of how switchbacks interact and exchange plasma and energy with the background solar wind. One major feature of switchbacks relevant to these points is that they have “sharp” boundaries, and their magnetic and velocity vectors rotate on a sphere in a specific way. Here we collate results that investigate switchback geometry and the properties of switchback boundaries, to shed light on the nature of these fluctuations. We first introduce occurrence statistics based on the classification of these structures as sharp deflections (Sect. 4.2.1). Second, we discuss their spatial scales and geometrical aspects in Sect. 4.2.2. Lastly, we present a series of discussions on the nature of the switchback boundaries: their non-Alfvénic characteristics (Sect. 4.2.3), their classification as discontinuities (Sect. 4.2.4), their relation to magnetic reconnection (Sect. 4.2.5), and lastly their relationship to electromagnetic wave activity (Sect. 4.2.6).

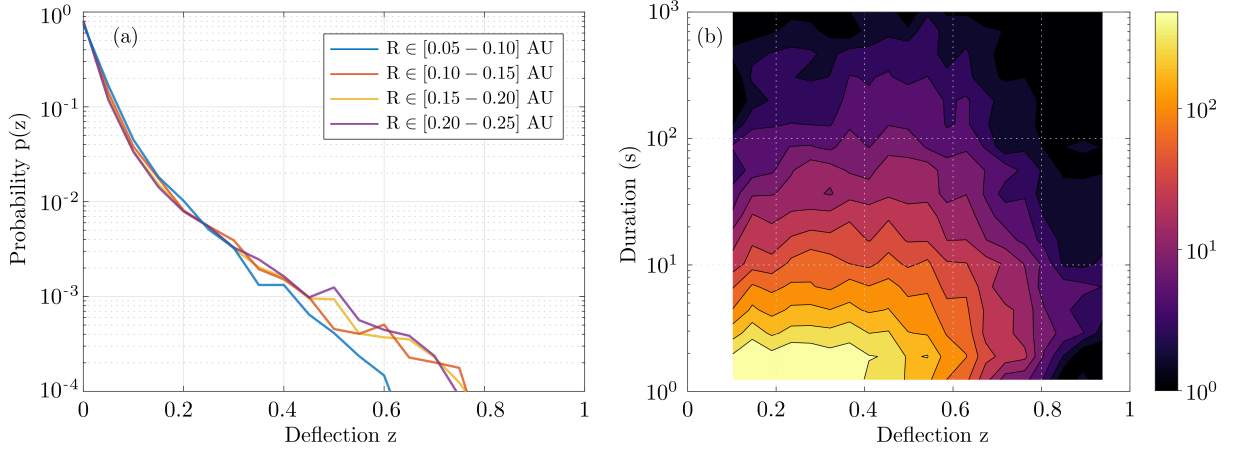


Fig. 7 Left panel (a): Probability distribution of the normalized deflection z for Parker data from E1 to E17, binned by distance from the Sun in AU. Right panel (b): 2D histogram versus the duration and the normalized deflection z for E1–E17, using the same dataset.

4.2.1 Deflection Angle and Duration Statistics

Establishing the distribution of switchback sizes, occurrence rates, and lifetimes provides powerful diagnostic information regarding their generation, decay, and physical nature. Automated identification and characterization of switchbacks (see Sect. 3) enable in-depth studies of these statistical properties. Here, we highlight some results based on a recent reanalysis of Parker data from E1 to E17, identifying switchbacks as sharp deflections from the Parker spiral as characterized by changes in the normalized deflection parameter, z (Dudok de Wit et al, 2020).

Figure 7 disaggregates what was previously shown in Fig. 5. In the left panel, the distribution of switchback deflections is shown for different distances from the Sun. These distributions are close to exponential except for an excess of very small deflections with $z < 0.1$. As mentioned before in Sect. 3, such small deflections are increasingly difficult to distinguish from stochastic fluctuations, and for that reason, ought to be discarded, even if this excludes some which technically meet the definition presented in Sect. 2. In what follows, we exclude these smallest deflections ($z < 0.1$) to avoid ambiguity with background solar wind.

From Fig. (7), we first observe a continuum of magnitudes with an abundance of smaller ones. Out of these, less than 2% can be called full-reversal switchbacks because they have a deflection of more than 90° . Numerous other statistical indicators (e.g., Dudok de Wit et al, 2020) suggest that small and large deflections belong to the same statistical distribution. This stresses the importance of considering all deflections as relevant, and not focusing only on full-reversal switchbacks of more than 90° . Secondly, Fig. 7a shows that the probability distribution remains remarkably constant when approaching the Sun, except for a growing deficit of large deflections within 0.1 AU (see also Bandyopadhyay et al, 2022; Larosa et al, 2024). The distribution does somewhat vary with solar wind conditions, i.e., velocity and other plasma parameters. However because all data are included in Fig. 7 one gets the (false) impression that the distribution is largely invariant with distance. Establishing what causes the distribution of z to vary will be crucial for constraining the generation mechanisms of switchbacks. This and other disambiguation of switchback occurrence by solar wind type currently remain largely understudied (see Sect. 5.2).

The same statistics allow us to investigate the connection between switchback lifetime and deflection. We show in Fig. 7b the joint distribution of these key parameters, which shows they are poorly correlated. Very short switchbacks with a duration of typically less than 2 s predominantly correspond to small deflections of much less than 90° . This may be due to the finite thickness of their boundaries (see Sect. 4.2.3), which may translate into a duration in the spacecraft frame which is greater ≥ 2 s (Larosa et al, 2021; Bzien et al, 2023) thus limiting the magnitude of the deflection for very short switchbacks. Though one sees that with increasing duration the contours of equal counts extend to greater deflections, the two parameters are essentially disconnected beyond a few seconds duration. This suggests that deflection and duration are most likely driven by different physical processes. These simple occurrence statistics, therefore, evidently contain powerful diagnostic information but are currently underutilized and underinterpreted.

4.2.2 Size, Shape, and Orientation

The size, shape, and orientation of switchback structures are important for understanding their origins, evolution, and impact on the solar wind. While many thousands of switchbacks have been measured, determining their characteristics is challenging: the structures are very variable in amplitude and duration; they contain considerable substructure; and as we have seen, different researchers have used differing criteria to define switchbacks so there is no observational standard. Nevertheless, it is possible to estimate the properties of switchbacks, at least in a statistical sense, if one assumes that these are the result of the structures passing over the spacecraft.

The angular distribution of magnetic fluctuations reveals an isotropic distribution of the smallest deflections (Dudok de Wit et al, 2020; Fargue et al, 2022). Large switchbacks in early Parker data (E1, E2), however, tend to deflect in the $+T$ direction of the RTN frame (Horbury et al, 2020; Meng et al, 2022). Fargue et al (2022), by splitting fluctuations into an isotropic core population and a non-isotropic tail, shows that this is statistically verified for several encounters (E1–E9), as the switchback magnetic field rotates preferentially in the clockwise direction in the ecliptic plane (i.e., $+T$ when the magnetic field polarity is negative, and $-T$ when the polarity is positive). Such an asymmetry also shows up in Helios observations (Macneil et al, 2020). This bias is typically what would be expected from an interchange reconnection process acting lower in the corona (Fisk and Kasper, 2020), and has been shown to be consistent with Alfvén waves propagating along the Parker spiral (Squire et al, 2022; Johnston et al, 2022). In each of these cases, the key underlying symmetry-breaking is the sense of solar rotation.

Over the time that a switchback is measured, a spacecraft travels at a constant velocity. Historically, this has been small compared to the solar wind speed, but for Parker near perihelion with spacecraft speeds over 150 km s^{-1} and rather slow wind speeds, this is not the case. We must therefore consider both the spacecraft and plasma velocities when determining how a switchback is sampled. With this in mind and motivated by the observation that switchbacks during E1 had on average a longer duration at the spacecraft when the field within them deflected in the $+T$ direction, Horbury et al (2020) calculated the velocity with which the spacecraft crosses through each structure (the vector sum of the spacecraft velocity with respect to the Sun and the plasma velocity within it). This analysis showed that the distribution of durations was consistent with approximately radially aligned structures, which were tens of thousands of km across, with high aspect ratios – that is, they were long and thin. This analysis is possible because of the Alfvénic nature of switchbacks, where, within a stream of a particular magnetic polarity, there is a consistent sense of correlation or anti-correlation between vector magnetic field and velocity deflections. That is, both the switchbacks and the local solar wind have well-defined, fixed common deHoffman-Teller frames (Horbury et al, 2020; Agapitov et al, 2023). Laker et al (2021) extended this work to multiple encounters, and with more detailed analysis, demonstrated that the apparent durations were consistent with structures with widths around 50 000 km and aspect ratios of order 10, with the major axis deflected away from the radial direction but in the sense of the Parker spiral – with consistent behavior within a stream, but quite different behavior from one stream to another. They therefore concluded that the switchbacks were approximately aligned with the Parker spiral, and, hence, could be propagating along it. Unlike in E1, there was not a preponderance of switchback deflections in the $+T$ direction, with different streams having different average deflection directions.

Independent estimates of the transverse size scale of individual switchbacks were also determined by (Krasnoselskikh et al, 2020), (Larosa et al, 2021) and (Bandyopadhyay et al, 2021), all yielding values in the range of 10^4 km . See Raouafi et al (2023) Table 1 for a numerical comparison. Lacking estimates which use more recent data (the latest data used for this purpose was up to E5 in Bandyopadhyay et al (2021)), it remains an open question as to how these size scales evolve with distance from the Sun and with Alfvén Mach number.

The importance of the deflection direction of switchbacks motivated Laker et al (2022) to consider them in more detail. The deflection direction of the magnetic field within a particular switchback is typically approximately constant: that is, they are arc-polarized structures, deflecting away from the background and returning along the same direction. This makes it possible to define a single deflection direction of each switchback and study its distribution. These directions are not isotropic, but within particular streams, they have a preponderance to particular directions (Laker et al, 2022; Fargue et al, 2022). As was seen in the first encounter, switchbacks that are close together in time often have the same deflection direction. Surprisingly, over the first eight Parker encounters, there seemed to be a preference for deflections in the tangential ($+T$ and $-T$) directions. Laker et al (2022) interpreted the clustering of deflection directions as possible evidence for a reconnection origin of switchbacks. Most recently, Laker et al (2024) interpreted this clustering as an indication that individual switchbacks can be part of a larger quasi-periodic structure with

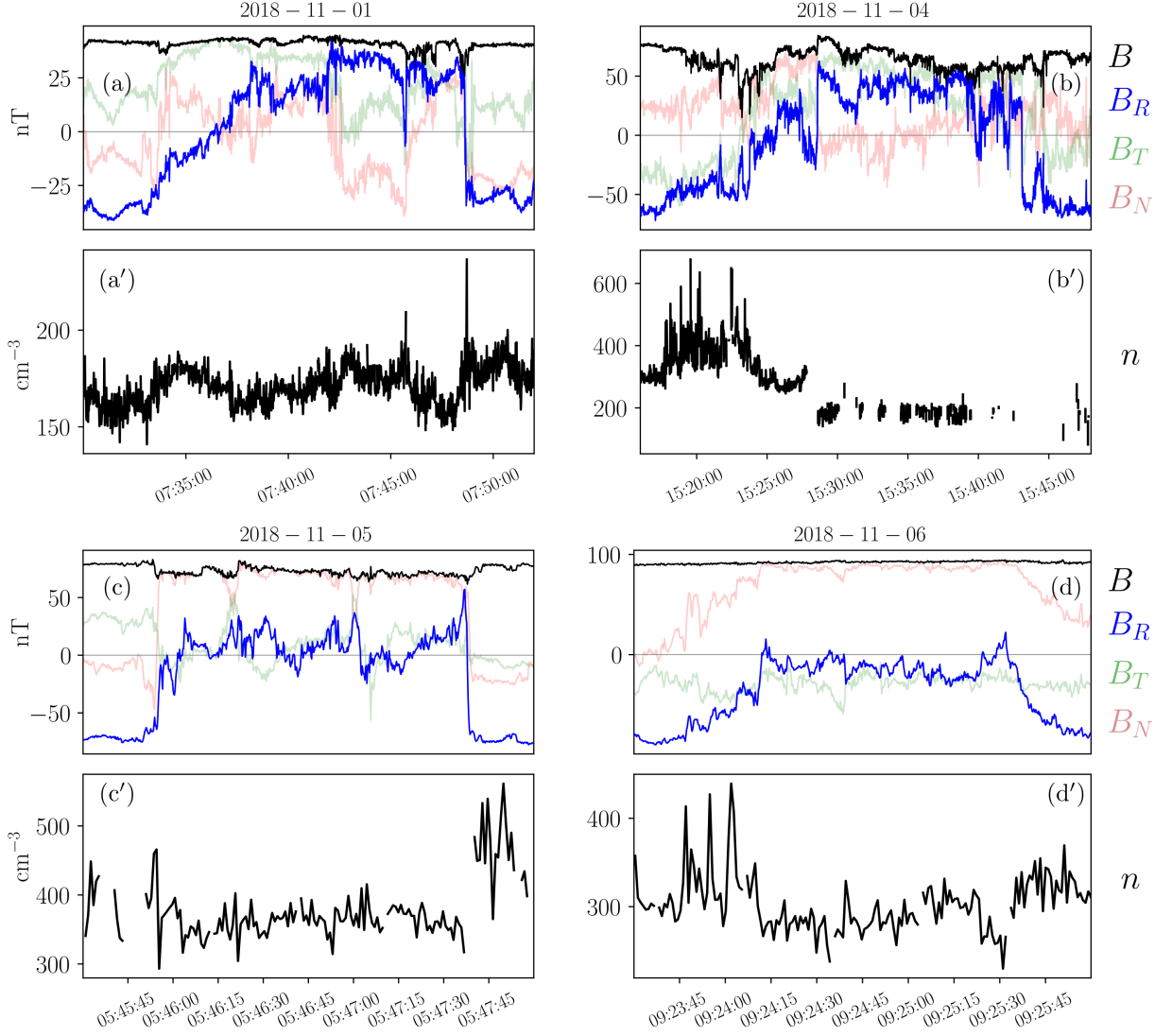


Fig. 8 Example of switchbacks observed with Parker, with a range of sharpness and properties observed at their boundaries, including substructures, density enhancements, and dips in magnetic field strength. For each example, we display the magnetic field components in the RTN frame from the FIELDS instrument (panels *a*, *b*, *c*, *d*) and the proton density from SWEAP/SPC (panels *a'*, *b'*, *c'*, and *d'*).

the same deflection sense and noted that this is consistent with simulations of the outflows from magnetic reconnection events (Wyper et al, 2022). Importantly, during the period of consistent switchback deflections, there was an overall increase in proton field-parallel temperature, as first noted by Woodham et al (2021), and this was above that expected from the well-known temperature-speed relation (Woolley et al, 2020). Again, this was interpreted as evidence of a possible reconnection-related origin of these events.

4.2.3 Non-Alfvénic Boundary Features

The boundaries of switchbacks, marking the separation between the switchback's internal structure and the ambient solar wind, are a key feature potentially holding clues for understanding the mass and energy exchange with the solar wind as well as the switchback formation mechanism and origin. As magnetic switchbacks are “deflections”, their boundaries sometimes exhibit non-Alfvénic properties indicative of current sheets. As detailed in Sect. 2, the boundaries are typically sharp, i.e., have small apparent duration in the magnetic field time series compared to the total duration of the structure crossing. However, more complicated boundaries can be encountered, as illustrated in Fig. 8, where we show a range of examples. The magnetic field rotation can sometimes be gradual, resulting in “blurry” edges in the magnetic field time series (see the leading edge of the structures in panels (a) and (b) of Fig. 8, and both edges of the switchback in panel (d) of Fig. 8). Some switchbacks can exhibit an asymmetry between the leading and trailing

edges, sometimes called a transition region (e.g., [Akhavan-Tafti et al, 2021, 2022](#); [Huang et al, 2023a,b](#)). The thickness of these regions was found to have sizes ranging from 10 km to 10 000 km, with most cases featuring boundaries with widths on the order of the MHD scale ([Larosa et al, 2021](#); [Bizien et al, 2023](#)). These results are, to date, mostly based on the analysis of Parker's E1 observations. This limitation may bias findings such as determining the normal to the switchback boundary, treated as an MHD discontinuity, which strongly depends on the method used, as explained later in the next paragraph (Sect. 4.2.4).

Compressive features are frequently observed at switchback boundaries, where the proton density often increases ([Agapitov et al, 2020](#); [Farrell et al, 2020](#); [Froment et al, 2021](#); [Larosa et al, 2021](#)). Examples of this are illustrated in Fig. 8 at the trailing edges of the top left (panel (a')) and bottom left (panel (c')) switchbacks, as well as the leading edge of the bottom right example (panel (d')). Superposed Epoch Analysis of E1 switchback observations shows that the proton density tends to increase by about 30% at switchback edges ([Farrell et al, 2020](#)), which may be related to the ballistic propagation of switchbacks relative to the background solar wind speed ([Agapitov et al, 2023](#)). This density increase could be explained by a compression region around a fast ejecta ([Liu et al, 2022](#)) or by the possible merging of switchbacks ([Agapitov et al, 2022](#)). However, these results on density variations must be interpreted with caution, as a more recent study using electron density measurements from the QTN method did not observe similar density variations ([Rasca et al, 2021](#)).

Frequent magnetic field magnitude depletions are also observed at switchback boundaries, sometimes named “magnetic dropouts” ([Farrell et al, 2020](#); [Rasca et al, 2022](#)) or “magnetic dips” ([Agapitov et al, 2020](#)). These dips are visible in panels *a*, *b* and *c* of Fig. 8. These dropouts are generally close to 10% ([Farrell et al, 2020](#)), but more dramatic dips can also be observed ([Froment et al, 2021](#); [Larosa et al, 2021](#)). The dips are usually not related to magnetic reconnection, as discussed in Sect. 4.2.5. They may be, however, the key ingredient for the generation of some of the waves observed at switchback boundaries (see Sect. 4.2.6).

Several explanations exist to explain the observation of these magnetic dropouts: They might originate from diamagnetic currents forming at switchback boundaries ([Krasnoselskikh et al, 2020](#); [Farrell et al, 2020, 2021](#); [Rasca et al, 2023](#)), which would be favored when the magnetic field vector rotates to an orientation quasi-perpendicular to the pressure gradient. Another model relates the dips to the development of switchback from the growth of Alfvén waves propagating in the expanding solar wind ([Squire et al, 2020](#); [Mallet et al, 2021](#); [Johnston et al, 2022](#); [Squire et al, 2022](#)). By studying the evolution of large amplitude Alfvén waves with a gradient scale of the order of the ion **inertial** length in a low β environment, [Mallet \(2023\)](#) showed that the boundary dips occur in order to avoid singularities in the solutions of the wave equation when the magnetic field undergoes a sharp rotation. Currently, the compressible nature of switchback boundaries is a property that many models do not address except for the Alfvén wave based ones ([Mallet et al, 2021](#); [Mallet, 2023](#)), and warrants deeper investigation overall. We further discuss the relationship between magnetic dropouts and the occurrence of electromagnetic waves in Sect. 4.2.6.

4.2.4 Discontinuity Classification

One straightforward question when studying switchback boundaries is to wonder what type of discontinuity is involved. Are switchbacks bound by rotational discontinuities (RDs), which are open boundaries propagating in the solar wind, or by tangential discontinuities (TDs), which are closed boundaries advected in the solar wind ([Hudson, 1970](#))? We know that switchbacks are Alfvénic structures and that their magnetic field vector is constrained to rotate on the surface of a sphere. Their boundaries are, moreover, contained in planes and thus are usually referred to as arc-shaped structures ([Tsurutani et al, 2018](#); [Horbury et al, 2020](#); [McManus et al, 2022](#); [Bizien et al, 2023](#)). We detail here the latest results regarding the nature of their boundaries as rotational or tangential discontinuities.

RDs and TDs can be distinguished through measurements of magnetic field fluctuations. Indeed, in ideal MHD, the magnetic field of RDs should present a component normal to the plane of the discontinuity, while TDs should not. The nature of the switchback boundary therefore relies on the estimation of B_n , where n designates the boundary normal. The discontinuity plane and its associated normal direction are usually obtained through minimum variance analysis (MVA, [Sonnerup and Cahill, 1967](#)). The classification of discontinuities can then be achieved by comparing the degree of collinearity of B_n/B with the variation in field magnitude across the discontinuity $\Delta B/B$ ([Neugebauer et al, 1984](#)). TDs classically present $B_n/B < 0.4$ and $\Delta B/B \geq 0.2$, while RDs present the opposite, with $B_n/B \geq 0.4$ and $\Delta B/B < 0.2$. Discontinuities falling outside of these parameter regions are unclassified and named “either” ($B_n/B < 0.4$ and $\Delta B/B < 0.2$) or “neither” discontinuities ([Neugebauer et al, 1984](#)). This classification applied to switchback boundaries, however, led to contrasting results. Switchbacks usually present low magnetic field magnitude variability on the timescale of the switchback itself, landing most of them as rotational discontinuities ([Akhavan-Tafti](#)

et al, 2021) or as “either” discontinuities (Larosa et al, 2021), consistent with Ulysses observations at larger distances (Yamauchi et al, 2002).

The MVA method, however, presents some serious limitations that lead to high uncertainties when computing the normal direction (Hausman et al, 2004; Knetter, 2005; Wang et al, 2023). The geometry of switchback boundaries, with their arc shape and the superimposed waves, prevents the use of MVA only for their classification. In a recent study, Buzien et al (2023) suggest that the use of the singular value decomposition (SVD, Golub and van Loan, 2013), instead of MVA, sheds new light on the nature of switchback boundaries. While both methods rely on a diagonalization of the magnetic field covariance matrix, MVA additionally subtracts the mean value of each magnetic field component. MVA, therefore, finds a plane centered on the orbit of the magnetic field and usually tangent to the sphere, while the SVD plane will always include the origin. In Fig. 9, we illustrate how switchback boundaries evolve on a sphere and the difference between TDs and RDs. Panel 9a shows the two types of boundaries in the ideal case, without any superimposed fluctuations. The blue plane includes the origin and corresponds to a TD, while the red plane represents an RD. Panels 9b and 9c show two examples of switchback boundaries measured during the first encounter of Parker, both presenting arc-shaped structures (see Buzien et al, 2023). Panel 9b shows the boundary of a switchback measured on November 7, 2018, at 20:53:15 UT, whose plane includes the origin and that is classified as a TD. Panel 9c shows a second example measured on November 2, 2018, at 18:33:33 UT, with a plane which clearly does not include the origin. This discontinuity thus presents a large normal component and corresponds to an RD. The use of SVD over MVA leads Buzien et al (2023) to conclude that the number of RDs has been previously overestimated compared to TDs, and that many switchback boundaries are TD-like discontinuities. These results have important implications for the evolution of the switchbacks in the solar wind (see Mallet et al, 2026, this collection). TD-like discontinuities are closed boundaries, which seems to indicate that switchbacks are stable structures that could survive as they propagate at larger heliocentric distances. The results of Buzien et al (2023) thus indicate that the nature of switchback boundaries is compatible with a solar origin in these structures. However, this is not enough evidence to rule out an *in situ* formation. Another important remark is that though not completely Alfvénic, switchback boundaries do preserve an outwardly propagating fluctuation correlation between velocity and magnetic field, a condition which is part of the definition of an RD, but a completely additional constraint for a TD. In other words, classifying the boundary as a TD does not use the full properties of the switchback boundary, and calls into question this interpretation. Electron temperature behavior across the discontinuities are another potential discriminator with TDs able to support a temperature jump and RDs not. Rivera et al (2024b) showed electron core temperature behavior across several switchback patches and did not observe variation correlated with the switchback deflections. Further statistical behavior of electron properties across switchbacks would be useful to further constrain the nature of their boundaries.

Having these contradictory results in mind (Larosa et al, 2021; Akhavan-Tafti et al, 2021; Buzien et al, 2023), additional properties of switchback boundaries were retrieved. The nature of switchback boundaries appears to be linked to properties of the solar wind, with apparent proton temperature sharply increasing by 29% across RD-type leading boundaries, enhancing the thermal pressure gradient while the plasma density drops slightly (Akhavan-Tafti et al, 2022), although as noted in Sect. 4.1.2 temperature signatures during large flow deflections measured by Parker remain somewhat controversial. Nevertheless, this evidence suggests switchback transition regions may not be in thermal equilibrium with their neighboring plasma, likely driven by plasma instabilities rather than magnetic reconnection. Significant heating mechanisms are possible, and the topic requires further investigation (Akhavan-Tafti et al, 2022). These conclusions are based, however, on the rotational nature of the boundary retrieved through the MVA method, and results may change if the SVD method was used. In parallel, the deflection does not seem to influence the nature of the discontinuity (Buzien et al, 2023), suggesting that switchbacks are self-similar, which is consistent with earlier studies (Dudok de Wit et al, 2020).

4.2.5 Switchbacks and Magnetic Reconnection

Magnetic reconnection is a fundamental plasma process that occurs at thin current sheets, where plasma is heated and accelerated by the release of energy stored in the magnetic field due to changes in the field topology (e.g., Gosling and Szabo, 2008; Gosling, 2012). Yet, the very nature of magnetic switchbacks as sudden deflection of the magnetic field goes hand in hand with an increased presence of current sheets in the solar wind. Switchback boundaries, therefore, seem like a potential favored place for magnetic reconnection to occur, and it is natural to wonder whether this process of magnetic reconnection, in addition to potentially playing a role in the formation of switchbacks, could also be responsible for their erosion and, ultimately,

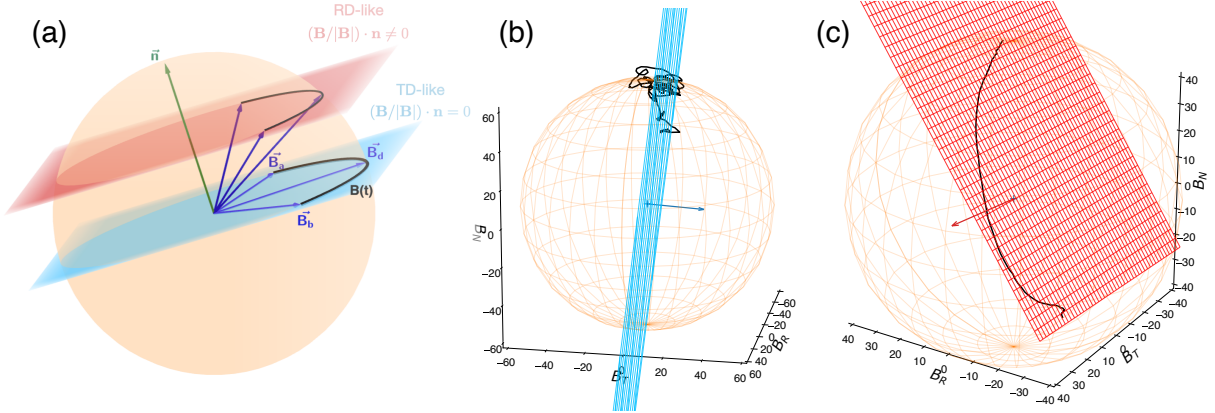


Fig. 9 Evolution of the magnetic field vector on a sphere for TDs and RDs. Panel (a) shows a schematic view of an arc-polarized switchback boundary. A discontinuity plane is represented in blue with its normal \mathbf{n} in green. For a TD, the tip of the field vector rotates in that plane, which includes the origin in that particular case. More generally, any arc-polarized boundary would be identified by the red plane, with the same normal but excluding the origin. The blue plane corresponds to a tangential-like boundary (small B_n/B) while the red plane corresponds to a rotational-like boundary (large B_n/B). Panels b and c show two switchback boundaries, the first (panel (b)) was observed on November 7, 2018, at 20:53:15 UT and corresponds to a TD, while the second (panel (c)) was observed on November 2, 2018, at 18:33:33 UT and corresponds to an RD. Figures reproduced with permission from [Bizien et al \(2023\)](#), copyright by AAS

Table 5 Table summarizing the properties of the rare instances of reconnection at switchback boundaries observed by Parker and Solar Orbiter. For further details, see [\(Froment et al, 2021\)](#) and [\(Suen et al, 2023\)](#).

Spacecraft	Heliocentric distance (AU)	Boundary	\mathbf{B} shear (°)	$ \mathbf{B} $ dip (%)	V increase (% V_A)
Parker	0.22	Leading	58	6	9
		Trailing	81	27	
Parker	0.22	Leading	67	16	10
		Trailing	60	12	
Parker	0.22	Leading	61	22	39
		Trailing	168	90	
SolO	0.72	Trailing	117	23	35
		Trailing	134	8	31
		Trailing	95	6	17

their dissipation. Here, we review results relating to magnetic reconnection and switchbacks in the solar wind.

Only a handful of switchback boundary reconnection events have been reported, suggesting that they are rare compared to reconnection at the heliospheric current sheet and ICMEs ([Phan et al, 2020](#)). Some properties of the reported reconnection at switchback boundaries ([Froment et al, 2021](#); [Suen et al, 2023](#)) are listed in Table 5. The few observations suggest that reconnection neither favors the leading nor trailing edge boundary of the switchback and can sometimes occur simultaneously at both boundaries, as illustrated in Fig. 10. Most of the reconnection events observed by Parker occur across boundaries with moderate magnetic shear angle, whereas events observed by the Solar Orbiter spacecraft tend to have larger shear angles ($> 100^\circ$, [Phan et al, 2010](#)). Interestingly, switchbacks with reconnection occurring at their boundaries exhibit modest velocity enhancements in their interior, especially when compared to those without boundary reconnection ([Froment et al, 2021](#); [Larosa et al, 2021](#)). Whether this is a consequence or a prerequisite of magnetic reconnection remains to be determined.

Figure 10 shows an example of switchback undergoing boundary reconnection observed by Parker on November 2, 2018, at ~ 0.2 AU (first event of Table 5). Reconnection outflows in the solar wind are characterized by a bifurcation of the reconnecting current sheet (i.e., a plateau in the field rotation), wherein the outflow region is bound by a pair of standing Alfvénic rotational discontinuities in the magnetic field ([Gosling et al, 2005](#)). In Fig. 10, both the leading and trailing edge boundaries of the switchback exhibit an increase in $\delta\mathbf{V}$ confined within a bifurcated current sheet layer. Fluctuations in \mathbf{B} and $\delta\mathbf{V}$ are correlated on one side of each outflow and anti-correlated on the other. These are characteristic signatures of magnetic reconnection observed *in situ*, as described by [Gosling et al \(2005\)](#).

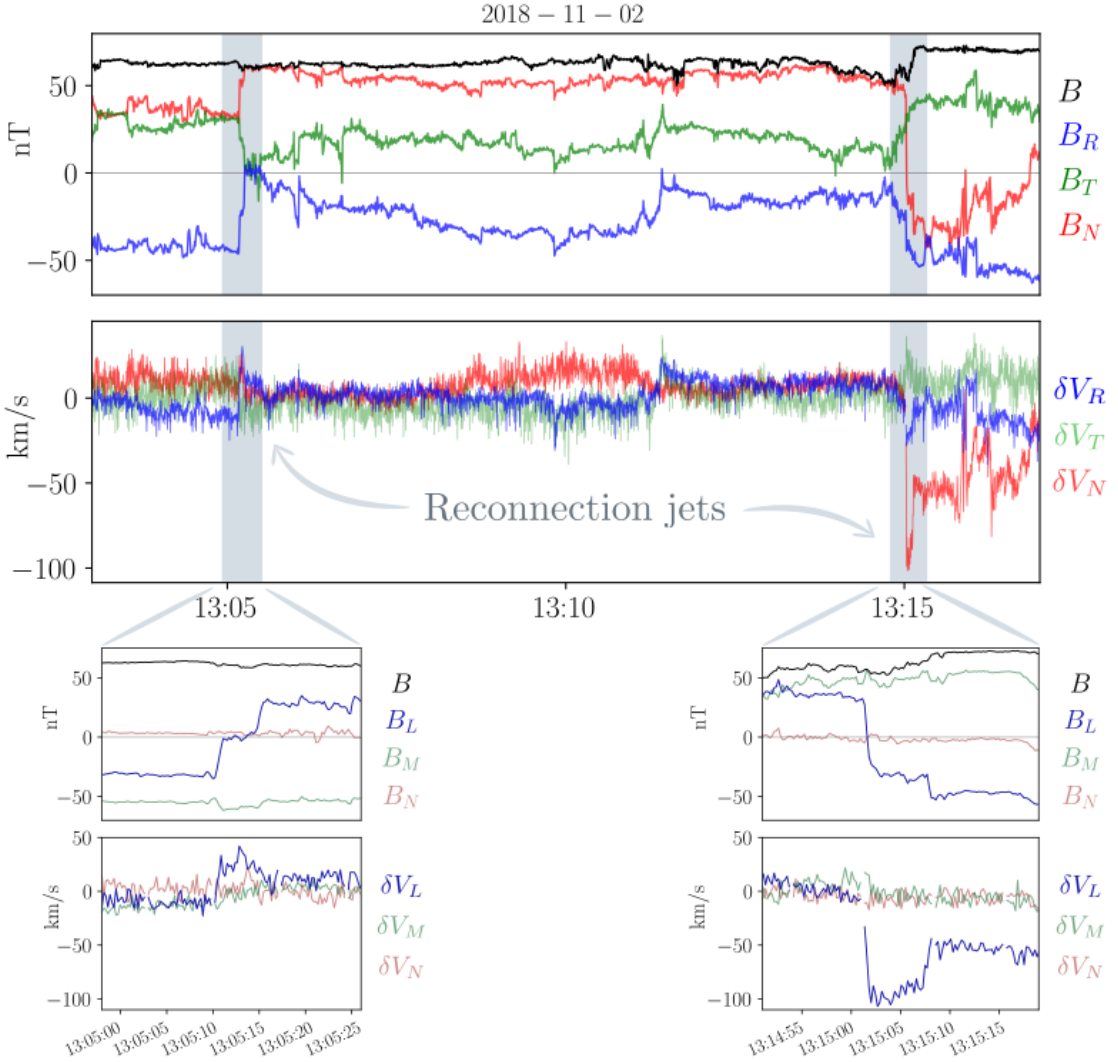


Fig. 10 Magnetic reconnection observed at switchback boundaries by Parker, first reported by Froment et al (2021). The top panels shows the magnetic field for the full switchback encounter as well as the ion velocity variation measured by SPC $\delta\mathbf{V} = \mathbf{V} - \bar{\mathbf{V}}$, where the average background solar wind speed $\bar{\mathbf{V}}$ is $[322, 6, 26]_{RTN}$ km s $^{-1}$ over this time interval. The shaded regions show the locations of the switchback boundaries. The insets zoom-in on the switchback boundaries and display \mathbf{B} and $\delta\mathbf{V}$ in the LMN current sheet aligned frame, where l points in the outflow direction, m in the X-line direction, and n is the current sheet normal direction.

Froment et al (2021) postulates that magnetic reconnection at switchback boundaries may destabilize the switchback structure, thus causing the velocity enhancements to decay. Using examples of reconnecting switchbacks observed at 0.6–0.7 AU by Solar Orbiter, Suen et al (2023) finds that boundary reconnection could erode a switchback in minutes or hours, making it an efficient erosion process. This short timescale could explain why switchback boundary reconnection is so rarely observed. A more detailed discussion of the erosion of switchback by magnetic reconnection can be found in Mallet et al (2026, this collection)

The lack of observations of magnetic reconnection at switchback boundaries may also suggest that reconnection is suppressed. This is confirmed by recent statistical studies of magnetic reconnection occurrence in the solar wind, which suggest that reconnection jets are not observed in the highly Alfvénic wind dominated by switchbacks (Fargette et al, 2023; Eriksson et al, 2024). Again one must remember that switchbacks are Alfvénic structures, and therefore across the boundary the current sheet coexists with a vorticity sheet and a strong velocity-magnetic field correlation. Shear flows across current sheets of magnitude comparable to the Alfvén speed suppress reconnection (Einaudi and Rubini, 1986; Owen and Cowley, 1987; Chen et al, 1997; Cassak and Otto, 2011; Shi et al, 2021). The reason is that, in incompressible MHD, the purely unidirectional Alfvén wave is an attracting nonlinear state, and should therefore be completely stable. However, including compressibility and only partial Alfvénicity, the tearing instability is quenched but not completely suppressed (Shi et al, 2021). This would explain the moderate velocity enhancements inside switchbacks

undergoing reconnection at their boundaries (see Table 5). Flow shears may also induce diamagnetic drifts that suppress reconnection if the shear angle across the current sheet θ is sufficiently large through the $\Delta\beta - \theta$ condition, where $\Delta\beta$ is the difference in plasma β across the sheet (Swisdak et al, 2003; Phan et al, 2010). Akhavan-Tafti et al (2021) show that the three Parker events of Table 5 fall within the regime set by the $\Delta\beta - \theta$ condition where reconnection is favored. The authors further argue that the negligible magnetic tension and the presence of strong $|\mathbf{B}|$ prevent instability formation and growth, therefore suppressing the triggers of magnetic reconnection. However, a recent study by Vasko et al (2021) shows that all current sheets, both reconnecting and non-reconnecting, fall within the $\Delta\beta - \theta$ regime where reconnection is favored. This suggests that the diamagnetic drift mechanism does not play a significant role in suppressing switchback boundary reconnection.

4.2.6 Waves at Switchback Boundaries

Coherent electromagnetic fluctuations from about the Hz to the MHz ranges have been reported inside and at the boundaries of switchbacks (e.g., Krasnoselskikh et al, 2020; Larosa et al, 2021; Malaspina et al, 2022). Most of the wave activity detailed in this section is linked to wave-particle interactions involving, in particular, electron beams (whistler and Langmuir waves) or particle transfer between the ambient solar wind and the switchbacks (surface waves).

Larosa et al (2021) used FIELDS Search Coil Magnetometer (SCM; Bale et al, 2016; Bowen et al, 2020a) data to show that, during Parker's first encounter, the amplitude of the broadband magnetic fluctuations above 3 Hz increased by 65% on average inside the structures. This increase of electromagnetic activity is illustrated in Fig. 11, which shows the enhancement of the magnetic power spectral density across a switchback interval. The wave activity then seems to decay with the heliocentric distance (Mozer et al, 2020b; Farrell et al, 2021; Mozer et al, 2020a), a topic covered in more depth in (Mallet et al, 2026, this collection).

Different types of waves have been found at switchback boundaries and inside switchbacks, such as ultra-low frequency (ULF) waves (Farrell et al, 2021), surface waves (Krasnoselskikh et al, 2020), as well as whistler waves discussed in the next paragraph. ULF waves were observed while considering the range 0.7 Hz to 1 Hz (Farrell et al, 2021). A large portion of the detected ULF waves presents a low amplitude compared to the magnitude of the background magnetic field (less than 3%). These waves might play a role in switchback degradation (Farrell et al, 2021). In parallel, waves with frequency close to the ion cyclotron frequency f_{ci} (i.e., a few Hz) were reported at switchback boundaries (Krasnoselskikh et al, 2020). The angle of about 60° between the wave normal angle and the normal to the boundary seems to indicate these are surface waves, which could increase the particle transfer across switchback boundaries. Both ULF waves and surface waves have been largely underexplored to date. More work is needed to understand their occurrence, generation, and importance for the evolution of switchbacks in the solar wind.

Parker observations revealed the occurrence of localized bursts of low-frequency whistler wave packets, collocated with magnetic field dips associated with switchback boundaries (Sect. 4.2.3) with a typical frequency range of 100 Hz to 300 Hz (0.05–0.2 f_{ce}) in the spacecraft frame (Agapitov et al, 2020; Karbashewski et al, 2023; Froment et al, 2023; Colomban et al, 2023; Colomban et al, 2024). However, whistler waves seem to only be observed in 15% of switchbacks, where they tend to have a shorter duration with respect to non-switchback intervals (Jagaramudi et al, 2021).

Whistler waves observed in the solar wind (not only at switchback boundaries) present wave amplitudes that peak at 2 nT, representing up to 5% of the background magnetic field magnitude. The polarization of these waves was found to be predominantly quasi-parallel to the background magnetic field (Froment et al, 2023; Karbashewski et al, 2023). Quasi-parallel propagation appears to be the predominant mode of whistler waves in the solar wind. Indeed, over the heliocentric distances covered by Parker and Solar Orbiter, the occurrence of quasi-perpendicular whistler waves (normal wave angle greater than 50°) was less than 1% (Kretzschmar et al, 2021). The direction of propagation is therefore the key factor in the efficiency of the wave-particle interaction: scattering of strahl electrons by counter-propagating (sunward) whistler waves is an order of magnitude more efficient than scattering by anti-sunward quasi-parallel waves (Colomban et al, 2024). Also, all whistler waves observed by Solar Orbiter at 0.5 – 1.0 AU were found to propagate from the Sun (Kretzschmar et al, 2021). Thus, sunward propagating whistler populations in the young solar wind (observed by Parker at 25–75 R_\odot) are potentially a key factor for the diffusion of the strahl electron population, which raises the question of the mechanism behind their local generation (to explain the range of generation of these waves reported by Cattell et al, 2022).

The generation mechanism for these sunward and anti-sunward propagating quasi-parallel whistler waves is presumably the cyclotron instability (suggested by the simultaneous generation of counter-propagating

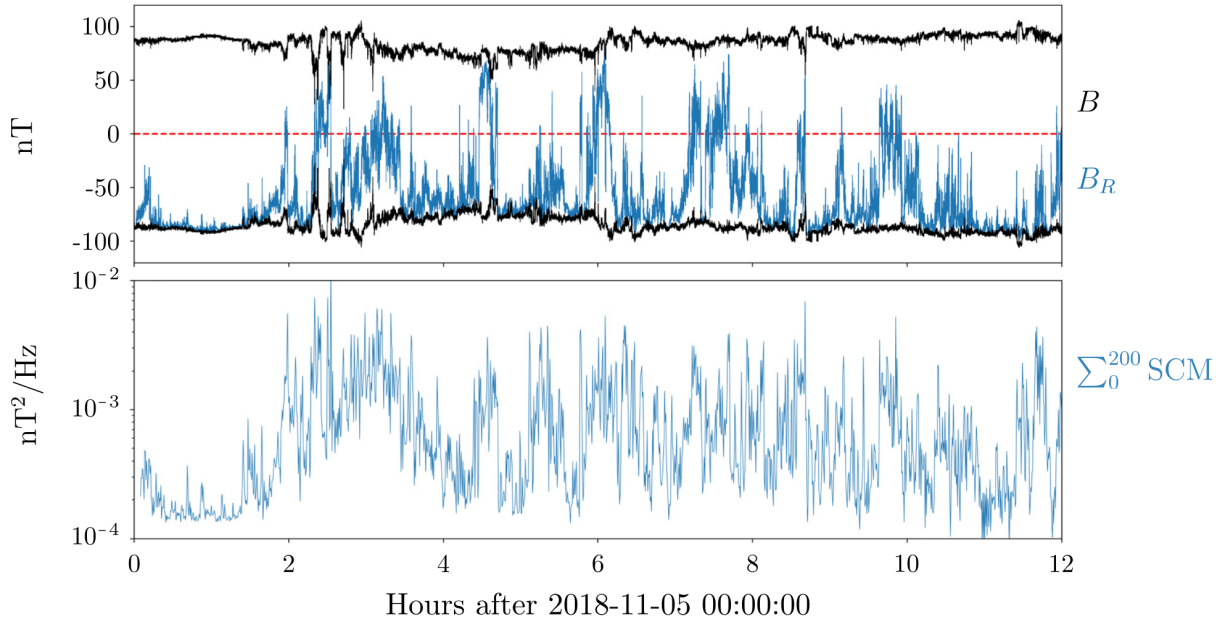


Fig. 11 Top panel: Radial component of the magnetic field with FIELDS/MAG Parker observations, showing a switchback interval. Bottom panel: Time series of the magnetic power spectral density, summed from 20 to 200 Hz from FIELDS/SCM data. Figure reproduced with permission from [Malaspina et al \(2022\)](#), copyright by AAS

wave bursts). The latter could be driven by a population of suprathermal electrons (~ 100 eV) trapped in magnetic field dips and/or by the strahl population, whose geometry is disturbed by local inhomogeneities in the magnetic field (such as abrupt rotations) at switchback boundaries. The derived difference in frequency of sunward and anti-sunward counter-propagating waves confirmed their simultaneous generation in the source region moving in the solar wind frame ([Karbasewski et al, 2023](#)).

A statistical study of whistler wave occurrence rates and their parameters in the young solar wind showed that the high-amplitude waves observed between $25\text{--}45 R_\odot$ were mostly tied to the magnetic dips or sharp rotations often associated with switchbacks and were propagating toward the Sun (antisunward waves were observed mostly above $40 R_\odot$ and without any relationship to magnetic field inhomogeneities) ([Choi et al, 2024](#)). This co-existence of sunward whistlers and magnetic field gradients (Fig. 12c, d) provides favorable conditions for the fast local scattering of the strahl electrons by the waves and can lead to broadening of the superthermal pitch-angle electron distribution seen in Fig. 12f ([Vo et al, 2024](#)).

[Rasca et al \(2023\)](#) found that magnetic dips, or dropouts, are both less frequent and of lower amplitude in the sub-Alfvénic solar wind. These dropouts may originate from diamagnetic effects stemming from a large magnetic field rotation at switchback boundaries (see Sect. 4.2.3). They hypothesize that the rarer observations of magnetic dips at switchback boundaries below the Alfvén critical surface may be linked to smaller magnetic field deflections (see also Sect. 5.3). This may be an avenue to explore to explain the apparent lack of whistler waves close to the Sun ([Cattell et al, 2022](#)).

Finally, we note that it remains unclear whether whistler wave activity at switchback boundaries is related to the emission near the electron plasma frequency f_{pe} reported by [Rasca et al \(2022\)](#). [Rasca et al \(2022\)](#) find an enhanced emission in LFR radio spectrograms near f_{pe} at switchback boundaries with a significant magnetic field dropout. They argue that these dropouts are creating electron currents that stimulate Langmuir waves, showing as f_{pe} emissions. Indeed, [Jagarlamudi et al \(2021\)](#) reported that whistlers were detected together with Langmuir waves about 85% of the time in Parker data, which is consistent with previous solar wind observation ([Kennel et al, 1980](#)). The relationship between these different types of waves at switchback boundaries remains to be investigated and will certainly shed light on the properties of switchbacks, their generation mechanisms, and evolution in the solar wind.

4.2.7 Geometry and Boundary Takeaways

The phenomenon that we call magnetic switchback is characterized by a self-similar distribution of deflection angle, where small and large deflections share the same properties (Sect. 4.2.1). It is thus important to consider all deflections as relevant, and not focus only on “polarity reversal” switchbacks of more than 90° . Switchbacks also seem to have a tendency to deflect in a preferential direction, and their orientation presents

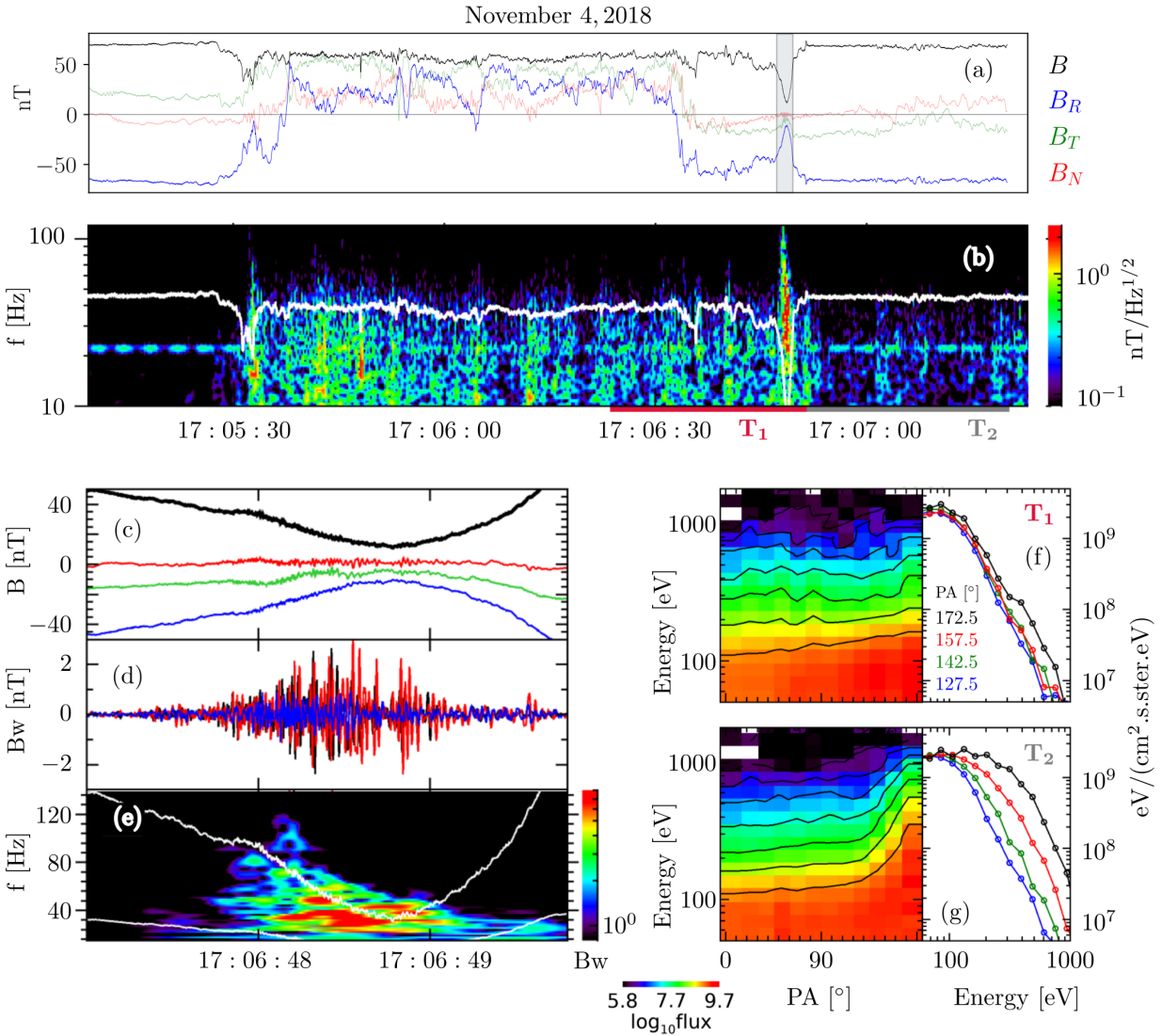


Fig. 12 Magnetic field dynamics associated with a switchback observed on November 4, 2018, from 17:05 to 17:07 UT. The magnetic field (a) exhibits an almost complete reversal of the radial component. Panel (b) represents the dynamic spectrum of magnetic field waveforms estimated from the combined MAG and SCM data (Bale et al. 2016; Bowen et al. 2020a), in which the solid white curve indicates the local lower hybrid frequency. Panels (c-e) present a zoomed interval covering the magnetic dip observed at the trailing edge of the switchback (shaded area in panel a) around 17:06:49 UT with (c) – the magnetic field components and magnitude from MAG; (d) the magnetic field high-frequency (>10 Hz) waveforms; (e) – the spectral power of the magnetic field perturbations. Panels (f) and (g) present the pitch-angle distribution electron functions in the vicinity of the magnetic dip (T1 in panel (b)) and the unperturbed solar wind (T2 in panel (b)). Figures reproduced with permission from Vo et al (2024), copyright by AAS

a clustering behavior (Sect. 4.2.2). Finding a physical mechanism able to reproduce the full distribution of deflection angles through simulations will be key to understanding the origins of switchbacks. This distribution may also vary depending on solar wind conditions or as the solar wind evolves, and clearly, establishing what causes the distribution of z to vary will be crucial for constraining the generation mechanisms of switchbacks.

Much remains to be studied about switchback boundaries, and understanding their properties and evolution will shed light on their interaction with the ambient solar wind. The compressible nature of switchback boundaries is, for now, only addressed by wave-based models and requires further investigation (Sect. 4.2.3). Arriving at a consensus on whether switchbacks are bound by rotational or tangential discontinuities, in combination with establishing if switchbacks contain distinct plasma populations, would provide evidence for determining a solar or *in situ* origin (Sect. 4.2.4). The lack of magnetic reconnection at switchback boundaries deserves more attention and could be explained by either it being an efficient erosion mechanism for switchbacks, or it being suppressed by *in situ* local conditions (Sect. 4.2.5). Finally, enhanced wave activity has often been observed at switchback boundaries, often associated with whistler waves. ULF and surface

waves have been underexplored to date. More work is needed to understand their occurrence, generation, and importance for the evolution of switchbacks in the solar wind (Sect. 4.2.6)

Overall, most studies on switchback geometry and boundaries focus on the early encounters of Parker with the Sun. Seeing how their properties (deflection direction, occurrence, compressibility, wave activity, magnetic reconnection occurrence, etc.) evolve in the latest encounters, i.e., closer to the Sun, could be an important step in understanding switchbacks' origins.

4.3 Switchbacks, Turbulence, and Ion-scale waves

In the regions explored by Parker and other spacecraft, switchbacks are typically embedded in the young solar wind's highly Alfvénic turbulent fluctuations (Bruno and Carbone, 2013; Chen et al, 2020; Sioulas et al, 2023; Wu et al, 2023; Brodiano et al, 2023; Sorriso-Valvo et al, 2023). Irrespective of their origin, the large magnetic and velocity gradients associated with switchbacks, as well as their modulation in patches, provide a source of energy that is expected to feed the turbulent cascade. They might, in fact, have a relevant role in setting or modulating the properties of turbulence in the expanding solar wind.

One major basic question arises: to what degree can switchbacks be considered as entities that are distinct from the turbulent field in which they are embedded, since when propagating away from the Sun, they eventually merge with it and become indistinguishable? Determining how turbulence and switchbacks interact and develop as the solar wind expands may provide answers to such questions.

4.3.1 Background on Alfvénic Turbulence

Various mechanisms, possibly involving photospheric motions or magnetic reconnection, lead to a predominance in the solar wind of anti-sunward propagating Alfvénic perturbations, a condition known as "imbalance". Such imbalance is usually quantified through the normalized cross-helicity spectrum $\sigma_c = (E^+ - E^-)/(E^+ + E^-)$, where E^\pm are the power spectral densities of the inward and outward Alfvénic modes which are defined in terms of the Elsasser fields (Elsasser, 1950, $\mathbf{z}^\pm = \mathbf{v} \pm \mathbf{b}$) as $E^\pm(\tau) = \frac{1}{2}\langle(\mathbf{z}^\pm)^2\rangle_\tau$ where $\langle\rangle_\tau$ indicates an ensemble average over a time window τ , \mathbf{v} is the bulk velocity fluctuation vector (also referred to as $\delta\mathbf{v}$ earlier) and $\mathbf{b} = \delta\mathbf{B}/\sqrt{\mu_0\rho}$ is the magnetic field fluctuation vector in velocity (Alfvén) units. Note that in addition to τ , the background vectors with which fluctuations are computed with respect to can vary between studies. Another closely related quantity is the residual energy spectrum $\sigma_r = (E^k - E^b)/(E^k + E^b)$, representing the level of balance between magnetic (E^b) and kinetic (E^k) energy in the fluctuations, such that $\sigma_r = 0$ if they are pure outwards traveling Alfvénic fluctuations and $\sigma_r < 0$ if there is an excess of magnetic with respect to kinetic energy. Here, $E^k = \frac{1}{2}\langle\mathbf{v}^2\rangle_\tau$ and $E^b = \frac{1}{2}\langle\mathbf{b}^2\rangle_\tau$. A related quantity is the Alfvén ratio, $r_A = E^k/E^b$, which can be used to describe the 'Alfvénicity' of the fluctuations, where the limit of $r_A = 1$ corresponds to perfect Alfvénic correlation between magnetic and kinetic fluctuations. Linear couplings of the outgoing modes to the large-scale inhomogeneity result in non-WKB (Wentzel-Kramers-Brillouin) reflections (Velli et al, 1989), providing the sunward propagating component that is necessary for the MHD non-linear interactions to be activated and for turbulent characteristics to emerge (Iroshnikov, 1963; Kraichnan, 1965).

When the turbulence is fully developed, nonlinear interactions among counter-propagating modes result in an energy cascade from large to small scales (Montgomery and Turner, 1981; Shebalin et al, 1983), highlighted by a broad range of power-law scaling forms for different statistical quantities as a function of fluctuation frequency, such as the power spectral density (PSD) and the high-order moments of the fields' fluctuations. The PSD (e.g., of magnetic fluctuations) is one of the most commonly studied turbulent quantities of space plasmas and exhibits key features such as a broken power law slope and a break frequency separating the two behaviors. The PSD amplitudes and power law exponents determines an apparent energy cascade rate (a rate of transfer of energy from one scale to another), and the location of the break frequency indicates a change in physics e.g. a transition from dissipation free (inertial-range) to dissipative scales where fluctuation energy can be efficiency transferred to random particle thermal motion (heating). The amplitude of the PSD also encodes the overall turbulent fluctuation strength at all scales. Various degrees of intermittency (most simply put, the departure of fluctuation statistics from a Gaussian distribution) also emerge (see, e.g., Frisch, 1995), associated with the inhomogeneous generation of highly energetic small-scale structures, and typically estimated using the anomalous scaling of the magnetic field and velocity fluctuations' statistics (Sorriso-Valvo et al, 1999). The cascade culminates at ion scales with the collisionless dissipation of fluctuating energy and ensuing heating of the plasma (see e.g., Verscharen et al, 2019).

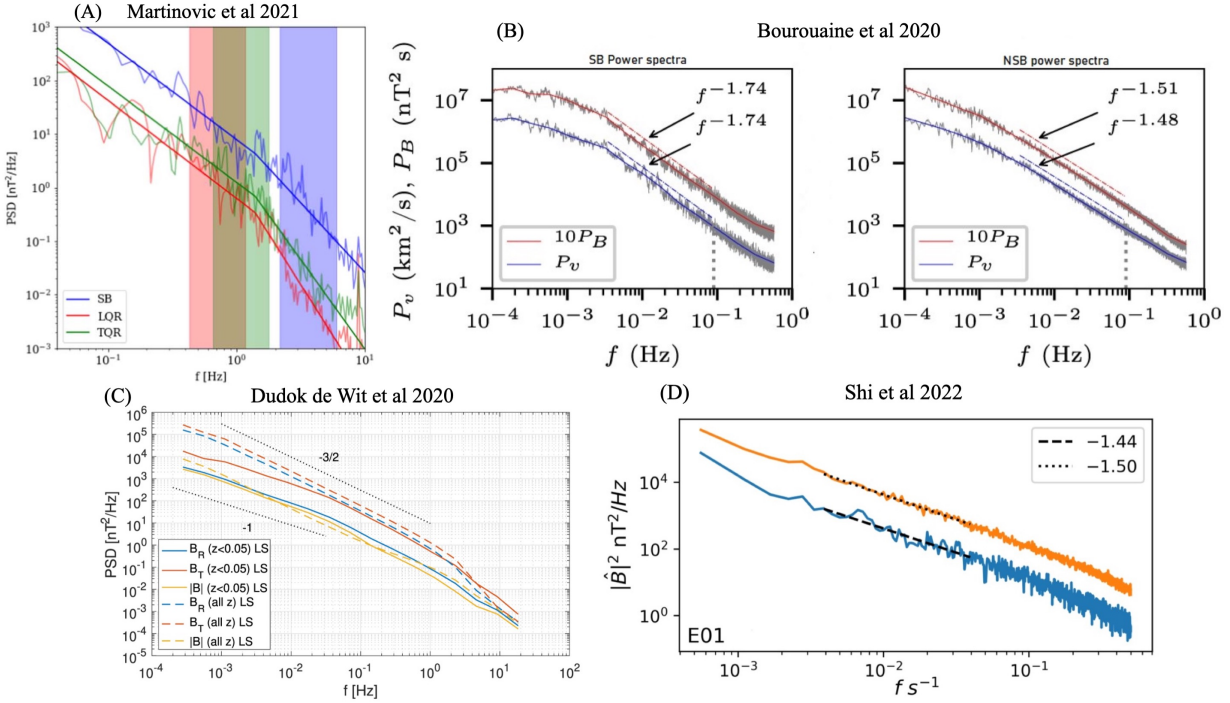


Fig. 13 Power spectral density (PSD) of magnetic field fluctuations during switchback and non-switchback intervals. In (A), Martinović et al (2021) compare the PSD of a switchback interval (blue) with the PSD of the surrounding leading quiet region (LQR, in red) and trailing quiet region (TQR, in green). In (B), Bourouaine et al (2020) show the PSD of both magnetic field (red) and velocity (blue) fluctuations, for switchback intervals (left panel) and non switchback intervals (right panel). In (C), Dudok de Wit et al (2020) compare the spectral properties of the quiescent periods where switchbacks have been removed (full lines, computed through the Lomb–Scargle (LS) method), and the spectral properties of the full time series, including switchbacks (dotted lines). In (D), Shi et al (2022a) show the PSD a quiescent interval (blue) and a switchback interval (orange) observed during E01. Linear fits of the PSD and their associated slopes are indicated in each figure. See Sect. 4.3.3 for discussion. Figures reproduced with permission from Martinović et al (2021); Bourouaine et al (2020); Dudok de Wit et al (2020); Shi et al (2022b), copyright by AAS

4.3.2 Approach to Turbulence Studies

In order to probe the relationship between switchbacks and turbulence, current research focuses on comparatively characterizing and modeling the major properties of the turbulent fluctuations (including those described in the previous section) in solar wind switchbacks and non-switchback intervals (see Sect. 3 for a discussion on different definitions of switchbacks). This can be done using different methodologies, so that the broadly used expressions “switchbacks interval” and “non-switchbacks interval” may correspond to at least four different selection criteria, as briefly summarized in the following. (i) Martinović et al (2021) examined the properties of turbulence in stationary intervals completely contained within each switchback structure, and in regions completely outside of them, then performing ensemble statistics over the different categories. This procedure ensures the study of homogeneous plasma, avoiding the sharp switchback boundaries. However, it severely reduces the low-frequency reach of the spectral analysis, preventing the study of large-scale properties. (ii) In a similar approach, Bourouaine et al (2020) performed a threshold-based conditioned correlation function analysis to study the turbulence inside and outside switchbacks in longer time series, retaining the homogeneity of the sample but also gaining access to lower frequencies. The two methodologies described above are appropriate for studying in a well-separated way the properties of turbulence in parcels of plasma entirely embedded in a switchback and in the regions with no switchbacks. (iii) On the other hand, Dudok de Wit et al (2020) separated quiescent regions (i.e., with very small magnetic field rotations), and then employed a technique for spectral analysis of unevenly sampled data (the Lomb–Scargle method) to compare the spectral properties of the quiescent ensemble with those of the whole time series, which included switchbacks. In this case, the switchback sharp boundaries were retained in the “switchback intervals”. (iv) Alternatively, Shi et al (2022b) and Hernández et al (2021) used hand-picked intervals or fixed-size running windows to obtain turbulence parameters in samples where regions inside, outside, and at the boundaries of a variable number of switchbacks could be mixed together. The latter two approaches are more appropriate for the study of global or regional interplay between turbulence and switchbacks (Mallet et al, 2026, this collection). The different methodologies described above may have profound differences, as for example (and primarily) the inclusion or exclusion of the sharp switchback boundaries, which can affect the statistical properties of the turbulent fields. It is therefore of utmost importance to give a clear and

explicit description of the chosen methodology in order to avoid misinterpretations of the observations and inappropriate comparisons between different studies.

4.3.3 Turbulent Spectra

Several studies based on the above methodologies were performed to compare the turbulence properties inside and outside, or with and without switchbacks. Such studies revealed substantial differences and similarities in spectral properties, intermittency, Alfvénicity, and turbulent cascade rate. Fig. 13 shows four examples of power spectral densities obtained from various Parker encounters in the works described above. The top-left panel (A) shows that, using several short intervals, [Martinović et al \(2021\)](#) found no major differences between the plasma inside the switchbacks and outside of them, except for a moderate excess of magnetic power. Similar larger magnetic power was found by [Bourouaine et al \(2020\)](#) (top-right panels, (B)), but in this case, the spectral index inside the switchbacks was ~ 1.7 (close to the Kolmogorov value $5/3$), while in the quieter intervals it was ~ 1.5 . [Dudok de Wit et al \(2020\)](#) (bottom-left panel, (C)) showed that a broader and steeper inertial range is present in the whole time series with respect to the extracted quiescent intervals between switchbacks. The magnetic power was also reduced in the quiescent regions, as expected when removing the larger fluctuations. Finally, [Shi et al \(2022b\)](#) (bottom-right panel, (D)) obtained slightly steeper spectral exponents and one order of magnitude enhanced power in the intervals containing switchbacks. While the above differences highlight the strong sensitivity of the selection methodology, the general picture that emerges is that solar wind intervals that include switchbacks have generally more developed turbulence, with enhanced power and steeper spectra. The magnetic spectral power also appears more isotropically distributed between the parallel and perpendicular direction to the magnetic field than in the ambient solar wind ([Sakshee et al, 2022](#)). However, it is important to note that due to the short duration of switchback intervals, large uncertainties may arise ([Dudok de Wit et al, 2013](#)). Consequently, a larger statistical dataset is required to further corroborate this observation. Additionally, [Tatum et al \(2024\)](#) have recently cautioned that the power spectral enhancement may be an effect related to the modulation of the sampling direction, following relative changes between the local magnetic and flow velocity. During large deflections (switchbacks), the stronger turbulent power typically associated to the perpendicular direction ([Horbury et al, 2008; Duan et al, 2021](#)), would contribute more to the instantaneous single-spacecraft measurement of the power spectrum. This effect also likely complicates determinations of the turbulent anisotropy during switchbacks. Disambiguation of single spacecraft effects from such measurements will likely require future multi-spacecraft missions such as Helioswarm.

4.3.4 Intermittency and Dissipation

The above results are supported by observations suggesting that both intervals containing switchbacks and intervals within switchbacks exhibit elevated levels of intermittency, as compared to quiet intervals ([Hernández et al, 2021](#)). This picture seems to be also confirmed by more recent Solar Orbiter observations ([Perrone et al, 2025](#)). The increased intermittency is evidenced by the enhanced occurrence of small-scale current sheets ([Martinović et al, 2021; Huang et al, 2023a](#)), also resulting in the fast deviation from Gaussian statistics of the scale-dependent field increments ([Hernández et al, 2021](#)). An additional signature of more developed turbulence is evident in the positive correlation between the cross-scale energy transfer, obtained using third-order moment scaling laws ([Marino and Sorriso-Valvo, 2023](#)), and the occurrence rate of switchbacks ([Hernández et al, 2021](#)). This observation suggests that the enhanced energy injected by the strong magnetic and velocity shears is rapidly redistributed to ion-scale structures, where it is eventually dissipated. Evidence suggests that the physical mechanisms behind turbulent dissipation may depend significantly on the level of imbalance, with studies indicating that strongly Alfvénic, high cross-helicity intervals lead to the generation of ion-scale waves that impart their energy into the plasma. Conversely, more balanced, low cross-helicity intervals preferentially cascade to form sub-ion scale structures ([Bowen et al, 2024](#)). These results connect MHD scales to kinetic dissipation and suggest that, as examples of highly Alfvénic, outwards propagating structures, switchbacks may be dissipated preferentially via cyclotron resonant processes.

4.3.5 Cross-helicity, Residual energy and Alfvénicity of the fluctuations

[Balogh et al \(1999\)](#) have discussed how the direction of propagation of high-frequency Alfvén waves during switchbacks (where high-frequency means much higher frequency than the frequency of the switchback itself) can be used as a diagnostics for their magnetic connectivity. In fact, they have shown that during switchbacks observed by Ulysses in the polar wind, the otherwise anti-Sunward flux of Alfvén waves reverses, becoming Sunward, following the bent field line. Such dynamics was confirmed in Parker observations ([McManus et al,](#)

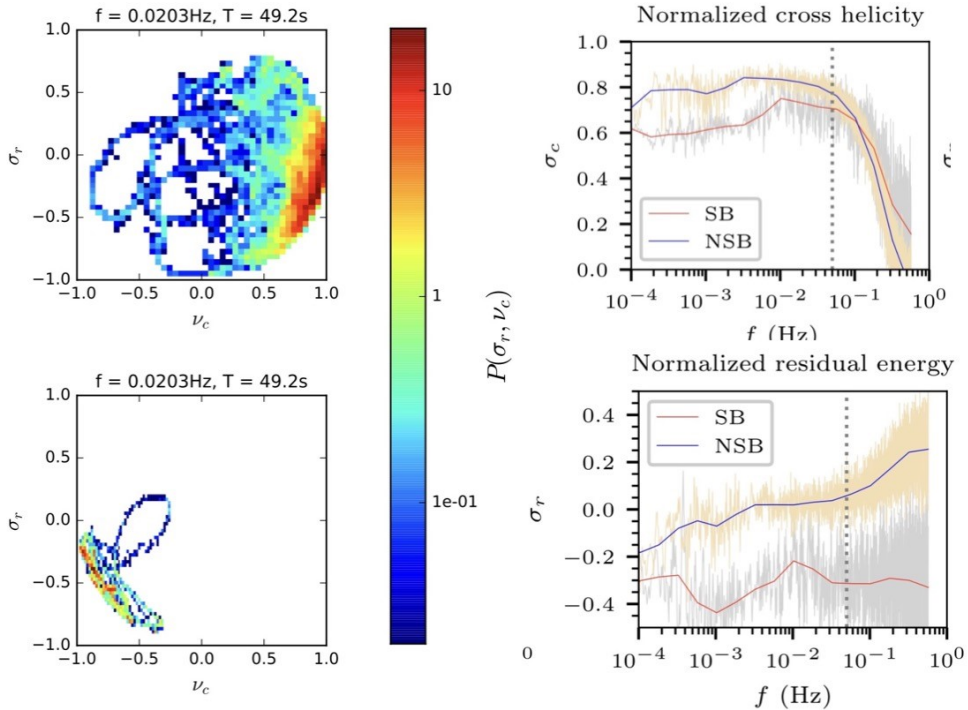


Fig. 14 Left: Distribution in the $\nu_c - \sigma_r$ plane for background turbulence (top) and switchbacks (bottom) where ν_c is the rectified cross-helicity. Figure reproduced with permission from (McManus et al. 2020), copyright by AAS. Right: Normalized Cross-Helicity (σ_c , top) and Normalized Residual Energy (σ_r , bottom) for different solar wind conditions: Switchback (SB, in red) and Non-Switchback (NSB, in blue) intervals, plotted against frequency. For frequencies $f \geq 5 \times 10^{-2}$ Hz (marked by a vertical dotted line), results are potentially subject to contamination from noise in velocity measurements. Figure reproduced with permission from Bourouaine et al (2020), copyright by AAS

2020), shown in Fig. 14, in terms of ν_c and σ_r where ν_c is the rectified cross-helicity such that the sign indicates fluctuations in the sunward or antisunward direction (as compared to σ_c whose sign reflects the direction with respect to the magnetic field orientation), with $\nu_c > 0$ indicating anti-sunward direction. As typically observed in the Alfvénic solar wind, most of the background fluctuations (top panel) lie near the edge of a circle in the $\sigma_c - \sigma_r$ plane. The same pattern is observed in switchbacks (bottom), once the reversal in the propagation direction, i.e., change of sign in ν_c , is accounted for.

More detailed Parker studies suggest that intervals with switchbacks present overall a slightly lower cross helicity (Bourouaine et al. 2020; Wu et al. 2021), as well as more negative residual energy (Bourouaine et al. 2020; Wu et al. 2021; Agapitov et al. 2023), in comparison to quiet intervals, as illustrated in the right-hand panels of Fig. 14. Agapitov et al (2023) further investigates cross-helicity, residual energy and ‘Alfvénicity’ at the scale of switchbacks themselves. They introduce an ‘Alfvénicity’ parameter (α) which is defined as $\alpha = \mathbf{v} \cdot \mathbf{b}/b^2$ where the fluctuation vectors \mathbf{v} and \mathbf{b} (in Alfvén units) are computed by a frame transformation to the deHoffman-Teller frame. Figure 15 illustrates both the detailed evolution of this quantity (in addition to the instantaneous¹ values of σ_c and σ_r) for a single event (left hand column) and statistics (right hand column) over many switchback events (yellow circles) in comparison to the general measurement population (black shading) from Parker E1. For a purely Alfvénic fluctuation, $\alpha = 1$ which corresponds to a fluctuation where $\mathbf{v} = \mathbf{b}$.

Figure 15(f, i) shows that σ_c clusters close to the geometric expectation for pure Alfvénic fluctuations (dashed black curves) compared to the solar wind, meaning \mathbf{b} and \mathbf{v} remain closely aligned inside switchbacks. However, the mean value of σ_c inside switchbacks is 0.66 ± 0.03 , which is close but slightly lower than the mean value of σ_c in the solar wind, 0.69 ± 0.01 (consistent with time scale decomposed values reported by Bourouaine et al (2020) and Wu et al (2021)). Other studies (Shi et al. 2022b) did not observe significant differences inside and outside of the switchbacks, but rather reduced cross-helicity at the switchback boundaries. The reason for the difference between those studies is not clear and should be addressed in future works.

¹Note: Here instantaneous means that the fluctuation vectors \mathbf{b} and \mathbf{v} are computed relative to a single background vector for each switchback event and σ_c and σ_r are no longer spectral/ensemble-averaged quantities but computed from the instantaneous variations of \mathbf{b} and \mathbf{v} .

The statistical behavior of σ_r is shown in Fig. 15(e,j). Switchback-related values are distributed from -1 to 0 with the mean value of -0.58 ± 0.07 , the solar wind-related intervals demonstrate values distributed around 0 with the mean value of -0.18 ± 0.04 .

More generally, a reduced cross-helicity and larger excess of negative residual energy could be attributed to an enhanced level of non-linear interactions between counter-propagating Alfvén waves within the switchbacks structures (Müller and Grappin, 2005; Boldyrev and Perez, 2012; Gogoheridze et al, 2012; Chandran et al, 2015), consistent with observations of the enhanced Alfvénic turbulence levels attributed to switchbacks close to the Sun (e.g., Dudok de Wit et al, 2020; Mozer et al, 2020b). This scenario would also be consistent with switchback periods presenting a more developed inertial range.

Returning to the Alfvénicity parameter itself, Fig. 15(g) shows evidence that switchbacks have a systematic reduction in α with increasing deflection angle. Moreover, these results suggest that the Alfvén speed may play a role in modulating this behavior. The black dashed curve in panel (g) and red dashed data in panel (c) show a geometric construction corresponding to the value α that would take as a function of deflection angle such that $|\mathbf{v}| = V_A$. The example event shown in panels (a–f) is seen to approach but remain below this limit. Statistically, the majority of the events (yellow markers) remain below this limit, but a significant number of them are observed above the limit. The distribution of α values increases towards 1 with decreasing deflection angle, and overall, α is below 1 in switchbacks (consistent with their generally exhibiting negative residual energy, and correspondingly having an Alfvén ratio < 1 Wu et al, 2021), with a maximum close to 0.8 for the largest deflections and approaching 1 for smaller deflections.

On the other hand, it is worth noting that high Alfvénicity ($\alpha \sim 1$) in large deflections has been reported elsewhere (e.g., Woolley et al, 2020; McManus et al, 2022; Bowen et al, 2025), including cases of switchbacks with speed enhancements above V_A . While then the Alfvén speed may be a reasonable term of comparison for the statistical behavior observed here, it is unlikely to be a true physical limitation, as can also be appreciated e.g. in Fig. 20. Nevertheless, this remains an interesting direction for further study, with particular attention to any changes in this behavior with distance from the sun, which may shed light on the interaction of Kelvin-Helmholtz or other instabilities on switchback evolution (Larosa et al, 2021; Mozer et al, 2020b).

4.3.6 Interaction with Ion Scale Waves

The suggestion of a modulation of solar wind turbulence properties with the presence of switchbacks hints at a connection to how switchback and turbulent energy is dissipated at small scales in the solar wind.

At ion-kinetic scales, the equations of MHD break down in favor of kinetic-plasma descriptions. Observations of the onset of kinetic effects include various signatures such as kinetic plasma waves and coherent structures that are thought to contribute to solar wind heating and turbulent dissipation. Signatures of ion-scale waves in the presence of switchbacks may help constrain processes behind their kinetic evolution and decay, and consequently their impacts on solar wind heating.

One primary signature associated with plasma waves is the magnetic helicity of the electromagnetic fields. Helicity signatures of turbulence at ion-kinetic scales have been studied as a constraint on turbulent heating mechanisms (Goldstein et al, 1994; Leamon et al, 1998b,a). Studies at 1 AU show that ion-kinetic scale helicity measurements vary depending on the angle between the solar wind and mean magnetic field (He et al, 2011; Podesta and Gary, 2011). A population of left-hand polarized waves is often observed when the mean magnetic field is roughly parallel to the flow direction, i.e., $\theta_{VB} \approx 0$, while a right-handed helicity emerges at perpendicular sampling angles, i.e., $\theta_{VB} \approx 90^\circ$.

It has been proposed that the right-handed helical signatures that appear at $\theta_{VB} \approx 90^\circ$ arise from a spectrum of oblique kinetic Alfvén waves (KAW) (Howes and Quataert, 2010; Podesta and Gary, 2011; He et al, 2011). Huang et al (2020b) reproduced results similar results during Parker's first encounter, demonstrating that right-handed polarization, consistent with KAWs, is evident when the local magnetic field is perpendicular to the mean flow direction, which may be preferentially during large-scale inversions associated with switchbacks, such that $\theta_{VB} \approx 90^\circ$.

In addition to right-handed ion-kinetic scale signatures that have been associated with anisotropic turbulence, observations at 1 AU show the presence of circularly polarized waves occurring at ion scales when $\theta_{VB} \approx 0^\circ$. These waves have been interpreted as a population of left-handed waves located near $k_{\parallel} d_i \sim 1$ (He et al, 2011; Podesta and Gary, 2011; Klein et al, 2014) where k_{\parallel} is the component of the wavevector parallel to the magnetic field and d_i is the ion inertial length. Statistical studies of parallel-propagating ion-scale waves consistently suggest a preference for the occurrence of these waves during intervals where the mean field is parallel to the background solar wind flow (Jian et al, 2010; Wicks et al, 2016; Boardsen et al, 2015). This statistical preference for the occurrence of circularly polarized waves during radial field

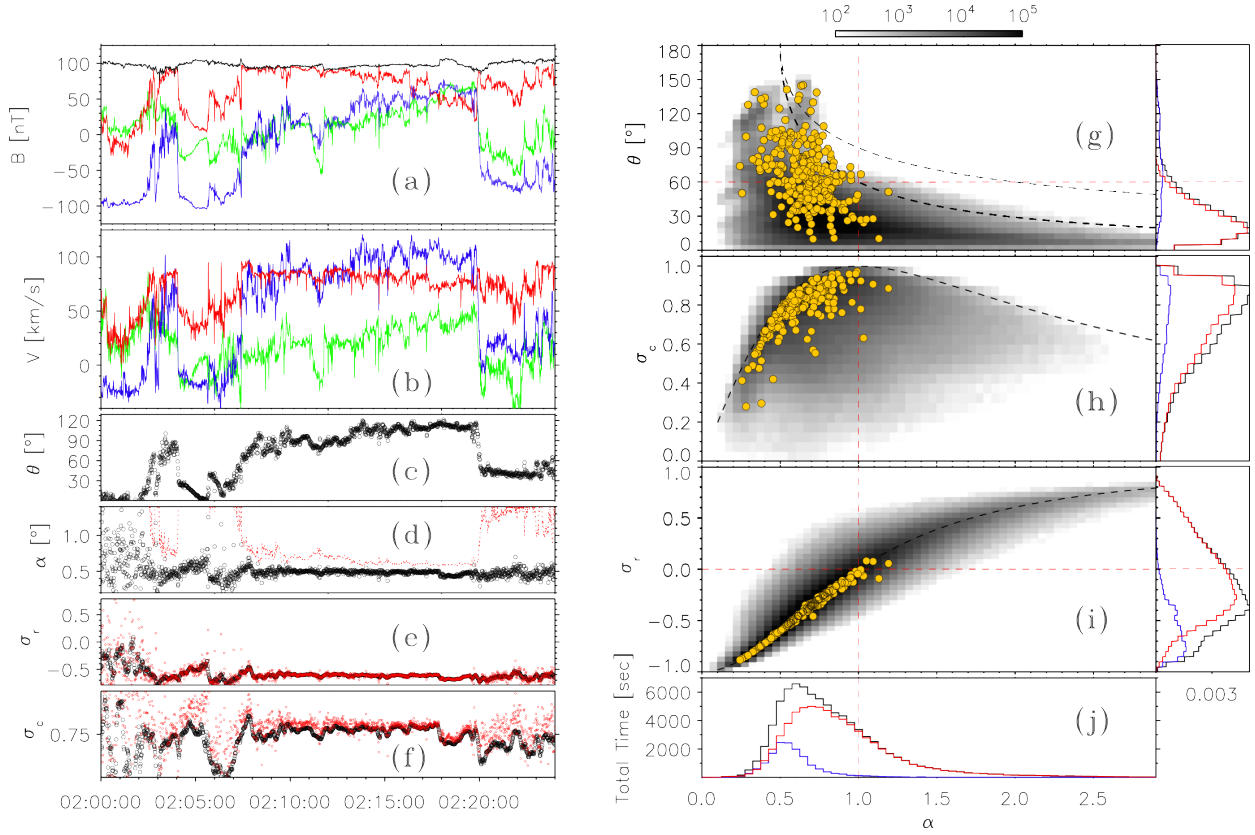


Fig. 15 Example and statistics of Alfvénicity, cross, and residual energy of switchback events from Parker E1. In the left hand column, panels (a)–(f) show timeseries of a switchback measured on Nov. 6, 2018 showing respectively the magnetic field in RTN (R blue, T green, R red and black shows the magnitude), proton bulk velocity with the DeHoffman-Teller velocity subtracted (see Agapitov et al, 2023), the angular deflection of field relative to the mean magnetic vector prior to the switchback, the instantaneous measured Alfvénicity parameter (α , black) and the geometric limit which would correspond to a velocity fluctuation of V_A (red), the instantaneous measured residual energy and cross helicity. In the right-hand column, statistics of individual events (yellow points) and instantaneous measured values (grey/black shading) are shown as a function of α for panels (g) deflection angle, (h) cross helicity, and (i) residual energy. The inset panels show 1D histograms of the different parameters subdivided into switchbacks (blue), non-switchbacks (red), and all measurements (black). Panel (j) shows the total time different values of α are sampled. The thicker dashed curve in panel (g) shows the geometric limit mentioned above. Figures reproduced with permission from Agapitov et al (2023), copyright by AAS

intervals, is consistent with observations from Parker (Bale et al, 2019; Bowen et al, 2020b; Verniero et al, 2020; Liu et al, 2023a). However, there are significant measurement effects associated with single-spacecraft sampling (Fredricks and Coroniti, 1976; Howes and Quataert, 2010) that complicate observation of parallel-propagating waves when the magnetic field and solar wind flow are not parallel (or anti-parallel). First, in the presence of anisotropic turbulence, increased amplitudes at perpendicular angles, i.e., in switchbacks, may obscure circularly polarized ion-scale waves (Bowen et al, 2020b). Second, the observed circularly polarized fluctuations in the solar wind are Doppler-shifted in the spacecraft measurement frame such that circularly polarized parallel propagating waves may not be evident at perpendicular sampling angles.

Bowen et al (2020b) constructed a simple 2D and slab model spectrum to test the observability of parallel-propagating waves in the presence of an anisotropic turbulent background. Their synthetic spectra, as well as their properties, strongly resembled the observations. The similarity between the observed spectra and synthetic spectra suggests that parallel propagating waves may be present during switchbacks, but that the Doppler shift and strong anisotropy of the solar wind turbulence may inhibit their observation.

Parker observations of radial (i.e., non-switchback) intervals, and especially near the heliospheric current sheet, demonstrate that pronounced proton beams exist simultaneously with ion-scale waves (Verniero et al, 2020; Verniero et al, 2022; Bowen et al, 2022) indicating such waves are either generated by proton beam instabilities, or pre-existing wave energies are being damped to create such beams *in situ* (a potential heating mechanism). Krasnoselskikh et al (2023), hypothesize that the proton beam itself may be coming from interchange reconnection which would support the former hypothesis. Given the interchange reconnection theory of switchback formation (see Wyper et al, 2026, this collection), it is therefore of interest to establish if such beam-wave correspondence is also present during switchback intervals. However, such an association

is currently hampered by the difficulty of observing coincident wave signatures during switchback intervals. One potential path forward is to use the fact that switchbacks exist with a spectrum of deflection angles and examine less extreme events to identify if non-instrumental wave signatures can be teased out.

4.3.7 Switchbacks & Turbulence Takeaways

The joint observation of enhanced energy spectra, intermittency, third-order moment scaling, and cross-helicity in intervals containing switchbacks suggests that these are a crucial component of the turbulence at large scales and that the turbulence is energized by the switchbacks. On the other hand, the recent results are not fully conclusive concerning possible intrinsic differences between the turbulent fluctuations inside and outside the switchbacks. In particular, evidence of enhanced wave-mediated turbulent dissipation during switchbacks is in question (Tatum et al, 2024). Evidence is also not yet conclusive on whether switchbacks of a certain size are meaningfully distinct from smaller amplitude fluctuations. Further studies of the interplay between turbulence and switchbacks are necessary to determine the origin of switchbacks and their evolution, but also to understand if they are an effective source of turbulence and its modulations. In carrying out these studies one should be always aware that the observations could be affected by the level of Alfvénicity, the presence of shears, and the geometry of the spacecraft crossing into the structures (see, e.g., Sioulas et al, 2022a; Cuesta et al, 2022; Zank et al, 2022) as well as the limitations of single spacecraft measurements in an anisotropically fluctuating field (Bowen et al, 2020a; Tatum et al, 2024).

5 The Underlying Structure of the Solar Wind

Up to this point, with the exception of the turbulence paragraphs above, the properties of switchbacks have mostly been discussed in terms of the properties of individual events. However, their aggregate behavior is just as remarkable and important to discuss, and may contain further clues to the origin of these structures. In this section, we discuss first the general observation that switchbacks occur in so-called “patches” close to the Sun. We then review current results on the relationship between switchback occurrence in different types of solar wind, including sub-Alfvénic intervals from the most recent Parker perihelia.

5.1 Switchback patches

Visual inspection of Parker’s first solar encounter, in November 2018, revealed almost two weeks of uninterrupted switchbacks in a slow Alfvénic solar wind (see Fig. 1). A striking feature was their occurrence in “patches”, with a series of large deflections that could last several hours (Bale et al, 2019). By examining the waiting times between successive switchbacks, Dudok de Wit et al (2020) found clear evidence of switchback aggregation. Chhiber et al (2020) and Sioulas et al (2022b) found similar evidence by examining intermittent events using the Partial Variance of Increments (PVI) method (Greco et al, 2018). The probability distribution of these waiting times has a power-law distribution, which is typical for sequences of correlated events. The distribution of switchback durations followed a very similar power-law distribution, suggesting that the physical mechanisms governing the rise and fall phases of each switchback were the same (Dudok de Wit et al, 2020). Switchbacks were thus unlike instabilities that are triggered by one mechanism and then relax when another mechanism comes into play. It is also interesting to note that the patches’ modulation in amplitude is more clear than their modulation in occurrence rate: that is small deflection events between patches occur almost as frequently as large deflection events occur in the middle of patches – see Fig. 7). Therefore, a subtle but important point is that when one identifies a switchback patch in Parker data, the key visual indicator is a rise and fall in switchback amplitude rather than a start or stop in switchback occurrence.

However, these results should be treated with caution, since power-law distributions of waiting times are known to occur even in non-stationary systems with uncorrelated events (Wheatland and Litvinenko, 2002). In addition, most analyses mixed different regimes of the solar wind and also different samplings of the switchbacks. During co-rotation periods, the spacecraft provided a temporal slice of their dynamics, while it provided a spatial slice elsewhere. In addition, Parker sampled the solar wind transversely near perihelion and radially farther out. Disentangling these different regimes is important to further understand switchbacks’ structures and properties.

Fargue et al (2021) and Bale et al (2021) studied the patch structure and its connection to solar source regions. In particular, both studies examined intervals where Parker moved rapidly prograde in Carrington longitude and therefore comprised a spatial cut through solar wind structure. This revealed a typical patch angular size of 5° , which is similar to the angular size of solar supergranular structure. As seen in Fig. 16 and in Bale et al (2021), typically the velocity spikes and field deflections show obvious patch structure, however

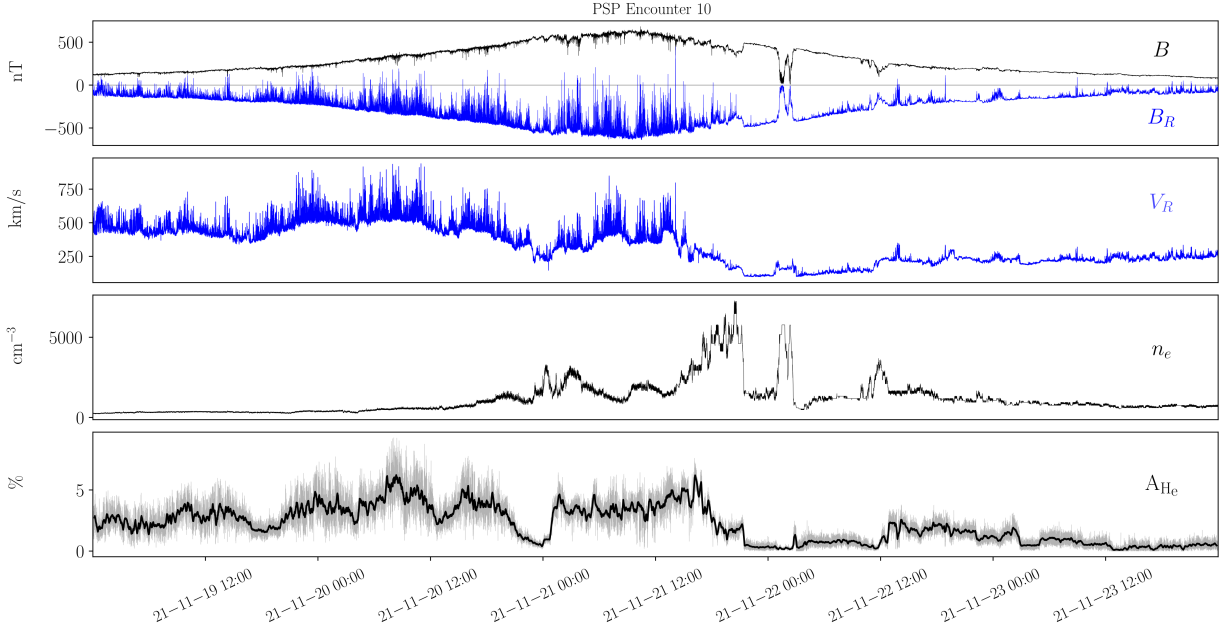


Fig. 16 Example *in situ* data from Parker E10. From top to bottom: radial component and amplitude of the magnetic field, solar wind radial velocity, electron density, and alpha particle abundance.

the alpha abundance is also seen to vary similarly in some cases (although it is not always correlated, see McManus et al. 2022)). The alpha abundance in particular was taken as further evidence of a connection to underlying coronal structure being the cause of the patches. Bale et al (2023) combined similar patch modulation from Parker’s 10th solar encounter with simultaneous observations of suprathermal ion tails with particle-in-cell simulation to further interpret the switchback patches as the remnants of bursty interchange reconnection organized on the solar supergranular network.

More recently, Rivera et al (2024b) used a well-aligned conjunction between Parker and Solar Orbiter (the same as studied in Rivera et al, 2024a) to use Solar Orbiter Heavy Ion Sensor (Livi et al, 2023) measurements as a proxy of the compositional characteristics of switchback patches, as well as direct measurements of the electron core temperature by Parker SPAN-e. They found similar characteristics inside and immediately adjacent to patches, with characteristics varying between patches, and also elemental abundance indicating source regions with open and closed field in close proximity to each other.

Horbury et al (2023) and Soni et al (2024) have similarly exploited Parker-Solar Orbiter alignments and observed patch-scale structure which appears to be preserved at consistent angular scales (at least out to distances probed by Solar Orbiter). They observe that these structures come to resemble “microstreams”, a feature identified historically in Ulysses polar fast wind data (Neugebauer et al, 1995).

While these studies provide evidence on the longitudinal structure of switchback patches, there is evidence that modulation of switchbacks may exist in the radial direction too. Switchback patches typically exhibit slow modulation in $|B|$ and V_R (see e.g., Fig. 16). Domains of nearly constant $|B|$ (i.e., magnetic pressure balance) often represent the space between switchbacks. For example, figure 1 of Ruffolo et al (2021) shows an example of the identification of such domains in Parker data near the 2nd perihelion. In some cases, either one or both boundaries of a switchback patch disrupt the domain structure, while there is a domain of nearly constant $|B|$ within the patch. Ruffolo et al (2021) characterized the aspect ratio of such domains by considering their duration as a function of either the total solar wind speed or a perpendicular speed relative to Parker, where “perpendicular” was relative to a possible axis of systematic domain elongation. They concluded that the domain shape could be isotropic (or spherical) and ruled out long aspect ratios either along the radial or Parker spiral direction. This is consistent with prior observations of isotropic density fluctuations or flocculæ in the super-Alfvénic solar wind (DeForest et al, 2016). Given that domains can be interrupted by switchback patch boundaries, this suggests that the spatial distribution of switchback patches (and the space between patches) is consistent with being isotropic, and the patches are not much more widely spaced along the radial or Parker spiral direction. This is in contrast to the switchbacks themselves, which are observed to have an elongated aspect ratio (Laker et al, 2021), which may play a role in the structures’ stability (Shi et al, 2024), see Sect. 4.2.

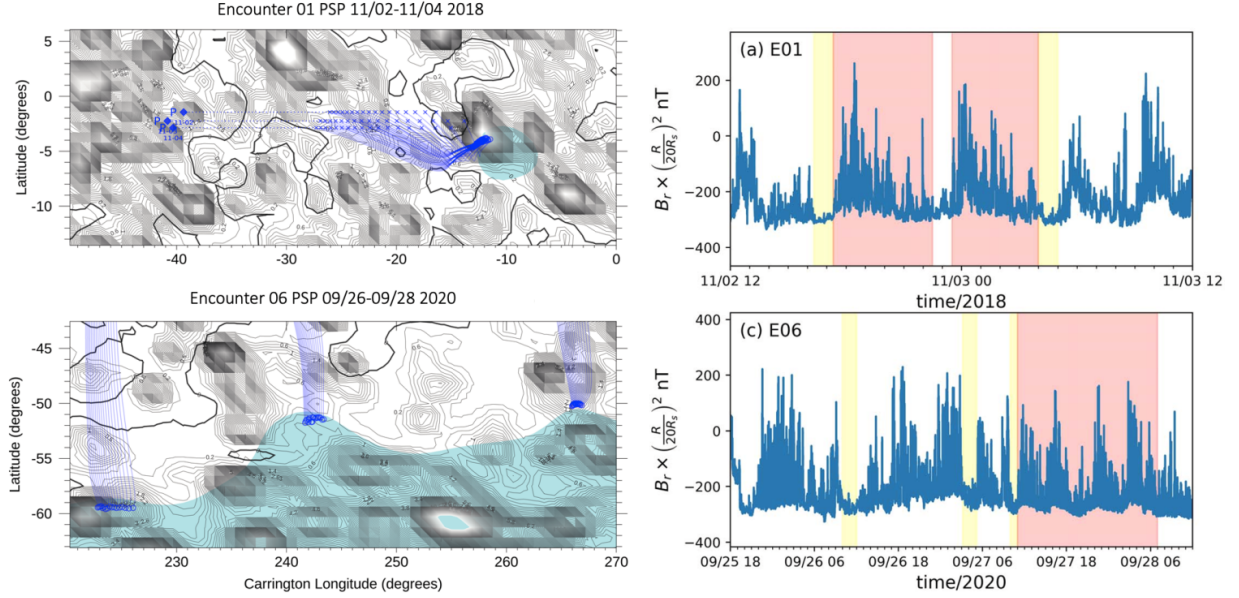


Fig. 17 Left hand column: Potential Field Source Surface mapping (Panasenco et al, 2020) of a time interval where Parker moved mostly radially during E01 (top) and mostly longitudinally during E06 (bottom). Right hand column: Corresponding time profiles of the radial magnetic field measured by Parker and multiplied by the square of its distance from the Sun. Yellow and pink shading indicates “quiescent” and switchback patch structure, respectively. Switchback patches are observed in both cases. Figure adapted with permission from Shi et al (2022b), copyright by AAS.

Similarly, Shi et al (2022b) examined data from Parker observations from E1–E10 during intervals both when the spacecraft is near co-rotation with the Sun and at intervals (as in Farglette et al, 2021; Bale et al, 2021, 2023) with rapid longitudinal motion. In both cases, switchback patches were visually identified (see Fig. 17). For cases where the motion was primarily longitudinal (bottom row of Fig. 17), Shi et al (2022b) arranged spatially just as in Bale et al (2021). However, for intervals near the co-rotating interval of Parker’s orbit (top row in Fig. 17) the spacecraft’s magnetic footprint on the source surface moved extremely slowly in Carrington longitude (top left panel), suggesting spatial modulation alone does not explain patches, but rather there must also be a time-dependent effect that the authors associated with flux emergence at the solar source.

These additional results suggest some switchback patches may have finite radial *and* longitudinal extent. While there is good physical motivation for coronal origin of the longitudinal extent, their radial behavior is a key area of further study that is necessary to understand their evolution with heliocentric distance and to explain why they are much less visually apparent farther from the Sun.

5.2 Switchback Occurrence in Different Solar Wind Streams

As discussed above, switchbacks do not occur randomly (Fig. 5) and are not omnipresent but rather are modulated in amplitude both on consistent spatial scales (see Sect. 5.1) and on a less well understood basis with different solar wind streams: The solar wind, as determined from statistical observations from 1 AU, is composed of a “fast” and “slow” component with a wind speed of 500 km s^{-1} at 1 AU used as a typical delineation (e.g., Kepko et al, 2016). Slow wind streams are observed to be further distinguishable according to their cross-helicity (or “Alfvénicity”) into slow Alfvénic solar wind and slow non-Alfvénic solar wind (e.g., D’Amicis et al, 2021). These different types of streams are thought to originate from different source regions and processes back at the Sun. It is therefore of interest to study the occurrence of switchbacks in different streams since a consistent difference according to solar wind type could indicate that the source region and associated energization method play a role in the creation of switchbacks.

At the time of writing, there are limited studies that have attempted to relate switchback occurrence to the type of solar wind in which they are embedded. We review these here but remark that they are mostly qualified as case studies, while more systematic and statistical investigations should be carried out to corroborate these findings. Further, as discussed in Sect. 3, there are numerous ways to quantify the presence of switchbacks, and in fact, the term “occurrence” depends on such a definition.

Rouillard et al (2020) studied the properties of switchbacks inside and outside the solar minimum streamer belt using observations from the second perihelion pass of Parker. They exploited coronagraphic

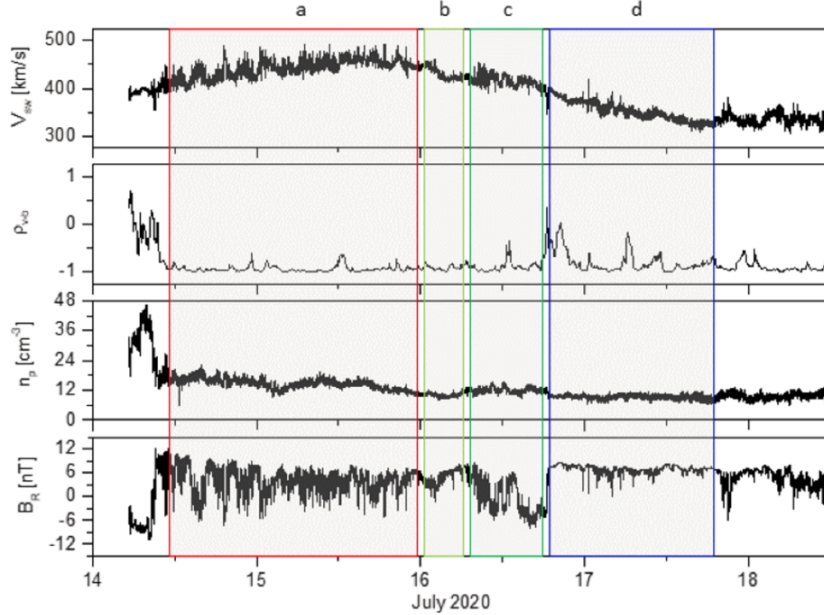


Fig. 18 Four solar wind intervals observed by Solar Orbiter labeled by solar source region. (a) faster wind from a northern polar coronal hole extension (b) wind from its eastern boundary, (c) negative open field area at the equator and (d) a slow transition across a pseudostreamer. Figure reproduced with permission from D'Amicis et al (2021), copyright by ESO

imagery recorded by the Solar and Heliospheric Observatory (SoHO; Domingo et al, 1995) to infer the types of solar winds measured by Parker during bursts of magnetic switchbacks. In this study, the proton speed measured by SWEAP was used to trace back (ballistically) the origin of the measured solar wind in the solar imaging taken by the Large Angle and Spectrometric COronagraph (LASCO; Brueckner et al. 1995) on SOHO. This back-mapping showed that during most of E2, Parker remained on the edges of the streamer belt. This was confirmed by the measurements *in situ* of high-density and highly variable wind flows, but no polarity inversion. As long as Parker remained inside the bright streamers, the density of the solar wind remained elevated, but as soon as it exited the streamers to enter solar wind flows produced by an isolated coronal hole, the wind density dropped by a factor of two to four. Rouillard et al (2020) showed that while switchbacks were observed in both streamer and coronal hole flows, the patches of switchbacks had different properties between the two types of slow winds with more pronounced reversals of the magnetic fields (Rouillard et al, 2020) and enhanced spectral power in the switchbacks transported in the streamer flows than in the coronal hole (Farglette et al, 2021). In addition, the patches of switchbacks in the streamer flows were associated with more significant compressive (density and magnetic field magnitude) variations than in the coronal hole flows. It is yet unclear if these density changes resulted from the formation of these switchbacks or were produced through distinct processes that are known to occur near the center of the streamer belt (Wang et al, 1998; Sanchez-Diaz et al, 2017b,a; Tripathi et al, 2026, this collection). This type of study should be repeated for more encounters.

Panasenco et al (2020) and D'Amicis et al (2021) identified intervals where Parker and Solar Orbiter traversed different types of solar wind, including pseudostreamers. Fig. 18 shows an example of *in situ* solar wind data taken by Solar Orbiter around 0.64 AU with segment (d) corresponding to pseudostreamer-type wind. They observe lower amplitude Alfvénic fluctuations with almost no deflections past 90° during a slow Alfvénic stream as compared to a prior fast stream (segment a in 18). Given this is based on data farther from the Sun, it is important that such studies be repeated with close approach Parker data when switchbacks are more unambiguously identified. In one such recent study, Rivera et al (2025) studied Parker E11 and showed the energy flux of large amplitude Alfvénic fluctuations was a larger fraction of the total solar wind energy budget in a slow Alfvénic wind stream as compared to a neighboring slow non-alfénic stream, but in both cases was lower than the fractional energy of such fluctuations in a neighboring fast stream.

Jagarlamudi et al (2023) performed a statistical study of switchback occurrence rates. While theirs and others' results examining the occurrence as a function of radial distance from the Sun are discussed at length in Mallet et al (2026, this collection), we briefly examine their results pertaining to separating switchbacks according to solar wind speed. In Fig. 19, switchback occurrence measured using a deflection threshold of 37° ($z > 0.1$) binned by deflection scale and radial distance, is shown for fast and slow wind speeds. The

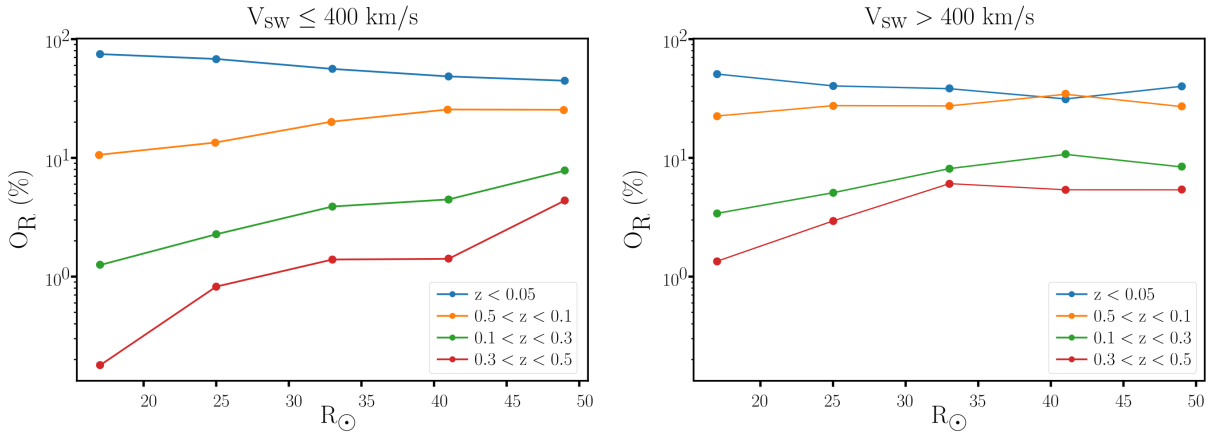


Fig. 19 Occurrence percentage of deflections (O_R) as a function of radial distance (R_\odot). For each radial distance bin, we show the fraction of deflections lying with a certain range of deflectiona angles, z . In panel *a* we showthis variation for the intervals with $V_{SW} \leq 400 \text{ km s}^{-1}$ and in panel *b* we show the variation of D for the intervals with $V_{SW} > 400 \text{ km s}^{-1}$ Figure reproduced with permission from [Jagarlamudi et al \(2023\)](#), copyright by AAS

main difference observed is that the deflection angles (D) are overall skewed to larger values in the faster wind streams.

The commonality in these studies is an observation that in slow Alfvénic solar wind, switchback amplitudes tend to be reduced, consistent with the inference that switchbacks are more energetically relevant to faster wind types ([Halekas et al, 2023](#); [Rivera et al, 2024a](#)). These three studies show this in the context of case studies of the streamer belt wind, pseudostreamer wind, or simply binning by local wind speed. A systematic separation of slow wind into different sub-types may reveal different variations of switchbacks among solar wind from different sources.

5.3 Switchbacks in Low Alfvén Mach Number Wind

Parker is the first heliospheric mission to routinely sample low Alfvén Mach number and sub-Alfvénic solar wind close to the Sun ([Kasper et al, 2021](#)). Since the Alfvénic fluctuations comprising switchbacks typically move on a sphere in velocity space of radius near the Alfvén speed ([McManus et al, 2022](#)), their behavior as this parameter changes, and in particular becomes comparable to the background flow speed, is of keen interest in understanding their nature and origin.

Early Parker observations and numerical simulations had predicted that switchbacks may be generated low in the corona (see e.g., [Fisk and Kasper, 2020](#); [Bale et al, 2023](#); [Tripathi et al, 2026, this collection](#); [Wyper et al, 2026, this collection](#)). For example, [Akhavan-Tafti et al \(2022\)](#) used discontinuity classification of switchbacks from the first eight Parker encounters to argue that switchbacks were most likely generated in the solar corona via interchange reconnection. They further went on to hypothesize that switchback evolution in the solar corona could contribute significantly to coronal heating. However, a clear deficit of switchbacks with full magnetic field reversals (deflection angle > 90 deg, see Sect. 3.1) is observed in the sub-Alfvénic solar corona both during observations in the earliest sub-Alfvénic streams ([Bandyopadhyay et al, 2022](#); [Pecora et al, 2022](#); [Jagarlamudi et al, 2023](#)) and more recently over the first 14 full orbits ([Akhavan-Tafti and Soni, 2024](#)). These observations indicate that switchbacks (as defined as reversals) are mostly either generated locally in the solar wind, or that magnetic switchbacks with deflection angle < 90 deg are generated in the solar corona and evolve to become full magnetic reversals in the super-Alfvénic solar wind as predicted by several models (see e.g. [Ruffolo et al, 2020](#); [Squire et al, 2020](#); [Schwadron and McComas, 2021](#); [Shoda et al, 2021](#); [Touesse et al, 2024](#)). See also [Wyper et al \(2026, this collection\)](#) for a complete review comparing and contrasting such model predictions.

Two subtleties of this inference should be noted, however. Firstly, switchbacks comprise local spikes in the radial velocity which become a sizable portion of the Alfvén speed for large deflections (see [Matteini et al, 2014](#)). When the magnetic field becomes more transverse or is even reversed (due to δB_R), δv_R is invariably positive, resulting in a localized increase in the wind bulk velocity. Therefore, even though switchbacks may be situated within a nominally sub-Alfvénic wind, the presence of these radial velocity jets can locally amplify the solar wind speed, temporarily pushing the local dynamics into a super-Alfvénic regime ([Sioulas](#)

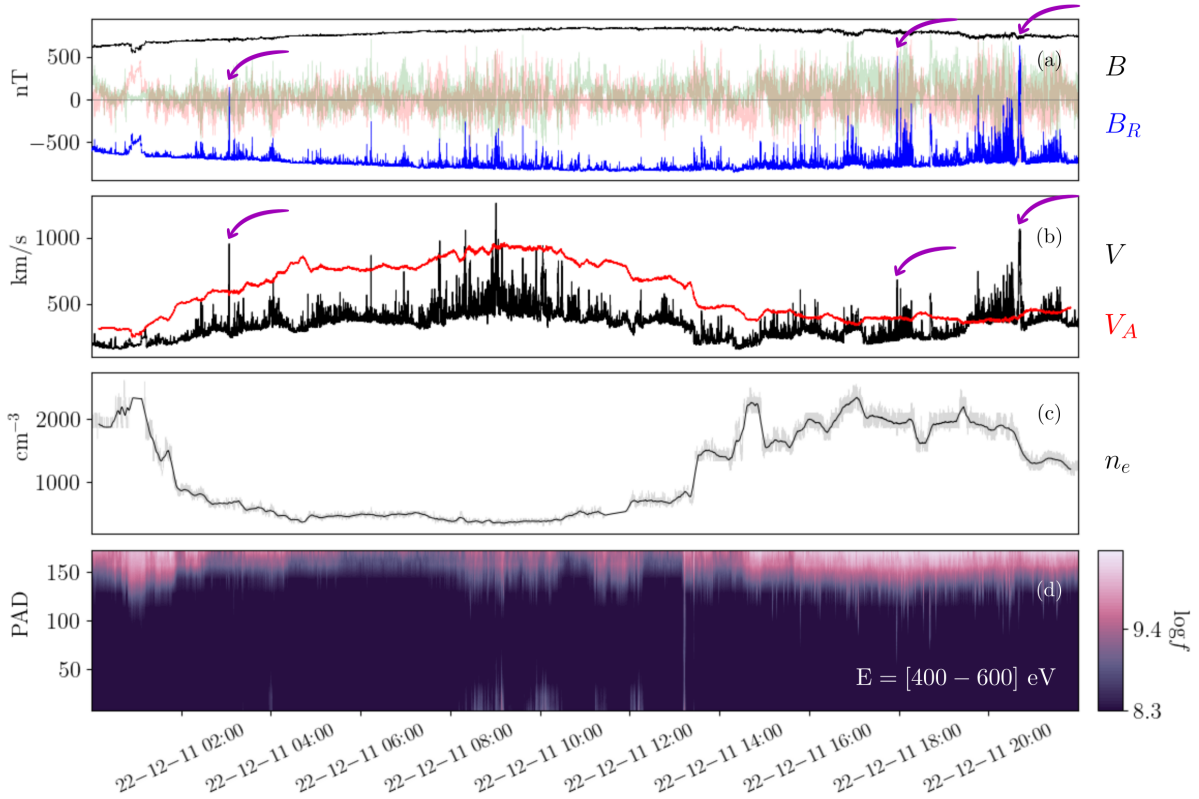


Fig. 20 Examples of magnetic field reversals embedded in otherwise sub-Alfvénic solar wind, indicated by purple arrows. Panels show from top to bottom: the magnetic field, the solar wind speed V and local Alfvén speed V_A , the electron density n_e and PAD of electrons within the 400–600 eV energy range.

et al, AGU Fall Meeting 2024²). Such an example is presented in Fig. 20. Therefore, if simply filtering data timeseries according to the instantaneous Alfvén Mach number, large deflections in otherwise sub-Alfvénic streams may be excluded by construction. To avoid this pitfall, an average background Alfvén speed should be used when studying switchbacks in a sub-Alfvénic solar wind.

Secondly, there are differences in the origin of sub-Alfvénic intervals in the Parker dataset to date. While several appear attributable to steady solar wind conditions and coronal source region properties (e.g., Kasper et al, 2021; Bandyopadhyay et al, 2022; Liu et al, 2023b; Badman et al, 2023), there is evidence that transient structures such as interplanetary coronal mass ejections (ICMEs) can also create long sub-Alfvénic wind intervals. Evidence is provided by Chané et al (2021) and Romeo et al (2023). In the study of Romeo et al (2023), it was shown that the passage of the CME created a huge density depletion region in its wake, which resulted in the creation of sub-Alfvénic wind streams with Alfvén points significantly farther out from the Sun than normal. So far, both types of intervals appear to be similar microphysically (i.e., the absence of magnetic reversals and high transverse fluctuations) but further work is needed to investigate whether this is true more generally, especially with the most recent, closest perihelia of Parker. It is important, therefore, to differentiate the source for the observation of sub-Alfvénic wind intervals before studying the properties of switchbacks in these intervals and connecting them to the global solar wind evolution.

5.4 Switchbacks Collective Behavior Takeaways

The organization of switchbacks into larger-scale patch structures is a key new observational feature from Parker Solar Probe that defines their appearance in the young solar wind and marks a difference from prior observations of individual field reversals farther from the Sun (although such reversals did appear within structures, called microstreams, in the Ulysses polar observations). The main takeaways are:

- Switchback patch longitudinal sizes match a key photospheric angular scale (supergranules) as judged by modulation of plasma parameters on patch scales not involved in the switchback fluctuations (i.e., density, potentially proton parallel temperature and sometimes alpha abundance). Temporal scales also

²See <https://ui.adsabs.harvard.edu/abs/2024AGUFMSH23F..03S>

match characteristics of supergranulation. This and compositional data indicative of open and closed field structures provide evidence that coronal magnetic field structure plays a role in their formation.

- Switchback patch properties (most clearly their amplitude) vary between different solar wind stream types (lower amplitudes typically observed in slower streams) suggesting their formation and evolution are affected by the type of stream they exist in.
- Growing evidence supports that the size of the deflection angle of switchbacks increases with Alfvén Mach number, and that it is rare to observe polarity reversals in sub-Alfvénic wind.

6 Summary and Open Questions

We have summarized the main properties of “magnetic switchbacks”, solar wind fluctuations which have been shown to be ubiquitous close to the Sun by Parker Solar Probe observations. In Sect. 2, we discussed how switchbacks’ essential features identify them as large amplitude Alfvénic fluctuations in which the magnetic field vector goes through a large, magnitude-conserving deflection while the radial velocity is simultaneously enhanced. The transition to the deflected state is sharp, meaning it occurs more rapidly than the time over which the deflection persists. Throughout this transition, field lines remain connected to the Sun as demonstrated by the fact that the electron heat flux remains aligned with the corresponding field line following the field line folds. At closest approach to the Sun, switchbacks are arranged into patches whose angular scales match those of coronal structures (supergranules).

In Sect. 3, we discussed the different methodologies used to detect switchbacks with *in situ* data. In particular, we highlight an overall dichotomy in the literature: while some studies simply examine the deflection angle of the field, others use all the defining features of switchbacks but require human intervention and are thus less statistically rich. The use of the rapidly growing field of machine learning or other AI tools may be a useful route to improve this limitation. Further, we highlight that deflection-based thresholding for switchback detection requires some choice of background field orientation, and choices vary throughout the literature.

Next, in Sect. 4 we listed some of the more detailed properties inferred in relation to switchbacks. These were sub-categorized into:

1. **The steady plasma properties of switchbacks as compared to their surroundings.** In line with their identification as Alfvénic structures, it was noted that the magnetic field magnitude and density of switchbacks changes only modestly compared to their surroundings. The inside-outside ratios form distributions which peak at the ideal incompressible (i.e., Alfvénic) case but with a finite population which exhibits some compression. Additionally, there is some evidence for increased proton temperatures inside individual switchbacks. This may suggest that switchbacks contain plasma distinct from their surroundings and indicative of an injection process at the source. However, these results need to be bolstered with additional evidence, both in terms of the plasma temperatures as well as other compositional properties.
2. **The properties of switchback boundaries, including boundary geometry, discontinuity classification, and boundary-associated electromagnetic wave activity.** We summarize how the processes at these boundaries offer clues on switchback generation and decay. The nature of their boundary discontinuity is important for establishing the extent to which switchbacks can mix with their surroundings and therefore lose memory of their origin and merge slowly, rather than rapidly via instabilities and rapid dynamical processes such as reconnection.
3. **The interaction between switchbacks, turbulence, and ion scale waves.** We summarize a general consensus of a more developed turbulence in the presence of switchbacks. As an energy source at large wavelengths, switchbacks are likely to be an important actor within the full spectrum of solar wind turbulence. Nevertheless, results differ in their details and a consensus picture of cause and effect between turbulence and switchbacks, and implications for whether switchbacks are carrying coronal information, is yet to be established.

Finally, in Sect. 5 we reviewed results on the collective behavior of switchbacks, most prominently their organization into patches, but also the extent to which their presence varies in different wind types. Specifically, we recounted how switchbacks patch spatial extent (with variation across a range of solar wind parameters) and solar supergranular structure are well associated. However, questions remain about the radial extent of patches, with some suggestion some are time-dependent structures. Comparing different solar wind types, a consensus emerges that switchbacks are generally most prominent, high amplitude, and energetically relevant in faster wind streams. More systematic approaches that bin wind, especially slow types, into different levels of Alfvénicity are needed to complete this. Lastly, we touched on the connection between switchbacks and low-Alfvén Mach number wind, where several authors report that polarity reversal

switchbacks are rare in such wind streams. However, counter-examples are possible to find, and additionally, further work is needed to distinguish the effects of transient wakes from steady sub-Alfvénic wind streams to fully understand the behavior of switchbacks at this transition point.

We close this summary with a list of some significant remaining gaps in our knowledge of the properties of magnetic switchbacks, whose resolution may provide evidence for the origin of these structures and their subsequent interaction with the solar wind.

6.1 Knowledge Gaps

Are Switchbacks Meaningfully Distinct from Alfvénic Turbulence?

Switchbacks are large amplitude Alfvénic fluctuations embedded in solar wind dominated by Alfvénic turbulence. Viewing the spectrum of solar wind fluctuations in terms of just Alfvénic fluctuation power or rotational increments (Larosa et al, 2024), switchbacks appear continuous with the background. However, switchbacks are also defined (Sect. 2) by geometrical constraints: sharp boundaries and continuous electron strahl. These aspects are not conditions generally applied to turbulent fluctuations, and also are not enforced for switchback detection methods (Sect. 3), which are based solely on magnetic deflection angle.

It remains to be robustly established how important applying these geometric criteria to switchbacks is in determining their properties and whether they are truly special fluctuation types with respect to background solar wind turbulence.

Do Switchbacks Contain a Different Plasma Population from the Surrounding Solar Wind?

Switchbacks are characterized by a number of properties that do not change much compared to their surroundings. Most notably, this is true of the magnetic field magnitude and density. This property supports the characterization of switchbacks as nearly incompressible Alfvénic fluctuations.

However, their thermal and compositional properties are not firmly established with respect to their surroundings. While the best indications to date suggest a potential enhancement in proton temperature and potential modulation of anisotropy (Woodham et al, 2021; Huang et al, 2023b; Laker et al, 2024), measurement and statistical limitations mean further work is needed to more concretely establish this. The presence of proton (and alpha) beams is also something that may be systematically affected by observational effects and therefore needs careful further attention. Moreover, it is not excluded that part of the observed modulation of the plasma pressure within switchbacks may occur locally, due to the coupling to velocity shears within the structure (Del Sarto and Pegoraro, 2018).

Direct *in situ* thermal compositional data is also limited by instrumentation at Parker to studying proton and alpha particles, and these results are also currently ambiguous (McManus et al, 2022). Possible inroads may also be made by the consideration of energetic particles by the IS \odot IS instrument on Parker (McDougall and Poduval, 2025), or by combining measurements farther out by the Solar Orbiter Heavy Ion Sensor (Livi et al, 2023) for well-aligned streams. This latter strategy was recently applied by Rivera et al (2024b) to examine the heavy ion composition of patches and did not reveal distinct differences inside patches to outside, but did find a range of compositional signatures indicating a solar wind source with open and closed field in close proximity. These additional insights are vital given that there are *in situ* instability mechanisms which may also lead to simple temperature differences occurring in the solar wind rather than being created at the source.

Answering these questions is of direct importance to the formation of switchbacks in that distinct thermal and compositional characteristics would imply they are created from distinct coronal sources. It should be cautioned, though, that the inverse is not necessarily true if there is significant mixing between switchbacks and their neighboring plasma, then such thermal or compositional information may be lost. This highlights the importance of establishing the discontinuity type of switchbacks since tangential discontinuities may inhibit such mixing.

What do Switchback Boundaries and Associated Wave Activity Tell us About How Switchbacks Form and Decay?

In this review, we highlighted the importance of switchback boundaries, which are unique features of the fluctuations. Investigations to date have focused on classifying the boundary type, looking for signatures of reconnection, and examining the zoo of different wave types produced there.

All of these aspects have important implications for how switchbacks will evolve, determining their stability and ability to mix with the surrounding plasma. As yet, there is no consensus nor unifying model

for the dynamics at the boundaries of switchbacks. Thus we still do not fully understand how they evolve and decay (and thereby lose their energy to the overall solar wind).

For example, certain electromagnetic waves could indicate switchback compression or merging. Rotational or tangential discontinuity types could indicate the extent to which switchback material can leak or mix with its neighboring plasma. Observations of reconnection could imply switchbacks impart energy impulsively to their surroundings. Departures from exact incompressibility are also of great importance to understanding this stability and evolution.

Do All Reported Switchback Properties Continue to Hold in Later Orbits and Closer Distances?

By the nature of the Parker Solar Probe mission, whose orbit has shrunk slowly over time to closer and closer perihelia, and the fact that switchbacks were prominently observed from the very first orbits, many results have been derived from these early encounters. As seen in various places in this review and discussed at length in [Mallet et al \(2026, this collection\)](#), switchbacks do evolve with radial distance. For example, polarity reversals become much less common closer to the Sun.

Therefore, it is important that observational results concerning switchbacks obtained from data in the earlier encounters be validated using observations over the full mission both to test if inferred properties remain robust with radial distance and to obtain larger statistical samples.

For example, conclusions about the limit to the velocity perturbations in switchbacks used measurements from the first encounter only ([Agapitov et al, 2023](#)). In another case, it has been observed that switchbacks whose boundaries show signs of reconnection have a smaller velocity enhancement relative to the Alfvén speed ([Suen et al, 2023](#)), but the number statistics where this is observed could be much improved using all available data. Lastly, it has been shown that Single Value Decomposition gives different results for classifying the discontinuity type at switchback boundaries ([Bizien et al, 2023](#)) as compared to prior Minimum Variance Analysis methods ([Akhavan-Tafti et al, 2021; Larosa et al, 2021](#)), and this finding and its implications for switchback physics should be applied to a much wider statistical population.

How Do Switchback Patches Evolve in both Time and Space?

The relationship between switchback patches and solar supergranulation scale size is an important linkage between these structures and the corona. However, there are some reports of switchback patch structure appearing in time while the spacecraft does not cross far in longitude ([Shi et al, 2022b](#)). This is an important phenomenon to investigate and determine statistically the relevant temporal and spatial scales.

6.2 Final Remarks

Magnetic switchbacks have provoked intense interest in heliophysics since their ubiquity was revealed by the launch of Parker Solar Probe. As discussed in Sect. 1, there are numerous reasons motivating this interest – both in how they interact and affect the dynamics of the solar wind and also the way in which they reveal its underlying physics and coronal connections. In this review, we have presented the major properties and areas of study of these complex phenomena. We highlight a consensus that magnetic switchbacks are of central importance to our understanding of the young solar wind, but also that their study is complicated by the need for consistent definitions and detection methodologies, as well as the encounter-based and time-evolving nature of the Parker mission. Future work, as more orbits and statistical datasets are built, is essential to fully understanding their role in shaping the inner Heliosphere.

Acknowledgments

STB and SBD were supported by the Parker Solar Probe project through the SAO/SWEAP subcontract 975569. MV acknowledges support from PSP through the FIELDS experiment on the Parker Solar Probe spacecraft was designed and developed under NASA contract NNN06AA01C. Parker Solar Probe was designed, built, and is now operated by the Johns Hopkins Applied Physics Laboratory as part of NASA's Living with a Star (LWS) program (contract NNN06AA01C). Support from the LWS management and technical team has played a critical role in the success of the Parker Solar Probe mission. We acknowledge the extraordinary contributions of the PSP mission operations and spacecraft engineering team at the Johns Hopkins University Applied Physics Laboratory. NF was supported by UKRI/STFC grant ST/W001071/1 and by the Centre National d'Etudes Spatiales (CNES). DR was supported by the National Science and Technology Development Agency (NSTDA) and National Research Council of Thailand (NRCT): High-Potential Research Team Grant Program (N42A650868), and from the NSRF via the Program Management Unit for

Human Resources & Institutional Development, Research and Innovation (B37G660015). N.B., T.D. and C.F. acknowledge funding from CNES. C.F. acknowledges funding from the CEFIPRA Research Project No. 6904-2. C.F, E.P & TDdW acknowledge the support of the French Agence Nationale de la Recherche (ANR) for the JET2SB project under grant ANR-25-CE31-7416. E.P. and A.P.R. acknowledge support by the Action Thématique Soleil-Terre (ATST) of CNRS/INSU PN Astro as well as from the APR program of CNES C.F., A.P.R., TDdW and N.B. acknowledge support from CNES (APR SCM). O.P. is supported by NSF SHINE grant # 2229566. J.H. is supported by NASA grants 80NSSC23K0737 and 80NSSC23K0450. M.M. acknowledges DFG grant WI 3211/8-2, project number 452856778, and the support of the Brain Pool program funded by the Ministry of Science and ICT through the National Research Foundation of Korea (RS-2024-00408396). A.L. is supported by STFC Consolidated Grant ST/T00018X/1. T.A.B is supported by NASA grant 80NSSC24K0272. L.S.-V. is supported by the Swedish Research Council (VR) Research Grant N. 2022-03352, by the projects “2022KL38BK– The ULtimate fate of TuRbulence from space to laboratory plAsmas (ULTRA)” (B53D23004850006) and ‘Data-based predictions of solar energetic particle arrival to the Earth: ensuring space data and technology integrity from hazardous solar activity events’ (H53D23011020001), funded by the Italian Ministry of University and Research through PRIN/NRRP-NextGenerationEU. VKJ acknowledges support from the Parker Solar Probe mission as part of NASA’s Living with a Star (LWS) program under contract NNN06AA01C. LM, MV, PO, and LSV are supported by the International Space Science Institute (ISSI) in Bern, through the ISSI International Team project #23-591 (Evolution of Turbulence in the Expanding Solar Wind). G.H.H.S. is partially supported by the Royal Society (RS) and the Consiglio Nazionale delle Ricerche (CNR) through the project ‘Multi-scale electrostatic energisation of plasma: comparison of collective processes in laboratory and space’ (IEC\R2\222050 and SAC.AD002.043.021). O.V.A. is supported by NASA grants 80NSSC21K1770, 80NSSC20K0218, and 80NSSC22K0433. The work done at the University of Michigan was supported by NASA contract Nos. NNN06AA01C, 80NSSC20K1847, 80NSSC20K1014, and 80NSSC21K1662. STB acknowledges Y. Rivera and M. Terres for helpful discussions on various sections of this work. Finally, all authors would like to thank ISSI for hosting the workshop that led to this review article. The work at AIP carried out by A.P.R. was supported by the Alexander von Humboldt foundation.

Statements and Declarations

The authors have no competing interests to declare that are relevant to the content of this article.

References

Agapitov OV, Dudok de Wit T, Mozer FS, et al (2020) Sunward-propagating Whistler Waves Collocated with Localized Magnetic Field Holes in the Solar Wind: Parker Solar Probe Observations at 35.7 Rs Radii. *The Astrophysical Journal* 891(1):L20. <https://doi.org/10.3847/2041-8213/ab799c>, URL <https://doi.org/10.3847%2F2041-8213%2Fab799c>

Agapitov OV, Drake JF, Swisdak M, et al (2022) Flux Rope Merging and the Structure of Switchbacks in the Solar Wind. *The Astrophysical Journal* 925(2):213. <https://doi.org/10.3847/1538-4357/ac4016>, [arXiv:2109.04016](https://arxiv.org/abs/2109.04016) [astro-ph.SR]

Agapitov OV, Drake JF, Swisdak M, et al (2023) Constraints on the Alfvénicity of Switchbacks. *ApJ Letters* 959(2):L21. <https://doi.org/10.3847/2041-8213/ad12a5>, [arXiv:2312.01011](https://arxiv.org/abs/2312.01011) [astro-ph.SR]

Akhavan-Tafti M, Soni SL (2024) In Situ Mechanisms are Necessary for Switchback Formation. *ApJ Letters* 970(2):L26. <https://doi.org/10.3847/2041-8213/ad60bc>

Akhavan-Tafti M, Kasper J, Huang J, et al (2021) Discontinuity analysis of the leading switchback transition regions. *Astronomy and Astrophysics* 650:A4. <https://doi.org/10.1051/0004-6361/202039508>

Akhavan-Tafti M, Kasper J, Huang J, et al (2022) Magnetic Switchbacks Heat the Solar Corona. *ApJ Letters* 937(2):L39. <https://doi.org/10.3847/2041-8213/ac913d>

Badman ST, Bale SD, Rouillard AP, et al (2021) Measurement of the open magnetic flux in the inner heliosphere down to 0.13 AU. *Astronomy and Astrophysics* 650:A18. <https://doi.org/10.1051/0004-6361/202039407>, [arXiv:2009.06844](https://arxiv.org/abs/2009.06844) [astro-ph.SR]

Badman ST, Riley P, Jones SI, et al (2023) Prediction and Verification of Parker Solar Probe Solar Wind Sources at 13.3 R_⊕. *Journal of Geophysical Research (Space Physics)* 128(4):e2023JA031359. <https://doi.org/10.1029/2023JA031359>, arXiv:2303.04852 [astro-ph.SR]

Bale SD, Goetz K, Harvey PR, et al (2016) The FIELDS Instrument Suite for Solar Probe Plus. Measuring the Coronal Plasma and Magnetic Field, Plasma Waves and Turbulence, and Radio Signatures of Solar Transients. *Space Science Reviews* 204(1-4):49–82. <https://doi.org/10.1007/s11214-016-0244-5>

Bale SD, Badman ST, Bonnell JW, et al (2019) Highly structured slow solar wind emerging from an equatorial coronal hole. *Nature* 576(7786):237–242. <https://doi.org/10.1038/s41586-019-1818-7>

Bale SD, Horbury TS, Velli M, et al (2021) A Solar Source of Alfvénic Magnetic Field Switchbacks: In Situ Remnants of Magnetic Funnels on Supergranulation Scales. *The Astrophysical Journal* 923(2):174. <https://doi.org/10.3847/1538-4357/ac2d8c>, arXiv:2109.01069 [astro-ph.SR]

Bale SD, Drake JF, McManus MD, et al (2023) Interchange reconnection as the source of the fast solar wind within coronal holes. *Nature* 618(7964):252–256. <https://doi.org/10.1038/s41586-023-05955-3>, arXiv:2208.07932 [astro-ph.SR]

Balogh A, Forsyth RJ, Lucek EA, et al (1999) Heliospheric magnetic field polarity inversions at high heliographic latitudes. *Geophysical Research Letters* 26(6):631–634. <https://doi.org/10.1029/1999GL900061>

Bandyopadhyay R, Matthaeus WH, McComas DJ, et al (2021) Energetic particle behavior in near-Sun magnetic field switchbacks from PSP. *Astronomy and Astrophysics* 650:L4. <https://doi.org/10.1051/0004-6361/202039800>

Bandyopadhyay R, Matthaeus WH, McComas DJ, et al (2022) Sub-Alfvénic Solar Wind Observed by the Parker Solar Probe: Characterization of Turbulence, Anisotropy, Intermittency, and Switchback. *ApJ Letters* 926(1):L1. <https://doi.org/10.3847/2041-8213/ac4a5c>, arXiv:2201.10718 [physics.space-ph]

Bizien N, Dudok de Wit T, Froment C, et al (2023) Are Switchback Boundaries Observed by Parker Solar Probe Closed? *The Astrophysical Journal* 958(1):23. <https://doi.org/10.3847/1538-4357/acf99a>, URL <https://dx.doi.org/10.3847/1538-4357/acf99a>

Boardsen SA, Jian LK, Raines JL, et al (2015) MESSENGER survey of in situ low frequency wave storms between 0.3 and 0.7 AU. *Journal of Geophysical Research (Space Physics)* 120(12):10,207–10,220. <https://doi.org/10.1002/2015JA021506>

Boldyrev S, Perez JC (2012) Spectrum of Kinetic-Alfvén Turbulence. *ApJ Letters* 758(2):L44. <https://doi.org/10.1088/2041-8205/758/2/L44>, arXiv:1204.5809 [astro-ph.SR]

Borovsky JE (2016) The plasma structure of coronal hole solar wind: Origins and evolution. *Journal of Geophysical Research (Space Physics)* 121(6):5055–5087. <https://doi.org/10.1002/2016JA022686>

Bourouaine S, Perez JC, Klein KG, et al (2020) Turbulence Characteristics of Switchback and Nonswitchback Intervals Observed by Parker Solar Probe. *ApJ Letters* 904(2):L30. <https://doi.org/10.3847/2041-8213/abbd4a>, arXiv:2010.00936 [physics.space-ph]

Bourouaine S, Perez JC, Raouafi NE, et al (2022) Features of Magnetic Field Switchbacks in Relation to the Local-field Geometry of Large-amplitude Alfvénic Oscillations: Wind and PSP Observations. *ApJ Letters* 932(2):L13. <https://doi.org/10.3847/2041-8213/ac67d9>, arXiv:2204.09800 [astro-ph.SR]

Bowen TA, Bale SD, Bonnell JW, et al (2020a) A Merged Search-Coil and Fluxgate Magnetometer Data Product for Parker Solar Probe FIELDS. *Journal of Geophysical Research (Space Physics)* 125(5):e27813. <https://doi.org/10.1029/2020JA027813>, arXiv:2001.04587 [astro-ph.IM]

Bowen TA, Mallet A, Huang J, et al (2020b) Ion-scale Electromagnetic Waves in the Inner Heliosphere. *ApJS* 246(2):66. <https://doi.org/10.3847/1538-4365/ab6c65>, arXiv:1912.02361 [astro-ph.SR]

Bowen TA, Chandran BDG, Squire J, et al (2022) In Situ Signature of Cyclotron Resonant Heating in the Solar Wind. *PRL* 129(16):165101. <https://doi.org/10.1103/PhysRevLett.129.165101>, arXiv:2111.05400

[astro-ph.SR]

Bowen TA, Bale SD, Chandran BDG, et al (2024) Mediation of collisionless turbulent dissipation through cyclotron resonance. *Nature Astronomy* <https://doi.org/10.1038/s41550-023-02186-4>

Bowen TA, Dunn CI, Mallet A, et al (2025) Nonlinear interactions in spherically polarized alfvénic turbulence. *The Astrophysical Journal* 985(1):49. <https://doi.org/10.3847/1538-4357/adc569>, URL <https://doi.org/10.3847/1538-4357/adc569>

Brodiano M, Dmitruk P, Andrés N (2023) A statistical study of the compressible energy cascade rate in solar wind turbulence: Parker solar probe observations. *Physics of Plasmas* 30(3):032903. <https://doi.org/10.1063/5.0109379>, https://pubs.aip.org/aip/pop/article-pdf/doi/10.1063/5.0109379/16796315/032903_1_online.pdf

Bruno R, Carbone V (2013) The Solar Wind as a Turbulence Laboratory. *Living Rev Sol Phys* 2:4–+

Burlaga LF (1969) Directional Discontinuities in the Interplanetary Magnetic Field. *Solar Physics* 7(1):54–71. <https://doi.org/10.1007/BF00148406>

Case AW, Kasper JC, Stevens ML, et al (2020) The solar probe cup on the parker solar probe. *The Astrophysical Journal Supplement Series* 246(2):43. <https://doi.org/10.3847/1538-4365/ab5a7b>, URL <https://doi.org/10.3847%2F1538-4365%2Fab5a7b>

Cassak PA, Otto A (2011) Scaling of the magnetic reconnection rate with symmetric shear flow. *Physics of Plasmas* 18(7):074501. <https://doi.org/10.1063/1.3609771>

Cattell C, Breneman A, Dombeck J, et al (2022) Parker Solar Probe Evidence for the Absence of Whistlers Close to the Sun to Scatter Strahl and to Regulate Heat Flux. *The Astrophysical Journal* 924:L33. <https://doi.org/10.3847/2041-8213/ac4015>, URL <https://ui.adsabs.harvard.edu/abs/2022ApJ...924L..33C>

Chandran BDG, Schekochihin AA, Mallet A (2015) Intermittency and Alignment in Strong RMHD Turbulence. *The Astrophysical Journal* 807(1):39. <https://doi.org/10.1088/0004-637X/807/1/39>, [arXiv:1403.6354](https://arxiv.org/abs/1403.6354) [astro-ph.SR]

Chané E, Schmieder B, Dasso S, et al (2021) Over-expansion of a coronal mass ejection generates sub-Alfvénic plasma conditions in the solar wind at Earth. *Astronomy and Astrophysics* 647:A149. <https://doi.org/10.1051/0004-6361/202039867>

Chen CHK, Bale SD, Bonnell JW, et al (2020) The Evolution and Role of Solar Wind Turbulence in the Inner Heliosphere. *ApJ Supplements* 246(2):53. <https://doi.org/10.3847/1538-4365/ab60a3>, [arXiv:1912.02348](https://arxiv.org/abs/1912.02348) [astro-ph.SR]

Chen Q, Otto A, Lee LC (1997) Tearing instability, Kelvin-Helmholtz instability, and magnetic reconnection. *Journal of Geophysical Research* 102(A1):151–162. <https://doi.org/10.1029/96JA03144>

Chhiber R, Goldstein ML, Maruca BA, et al (2020) Clustering of intermittent magnetic and flow structures near parker solar probe's first perihelion—a partial-variance-of-increments analysis. *The Astrophysical Journal Supplement Series* 246(2):31. <https://doi.org/10.3847/1538-4365/ab53d2>

Choi KE, Agapitov O, Colombari L, et al (2024) Whistler Waves in the Young Solar Wind: Statistics of Amplitude and Propagation Direction from Parker Solar Probe Encounters 1–11. *The Astrophysical Journal* 971(2):177. <https://doi.org/10.3847/1538-4357/ad54c4>, [arXiv:2408.00736](https://arxiv.org/abs/2408.00736) [physics.space-ph]

Colombari L, Agapitov OV, Krasnoselskikh V, et al (2023) Reconstruction of Polarization Properties of Whistler Waves From Two Magnetic and Two Electric Field Components: Application to Parker Solar Probe Measurements. *Journal of Geophysical Research: Space Physics* 128(10):e2023JA031427. <https://doi.org/10.1029/2023JA031427>, [eprint: https://onlinelibrary.wiley.com/doi/pdf/10.1029/2023JA031427](https://onlinelibrary.wiley.com/doi/pdf/10.1029/2023JA031427)

Colombari L, Kretzschmar M, Krasnoselskikh V, et al (2024) Quantifying the diffusion of suprathermal electrons by whistler waves between 0.2 and 1 AU with Solar Orbiter and Parker Solar Probe. *Astronomy and Astrophysics* 684:A143. <https://doi.org/10.1051/0004-6361/202347489>, [arXiv:2402.06016](https://arxiv.org/abs/2402.06016) [astro-ph.SR]

Cuesta ME, Parashar TN, Chhiber R, et al (2022) Intermittency in the Expanding Solar Wind: Observations from Parker Solar Probe (0.16 au), Helios 1 (0.3-1 au), and Voyager 1 (1-10 au). *ApJ Supplements*259(1):23. <https://doi.org/10.3847/1538-4365/ac45fa>, arXiv:2202.01874 [physics.space-ph]

D'Amicis R, Bruno R, Panasenco O, et al (2021) First Solar Orbiter observation of the Alfvénic slow wind and identification of its solar source. *Astronomy and Astrophysics*656:A21. <https://doi.org/10.1051/0004-6361/202140938>

DeForest CE, Matthaeus WH, Viall NM, et al (2016) Fading Coronal Structure and the Onset of Turbulence in the Young Solar Wind. *The Astrophysical Journal*828(2):66. <https://doi.org/10.3847/0004-637X/828/2/66>, arXiv:1606.07718 [astro-ph.SR]

Del Sarto D, Pegoraro F (2018) Shear-induced pressure anisotropization and correlation with fluid vorticity in a low collisionality plasma. *Monthly Notices of the Royal Astronomical Society*475(1):181–192. <https://doi.org/10.1093/mnras/stx3083>

Domingo V, Fleck B, Poland AI (1995) The SOHO Mission: an Overview. *Solar Physics*162(1-2):1–37. <https://doi.org/10.1007/BF00733425>

Drake JF, Agapitov O, Swisdak M, et al (2021) Switchbacks as signatures of magnetic flux ropes generated by interchange reconnection in the corona. *Astronomy and Astrophysics*650:A2. <https://doi.org/10.1051/0004-6361/202039432>, arXiv:2009.05645 [astro-ph.SR]

Duan D, He J, Bowen TA, et al (2021) Anisotropy of solar wind turbulence in the inner heliosphere at kinetic scales: Psp observations. *The Astrophysical Journal Letters* 915(1):L8. <https://doi.org/10.3847/2041-8213/ac07ac>, URL <https://dx.doi.org/10.3847/2041-8213/ac07ac>

Dudok de Wit T, Alexandrova O, Furno I, et al (2013) Methods for Characterising Microphysical Processes in Plasmas. *Space Science Reviews*178(2-4):665–693. <https://doi.org/10.1007/s11214-013-9974-9>, arXiv:1306.5303 [physics.plasm-ph]

Dudok de Wit T, Krasnoselskikh VV, Bale SD, et al (2020) Switchbacks in the Near-Sun Magnetic Field: Long Memory and Impact on the Turbulence Cascade. *ApJ Supplements*246(2):39. <https://doi.org/10.3847/1538-4365/ab5853>, arXiv:1912.02856 [astro-ph.SR]

Einaudi G, Rubini F (1986) Resistive instabilities in a flowing plasma: I. Inviscid case. *Physics of Fluids* 29(8):2563–2568. <https://doi.org/10.1063/1.865548>

Elsasser WM (1950) The hydromagnetic equations. *Phys Rev* 79:183–183. <https://doi.org/10.1103/PhysRev.79.183>, URL <https://link.aps.org/doi/10.1103/PhysRev.79.183>

Eriksson S, Swisdak M, Mallet A, et al (2024) Parker Solar Probe Observations of Magnetic Reconnection Exhausts in Quiescent Plasmas near the Sun. *The Astrophysical Journal*965(1):76. <https://doi.org/10.3847/1538-4357/ad25f0>

Farglette N (2022) The role of magnetic reconnection in the formation of flux ropes and switchbacks in the heliosphere. *Theses, Université Paul Sabatier - Toulouse III*, URL <https://theses.hal.science/tel-03936235>

Farglette N, Lavraud B, Rouillard AP, et al (2021) Characteristic Scales of Magnetic Switchback Patches Near the Sun and Their Possible Association With Solar Supergranulation and Granulation. *The Astrophysical Journal*919(2):96. <https://doi.org/10.3847/1538-4357/ac1112>, arXiv:2109.01519 [astro-ph.SR]

Farglette N, Lavraud B, Rouillard AP, et al (2022) The preferential orientation of magnetic switchbacks and its implications for solar magnetic flux transport. *Astronomy and Astrophysics*663:A109. <https://doi.org/10.1051/0004-6361/202243537>, arXiv:2203.14591 [astro-ph.SR]

Farglette N, Lavraud B, Rouillard AP, et al (2023) Clustering of magnetic reconnection exhausts in the solar wind: An automated detection study. *Astronomy and Astrophysics*674:A98. <https://doi.org/10.1051/0004-6361/202346043>

Farrell WM, MacDowall RJ, Gruesbeck JR, et al (2020) Magnetic Field Dropouts at Near-Sun Switchback Boundaries: A Superposed Epoch Analysis. *ApJ Supplements* 249(2):28. <https://doi.org/10.3847/1538-4365/ab9eba>

Farrell WM, Rasca AP, MacDowall RJ, et al (2021) Switchback Boundary Dissipation and Relative Age. *The Astrophysical Journal* 915(1):68. <https://doi.org/10.3847/1538-4357/ac005b>

Fedorov A, Louarn P, Owen CJ, et al (2021) Switchback-like structures observed by Solar Orbiter. *Astronomy and Astrophysics* 656:A40. <https://doi.org/10.1051/0004-6361/202141246>

Fisk LA, Kasper JC (2020) Global Circulation of the Open Magnetic Flux of the Sun. *ApJ Letters* 894(1):L4. <https://doi.org/10.3847/2041-8213/ab8acd>

Fox NJ, Velli MC, Bale SD, et al (2016) The Solar Probe Plus Mission: Humanity's First Visit to Our Star. *Space Science Reviews* 204(1-4):7–48. <https://doi.org/10.1007/s11214-015-0211-6>

Fredricks RW, Coroniti FV (1976) Ambiguities in the deduction of rest frame fluctuation spectrums from spectrums computed in moving frames. *JGR* 81(A31):5591–5595. <https://doi.org/10.1029/JA081i031p05591>

Frisch U (1995) Turbulence. The legacy of A.N. Kolmogorov. Cambridge University Press

Froment C, Krasnoselskikh V, Dudok de Wit T, et al (2021) Direct evidence for magnetic reconnection at the boundaries of magnetic switchbacks with Parker Solar Probe. *Astronomy and Astrophysics* 650:A5. <https://doi.org/10.1051/0004-6361/202039806>, arXiv:2101.06279 [astro-ph.SR]

Froment C, Agapitov OV, Krasnoselskikh V, et al (2023) Whistler waves generated inside magnetic dips in the young solar wind: Observations of the search-coil magnetometer on board Parker Solar Probe. *Astronomy and Astrophysics* 672:A135. <https://doi.org/10.1051/0004-6361/202245140>, URL <https://ui.adsabs.harvard.edu/abs/2023A&A...672A.135F>

Gogoberidze G, Chapman SC, Hnat B (2012) Generation of residual energy in the turbulent solar wind. *Physics of Plasmas* 19(10):102310. <https://doi.org/10.1063/1.4764469>

Goldstein ML, Roberts DA, Fitch CA (1994) Properties of the fluctuating magnetic helicity in the inertial and dissipation ranges of solar wind turbulence. *Journal of Geophysical Research* 99(A6):11519–11538. <https://doi.org/10.1029/94JA00789>

Golub GH, van Loan CF (2013) Matrix Computations. 4th edn.; Baltimore, MD: Johns Hopkins University Press

Gosling JT (2012) Magnetic Reconnection in the Solar Wind. *Space Science Reviews* 172(1-4):187–200. <https://doi.org/10.1007/s11214-011-9747-2>

Gosling JT, Szabo A (2008) Bifurcated current sheets produced by magnetic reconnection in the solar wind. *Journal of Geophysical Research (Space Physics)* 113(A10):A10103. <https://doi.org/10.1029/2008JA013473>

Gosling JT, Skoug RM, McComas DJ, et al (2005) Direct evidence for magnetic reconnection in the solar wind near 1 AU. *Journal of Geophysical Research (Space Physics)* 110(A1):A01107. <https://doi.org/10.1029/2004JA010809>

Gosling JT, McComas DJ, Roberts DA, et al (2009) A One-Sided Aspect of Alfvénic Fluctuations in the Solar Wind. *ApJ Letters* 695(2):L213–L216. <https://doi.org/10.1088/0004-637X/695/2/L213>

Greco A, Matthaeus WH, Perri S, et al (2018) Partial Variance of Increments Method in Solar Wind Observations and Plasma Simulations. *Space Science Reviews* 214(1):1. <https://doi.org/10.1007/s11214-017-0435-8>

Halekas JS, Bale SD, Berthomier M, et al (2023) Quantifying the Energy Budget in the Solar Wind from 13.3 to 100 Solar Radii. *The Astrophysical Journal* 952(1):26. <https://doi.org/10.3847/1538-4357/acd769>

arXiv:2305.13424 [astro-ph.SR]

Hausman BA, Michel FC, Espley JR, et al (2004) On determining the nature and orientation of magnetic directional discontinuities: Problems with the minimum variance method. *JGRA* 109(A11). <https://doi.org/10.1029/2004JA010670>

He J, Marsch E, Tu C, et al (2011) Possible Evidence of Alfvén-cyclotron Waves in the Angle Distribution of Magnetic Helicity of Solar Wind Turbulence. *The Astrophysical Journal* 731(2):85. <https://doi.org/10.1088/0004-637X/731/2/85>

Hernández CS, Sorriso-Valvo L, Bandyopadhyay R, et al (2021) Impact of Switchbacks on Turbulent Cascade and Energy Transfer Rate in the Inner Heliosphere. *ApJ Letters* 922(1):L11. <https://doi.org/10.3847/2041-8213/ac36d1>

Horbury TS, Burgess D, Fränz M, et al (2001) Three spacecraft observations of solar wind discontinuities. *Geophysical Research Letters* 28(4):677–680. <https://doi.org/10.1029/2000GL000121>

Horbury TS, Forman M, Oughton S (2008) Anisotropic Scaling of Magnetohydrodynamic Turbulence. *PRL* 101(17):175005. <https://doi.org/10.1103/PhysRevLett.101.175005>, arXiv:0807.3713 [physics.plasm-ph]

Horbury TS, Matteini L, Stansby D (2018) Short, large-amplitude speed enhancements in the near-Sunfast solar wind. *Monthly Notices of the Royal Astronomical Society* 478(2):1980–1986. <https://doi.org/10.1093/mnras/sty953>

Horbury TS, Woolley T, Laker R, et al (2020) Sharp Alfvénic Impulses in the Near-Sun Solar Wind. *ApJ Supplements* 246(2):45. <https://doi.org/10.3847/1538-4365/ab5b15>

Horbury TS, Bale SD, McManus MD, et al (2023) Switchbacks, microstreams, and broadband turbulence in the solar wind. *Physics of Plasmas* 30(8):082905. <https://doi.org/10.1063/5.0123250>

Howes GG, Quataert E (2010) On the Interpretation of Magnetic Helicity Signatures in the Dissipation Range Of Solar Wind Turbulence. *The Astrophysical Journal Letters* 709(1):L49–L52. <https://doi.org/10.1088/2041-8205/709/1/L49>, arXiv:0910.5023 [astro-ph.EP]

Huang J, Kasper JC, Vech D, et al (2020a) Proton Temperature Anisotropy Variations in Inner Heliosphere Estimated with the First Parker Solar Probe Observations. *ApJ Supplements* 246(2):70. <https://doi.org/10.3847/1538-4365/ab74e0>, arXiv:1912.03871 [physics.space-ph]

Huang J, Kasper JC, Fisk LA, et al (2023a) The Structure and Origin of Switchbacks: Parker Solar Probe Observations. *The Astrophysical Journal* 952(1):33. <https://doi.org/10.3847/1538-4357/acd17e>, arXiv:2301.10374 [physics.space-ph]

Huang J, Kasper JC, Larson DE, et al (2023b) The Temperature, Electron, and Pressure Characteristics of Switchbacks: Parker Solar Probe Observations. *The Astrophysical Journal* 954(2):133. <https://doi.org/10.3847/1538-4357/ace694>, arXiv:2306.04773 [physics.space-ph]

Huang SY, Zhang J, Sahraoui F, et al (2020b) Kinetic Scale Slow Solar Wind Turbulence in the Inner Heliosphere: Coexistence of Kinetic Alfvén Waves and Alfvén Ion Cyclotron Waves. *ApJL* 897(1):L3. <https://doi.org/10.3847/2041-8213/ab9abb>, arXiv:2006.04665 [physics.space-ph]

Hudson PD (1970) Discontinuities in an anisotropic plasma and their identification in the solar wind. *P&SS* 18(11):1611–1622. [https://doi.org/10.1016/0032-0633\(70\)90036-X](https://doi.org/10.1016/0032-0633(70)90036-X), URL <https://www.sciencedirect.com/science/article/pii/003206337090036X>

Iroshnikov PS (1963) Turbulence of a Conducting Fluid in a Strong Magnetic Field. *Astronomicheskii Zhurnal* 40:742. ADS Bibcode: 1963AZh....40..742I

Jagarlamudi VK, Dudok de Wit T, Froment C, et al (2021) Whistler wave occurrence and the interaction with strahl electrons during the first encounter of Parker Solar Probe. *Astronomy & Astrophysics* 650:A9. <https://doi.org/10.1051/0004-6361/202039808>, URL <https://www.aanda.org/10.1051/0004-6361/202039808>

Jagarlamudi VK, Raouafi NE, Bourouaine S, et al (2023) Occurrence and Evolution of Switchbacks in the Inner Heliosphere: Parker Solar Probe Observations. *ApJ Letters* 950(1):L7. <https://doi.org/10.3847/2041-8213/acd778>

Jian LK, Russell CT, Luhmann JG, et al (2010) Observations of ion cyclotron waves in the solar wind near 0.3 AU. *Journal of Geophysical Research (Space Physics)* 115(A12):A12115. <https://doi.org/10.1029/2010JA015737>

Johnston Z, Squire J, Mallet A, et al (2022) On the properties of Alfvénic switchbacks in the expanding solar wind: Three-dimensional numerical simulations. *Physics of Plasmas* 29(7):072902. <https://doi.org/10.1063/5.0097983>

Kahler SW, Crooker NU, Gosling JT (1996) The topology of intrasector reversals of the interplanetary magnetic field. *Journal of Geophysical Research* 101(A11):24373–24382. <https://doi.org/10.1029/96JA02232>

Karbashewski S, Agapitov OV, Kim HY, et al (2023) Whistler Wave Observations by Parker Solar Probe During Encounter 1: Counter-propagating Whistlers Collocated with Magnetic Field Inhomogeneities and their Application to Electric Field Measurement Calibration. *The Astrophysical Journal* 947:73. <https://doi.org/10.3847/1538-4357/acc527>, URL <https://ui.adsabs.harvard.edu/abs/2023ApJ...947...73K>

Kasper JC, Lazarus AJ, Gary SP (2002) Wind/SWE observations of firehose constraint on solar wind proton temperature anisotropy. *Geophysical Research Letters* 29(17):1839. <https://doi.org/10.1029/2002GL015128>

Kasper JC, Abiad R, Austin G, et al (2016) Solar Wind Electrons Alphas and Protons (SWEAP) Investigation: Design of the Solar Wind and Coronal Plasma Instrument Suite for Solar Probe Plus. *Space Science Reviews* 204:131–186. <https://doi.org/10.1007/s11214-015-0206-3>

Kasper JC, Bale SD, Belcher JW, et al (2019) Alfvénic velocity spikes and rotational flows in the near-Sun solar wind. *Nature* 576(7786):228–231. <https://doi.org/10.1038/s41586-019-1813-z>

Kasper JC, Klein KG, Lichko E, et al (2021) Parker Solar Probe Enters the Magnetically Dominated Solar Corona. *Physical Review Letters* 127(25):255101. <https://doi.org/10.1103/PhysRevLett.127.255101>

Kennel CF, Scarf FL, Coroniti FV, et al (1980) Correlated whistler and electron plasma oscillation bursts detected on ISEE-3. *Geophysical Research Letters* 7(2):129–132. <https://doi.org/10.1029/GL007i002p00129>

Kepko L, Viall NM, Antiochos SK, et al (2016) Implications of l1 observations for slow solar wind formation by solar reconnection. *Geophysical Research Letters* 43(9):4089–4097. <https://doi.org/https://doi.org/10.1002/2016GL068607>, <https://agupubs.onlinelibrary.wiley.com/doi/pdf/10.1002/2016GL068607>

Klein KG, Howes GG, TenBarge JM, et al (2014) Physical Interpretation of the Angle-dependent Magnetic Helicity Spectrum in the Solar Wind: The Nature of Turbulent Fluctuations near the Proton Gyroradius Scale. *ApJ* 785(2):138. <https://doi.org/10.1088/0004-637X/785/2/138>, arXiv:1403.2306 [physics.plasm-ph]

Knetter T (2005) A new perspective of the solar wind micro-structure due to multi-point observations of discontinuities. PhD thesis, Universität zu Köln

Knetter T, Neubauer FM, Horbury T, et al (2003) Discontinuity observations with cluster. *Advances in Space Research* 32(4):543–548. [https://doi.org/10.1016/S0273-1177\(03\)00335-1](https://doi.org/10.1016/S0273-1177(03)00335-1)

Knetter T, Neubauer FM, Horbury T, et al (2004) Four-point discontinuity observations using Cluster magnetic field data: A statistical survey. *Journal of Geophysical Research (Space Physics)* 109(A6):A06102. <https://doi.org/10.1029/2003JA010099>

Kraichnan RH (1965) Inertial-range spectrum of hydromagnetic turbulence. *The Physics of Fluids* 8(7):1385–1387. Publisher: American Institute of Physics

Krasnoselskikh V, Larosa A, Agapitov O, et al (2020) Localized Magnetic-field Structures and Their Boundaries in the Near-Sun Solar Wind from Parker Solar Probe Measurements. *The Astrophysical Journal* 893(2):93. <https://doi.org/10.3847/1538-4357/ab7f2d>, arXiv:2003.05409 [physics.space-ph]

Krasnoselskikh V, Zaslavsky A, Artemyev A, et al (2023) Ion kinetics of plasma interchange reconnection in the lower solar corona. *The Astrophysical Journal* 959(1):15. <https://doi.org/10.3847/1538-4357/ad046b>, URL <https://dx.doi.org/10.3847/1538-4357/ad046b>

Kretzschmar M, Chust T, Krasnoselskikh V, et al (2021) Whistler waves observed by Solar Orbiter/RPW between 0.5 AU and 1 AU. *Astronomy & Astrophysics* 656:A24. <https://doi.org/10.1051/0004-6361/202140945>, URL <https://ui.adsabs.harvard.edu/abs/2021A%26656A..24K/abstract>

Laker R, Horbury TS, Bale SD, et al (2021) Statistical analysis of orientation, shape, and size of solar wind switchbacks. *Astronomy and Astrophysics* 650:A1. <https://doi.org/10.1051/0004-6361/202039354>, arXiv:2010.10211 [physics.space-ph]

Laker R, Horbury TS, Matteini L, et al (2022) Switchback deflections beyond the early parker solar probe encounters. *Monthly Notices of the Royal Astronomical Society* 517(1):1001–1005. <https://doi.org/10.1093/mnras/stac2477>, arXiv:2204.12980 [physics.space-ph]

Laker R, Horbury TS, Woodham LD, et al (2024) Coherent deflection pattern and associated temperature enhancements in the near-Sun solar wind. *Monthly Notices of the Royal Astronomical Society* 527(4):10440–10447. <https://doi.org/10.1093/mnras/stad3351>, arXiv:2309.13683 [physics.space-ph]

Landi S, Hellinger P, Velli M (2006) Heliospheric magnetic field polarity inversions driven by radial velocity field structures. *Geophysical Research Letters* 33(14):L14101. <https://doi.org/10.1029/2006GL026308>

Larosa A, Krasnoselskikh V, Dudok de Wit T, et al (2021) Switchbacks: statistical properties and deviations from Alfvénicity. *Astronomy and Astrophysics* 650:A3. <https://doi.org/10.1051/0004-6361/202039442>, arXiv:2012.10420 [astro-ph.SR]

Larosa A, Chen CHK, McIntyre JR, et al (2024) Evolution of the magnetic field rotation distributions in the inner heliosphere. *Astronomy and Astrophysics* 686:A238. <https://doi.org/10.1051/0004-6361/202450030>

Leamon RJ, Matthaeus WH, Smith CW, et al (1998a) Contribution of Cyclotron-resonant Damping to Kinetic Dissipation of Interplanetary Turbulence. *The Astrophysical Journal Letters* 507(2):L181–L184. <https://doi.org/10.1086/311698>, arXiv:astro-ph/9809017 [astro-ph]

Leamon RJ, Smith CW, Ness NF, et al (1998b) Observational constraints on the dynamics of the interplanetary magnetic field dissipation range. *Journal of Geophysical Research* 103(A3):4775–4788. <https://doi.org/10.1029/97JA03394>

Li B, Cairns IH, Owens MJ, et al (2016) Magnetic field inversions at 1 AU: Comparisons between mapping predictions and observations. *Journal of Geophysical Research (Space Physics)* 121(11):10,728–10,743. <https://doi.org/10.1002/2016JA023023>

Liu R, Liu YCM, Huang J, et al (2022) Density Compressions at Magnetic Switchbacks Associated With Fast Plasma: A Superposed Epoch Analysis. *Journal of Geophysical Research (Space Physics)* 127(5):e30382. <https://doi.org/10.1029/2022JA030382>

Liu W, Zhao J, Wang T, et al (2023a) The Radial Distribution of Ion-scale Waves in the Inner Heliosphere. *The Astrophysical Journal* 951(1):69. <https://doi.org/10.3847/1538-4357/acd53b>, arXiv:2305.08424 [astro-ph.SR]

Liu YD, Ran H, Hu H, et al (2023b) On the Generation and Evolution of Switchbacks and the Morphology of the Alfvénic Transition: Low Mach-number Boundary Layers. *The Astrophysical Journal* 944(2):116. <https://doi.org/10.3847/1538-4357/acb345>, arXiv:2301.05829 [astro-ph.SR]

Livi R, Larson DE, Kasper JC, et al (2022) The solar probe analyzer—ions on the parker solar probe. *The Astrophysical Journal* 938(2):138. <https://doi.org/10.3847/1538-4357/ac93f5>, URL <https://dx.doi.org/10.3847/1538-4357/ac93f5>

Livi S, Lepri ST, Raines JM, et al (2023) First results from the Solar Orbiter Heavy Ion Sensor. *Astronomy and Astrophysics* 676:A36. <https://doi.org/10.1051/0004-6361/202346304>

Macneil AR, Owens MJ, Wicks RT, et al (2020) The evolution of inverted magnetic fields through the inner heliosphere. *Monthly Notices of the Royal Astronomical Society* 494(3):3642–3655. <https://doi.org/10.1093/mnras/staa951>, arXiv:2004.05449 [physics.space-ph]

Malaspina DM, Ergun RE, Bolton M, et al (2016) The Digital Fields Board for the FIELDS instrument suite on the Solar Probe Plus mission: Analog and digital signal processing. *Journal of Geophysical Research (Space Physics)* 121(6):5088–5096. <https://doi.org/10.1002/2016JA022344>

Malaspina DM, Chasapis A, Tatum P, et al (2022) Inhomogeneous Kinetic Alfvén Waves in the Near-Sun Solar Wind. *The Astrophysical Journal* 936(2):128. <https://doi.org/10.3847/1538-4357/ac87a7>, URL <https://doi.org/10.3847/1538-4357/ac87a7>

Mallet A (2023) Nonlinear dynamics of large-amplitude, small-scale Alfvén waves. *Physics of Plasmas* 30(12):122103. <https://doi.org/10.1063/5.0170226>, arXiv:2311.05068 [physics.plasm-ph]

Mallet A, Squire J, Chandran BDG, et al (2021) Evolution of Large-amplitude Alfvén Waves and Generation of Switchbacks in the Expanding Solar Wind. *The Astrophysical Journal* 918(2):62. <https://doi.org/10.3847/1538-4357/ac0c12>, arXiv:2104.08321 [physics.space-ph]

Mallet A, Shi C, Terenani A, et al (2026, this collection) Evolution and impact of switchbacks throughout the heliosphere. *SSR*, in preparation, this issue

Marino R, Sorriso-Valvo L (2023) Scaling laws for the energy transfer in space plasma turbulence. *Physics Reports* 1006:1–144. <https://doi.org/https://doi.org/10.1016/j.physrep.2022.12.001>, URL <https://www.sciencedirect.com/science/article/pii/S0370157322003969>

Martinović MM, Klein KG, Huang J, et al (2021) Multiscale Solar Wind Turbulence Properties inside and near Switchbacks Measured by the Parker Solar Probe. *The Astrophysical Journal* 912(1):28. <https://doi.org/10.3847/1538-4357/abebe5>, arXiv:2103.00374 [astro-ph.SR]

Matteini L, Horbury TS, Neugebauer M, et al (2014) Dependence of solar wind speed on the local magnetic field orientation: Role of Alfvénic fluctuations. *Geophysical Research Letters* 41(2):259–265. <https://doi.org/10.1002/2013GL058482>

Matteini L, Horbury TS, Pantellini F, et al (2015) Ion Kinetic Energy Conservation and Magnetic Field Strength Constancy in Multi-fluid Solar Wind Alfvénic Turbulence. *The Astrophysical Journal* 802(1):11. <https://doi.org/10.1088/0004-637X/802/1/11>, arXiv:1501.00702 [physics.space-ph]

Matteini L, Tenerani A, Landi S, et al (2024) Alfvénic fluctuations in the expanding solar wind: Formation and radial evolution of spherical polarization. *Physics of Plasmas* 31(3):032901. <https://doi.org/10.1063/5.0177754>

McComas DJ, Alexander N, Angold N, et al (2016) Integrated Science Investigation of the Sun (ISIS): Design of the Energetic Particle Investigation. *Space Science Reviews* 204(1-4):187–256. <https://doi.org/10.1007/s11214-014-0059-1>

McCracken KG, Ness NF (1966) The Collimation of Cosmic Rays by the Interplanetary Magnetic Field. *Journal of Geophysical Research* 71(13):3315–3318. <https://doi.org/10.1029/JZ071i013p03315>

McDougall E, Poduval B (2025) Energetic ion composition as a means of investigating the physical origins of alpha particle heavy magnetic switchbacks. *The Astrophysical Journal* 984(1):6. <https://doi.org/10.3847/1538-4357/adc2ff>, URL <https://dx.doi.org/10.3847/1538-4357/adc2ff>

McManus MD, Bowen TA, Mallet A, et al (2020) Cross Helicity Reversals in Magnetic Switchbacks. *ApJ Supplements*246(2):67. <https://doi.org/10.3847/1538-4365/ab6dce>, arXiv:1912.07823 [physics.space-ph]

McManus MD, Verniero J, Bale SD, et al (2022) Density and Velocity Fluctuations of Alpha Particles in Magnetic Switchbacks. *The Astrophysical Journal*933(1):43. <https://doi.org/10.3847/1538-4357/ac6ba3>, arXiv:2204.13801 [astro-ph.SR]

Meng MM, Liu YD, Chen C, et al (2022) Analysis of the Distribution, Rotation and Scale Characteristics of Solar Wind Switchbacks: Comparison between the First and Second Encounters of Parker Solar Probe. *Research in Astronomy and Astrophysics* 22(3):035018. <https://doi.org/10.1088/1674-4527/ac49e4>, arXiv:2201.08069 [astro-ph.SR]

Michel FC (1967) Model of Solar Wind Structure. *Journal of Geophysical Research*72:1917. <https://doi.org/10.1029/JZ072i007p01917>

Moncuquet M, Meyer-Vernet N, Issautier K, et al (2020) First In Situ Measurements of Electron Density and Temperature from Quasi-thermal Noise Spectroscopy with Parker Solar Probe/FIELDS. *ApJ Supplements*246(2):44. <https://doi.org/10.3847/1538-4365/ab5a84>, arXiv:1912.02518 [astro-ph.SR]

Montgomery D, Turner L (1981) Anisotropic magnetohydrodynamic turbulence in a strong external magnetic field. *The Physics of Fluids* 24(5):825–831. <https://doi.org/10.1063/1.863455>, URL <https://aip.scitation.org/doi/abs/10.1063/1.863455>, <https://aip.scitation.org/doi/pdf/10.1063/1.863455>

Mozer FS, Agapitov OV, Bale SD, et al (2020a) DC and Low-Frequency Electric Field Measurements on the Parker Solar Probe. *Journal of Geophysical Research (Space Physics)* 125(9):e27980. <https://doi.org/10.1029/2020JA027980>

Mozer FS, Agapitov OV, Bale SD, et al (2020b) Switchbacks in the Solar Magnetic Field: Their Evolution, Their Content, and Their Effects on the Plasma. *ApJ Supplements*246(2):68. <https://doi.org/10.3847/1538-4365/ab7196>

Mozer FS, Bale SD, Bonnell JW, et al (2021) On the Origin of Switchbacks Observed in the Solar Wind. *The Astrophysical Journal*919(1):60. <https://doi.org/10.3847/1538-4357/ac110d>, arXiv:2105.07601 [astro-ph.SR]

Müller WC, Grappin R (2005) Spectral energy dynamics in magnetohydrodynamic turbulence. *Physical Review Letters* 95(11):114502

Neugebauer M, Goldstein BE (2013) Double-proton beams and magnetic switchbacks in the solar wind. In: Zank GP, Borovsky J, Bruno R, et al (eds) *Solar Wind 13*, American Institute of Physics Conference Series, vol 1539. AIP, pp 46–49, <https://doi.org/10.1063/1.4810986>

Neugebauer M, Clay DR, Goldstein BE, et al (1984) A reexamination of rotational and tangential discontinuities in the solar wind. *Journal of Geophysical Research*89(A7):5395–5408. <https://doi.org/10.1029/JA089iA07p05395>

Neugebauer M, Goldstein BE, McComas DJ, et al (1995) Ulysses observations of microstreams in the solar wind from coronal holes. *Journal of Geophysical Research*100(9):23389–23396

Owen CJ, Cowley SWH (1987) A note on current sheet stress balance in the geomagnetic tail for asymmetrical tail lobe plasma conditions. *Planetary and Space Science*35(4):467–474. [https://doi.org/10.1016/0032-0633\(87\)90103-6](https://doi.org/10.1016/0032-0633(87)90103-6)

Owen CJ, Bruno R, Livi S, et al (2020) The Solar Orbiter Solar Wind Analyser (SWA) suite. *Astronomy and Astrophysics*642:A16. <https://doi.org/10.1051/0004-6361/201937259>

Owens MJ, Forsyth RJ (2013) The Heliospheric Magnetic Field. *Living Reviews in Solar Physics* 10(1):5. <https://doi.org/10.12942/lrsp-2013-5>

Panasenco O, Velli M, D'Amicis R, et al (2020) Exploring Solar Wind Origins and Connecting Plasma Flows from the Parker Solar Probe to 1 au: Nonspherical Source Surface and Alfvénic Fluctuations. *ApJ*

Supplements246(2):54. <https://doi.org/10.3847/1538-4365/ab61f4>

Pecora F, Matthaeus WH, Primavera L, et al (2022) Magnetic Switchback Occurrence Rates in the Inner Heliosphere: Parker Solar Probe and 1 au. *ApJ Letters*929(1):L10. <https://doi.org/10.3847/2041-8213/ac62d4>, [arXiv:2202.04216](https://arxiv.org/abs/2202.04216) [astro-ph.SR]

Perrone D, Chiappetta F, Settino A, et al (2025) Switchbacks and their role in the turbulent cascade: Solar Orbiter observations. *Astronomy and Astrophysics*696:A192. <https://doi.org/10.1051/0004-6361/202453094>

Phan TD, Gosling JT, Paschmann G, et al (2010) The Dependence of Magnetic Reconnection on Plasma β and Magnetic Shear: Evidence from Solar Wind Observations. *ApJ Letters*719(2):L199–L203. <https://doi.org/10.1088/2041-8205/719/2/L199>

Phan TD, Bale SD, Eastwood JP, et al (2020) Parker Solar Probe In Situ Observations of Magnetic Reconnection Exhausts during Encounter 1. *ApJ Supplements*246(2):34. <https://doi.org/10.3847/1538-4365/ab55ee>

Podesta JJ, Gary SP (2011) Magnetic Helicity Spectrum of Solar Wind Fluctuations as a Function of the Angle with Respect to the Local Mean Magnetic Field. *The Astrophysical Journal* 734(1):15. <https://doi.org/10.1088/0004-637X/734/1/15>

Pulupa M, Bale SD, Bonnell JW, et al (2017) The Solar Probe Plus Radio Frequency Spectrometer: Measurement requirements, analog design, and digital signal processing. *Journal of Geophysical Research (Space Physics)* 122(3):2836–2854. <https://doi.org/10.1002/2016JA023345>

Raouafi NE, Matteini L, Squire J, et al (2023) Parker Solar Probe: Four Years of Discoveries at Solar Cycle Minimum. *Space Science Reviews*219(1):8. <https://doi.org/10.1007/s11214-023-00952-4>, [arXiv:2301.02727](https://arxiv.org/abs/2301.02727) [astro-ph.SR]

Rasca AP, Farrell WM, MacDowall RJ, et al (2021) Near-Sun Switchback Boundaries: Dissipation with Solar Distance. *The Astrophysical Journal*916(2):84. <https://doi.org/10.3847/1538-4357/ac079f>

Rasca AP, Farrell WM, Whittlesey PL, et al (2022) Magnetic Field Dropouts and Associated Plasma Wave Emission near the Electron Plasma Frequency at Switchback Boundaries as Observed by the Parker Solar Probe. *The Astrophysical Journal*935(2):81. <https://doi.org/10.3847/1538-4357/ac80c3>

Rasca AP, Farrell WM, Gruesbeck JR, et al (2023) Switchbacks and Associated Magnetic Holes Observed near the Alfvén Critical Surface. *The Astrophysical Journal* 959(1):10. <https://doi.org/10.3847/1538-4357/ad06b4>, URL <https://dx.doi.org/10.3847/1538-4357/ad06b4>

Rivera YJ, Badman ST, Stevens ML, et al (2024a) In situ observations of large-amplitude alfvén waves heating and accelerating the solar wind. *Science* 385(6712):962–966. <https://doi.org/10.1126/science.adk6953>, URL <https://www.science.org/doi/abs/10.1126/science.adk6953>, <https://www.science.org/doi/pdf/10.1126/science.adk6953>

Rivera YJ, Badman ST, Stevens ML, et al (2024b) Mixed source region signatures inside magnetic switchback patches inferred by heavy ion diagnostics. *The Astrophysical Journal* 974(2):198. <https://doi.org/10.3847/1538-4357/ad7815>, URL <https://dx.doi.org/10.3847/1538-4357/ad7815>

Rivera YJ, Badman ST, Verniero JL, et al (2025) Differentiating the Acceleration Mechanisms in the Slow and Alfvénic Slow Solar Wind. *The Astrophysical Journal*980(1):70. <https://doi.org/10.3847/1538-4357/ada699>, [arXiv:2501.02163](https://arxiv.org/abs/2501.02163) [astro-ph.SR]

Romeo OM, Braga CR, Badman ST, et al (2023) Near-Sun In Situ and Remote-sensing Observations of a Coronal Mass Ejection and its Effect on the Heliospheric Current Sheet. *The Astrophysical Journal*954(2):168. <https://doi.org/10.3847/1538-4357/ace62e>

Rouillard AP, Kouloumvakos A, Vourlidas A, et al (2020) Relating Streamer Flows to Density and Magnetic Structures at the Parker Solar Probe. *ApJ Supplements*246(2):37. <https://doi.org/10.3847/1538-4365/ab55ee>

ab579a, arXiv:2001.01993 [astro-ph.SR]

Ruffolo D, Matthaeus WH, Chhiber R, et al (2020) Shear-driven Transition to Isotropically Turbulent Solar Wind Outside the Alfvén Critical Zone. *The Astrophysical Journal*902(2):94. <https://doi.org/10.3847/1538-4357/abb594>, arXiv:2009.06537 [physics.space-ph]

Ruffolo D, Ngampoopun N, Bhora YR, et al (2021) Domains of Magnetic Pressure Balance in Parker Solar Probe Observations of the Solar Wind. *The Astrophysical Journal*923(2):158. <https://doi.org/10.3847/1538-4357/ac2ee3>, arXiv:2110.08506 [astro-ph.SR]

Sakshee S, Bandyopadhyay R, Banerjee S (2022) MHD-scale anisotropy in solar wind turbulence near the Sun using Parker solar probe data. *Monthly Notices of the Royal Astronomical Society*514(1):1282–1288. <https://doi.org/10.1093/mnras/stac1449>

Sanchez-Diaz E, Rouillard AP, Davies JA, et al (2017a) The Temporal and Spatial Scales of Density Structures Released in the Slow Solar Wind During Solar Activity Maximum. *The Astrophysical Journal*851(1):32. <https://doi.org/10.3847/1538-4357/aa98e2>, arXiv:1711.02486 [astro-ph.SR]

Sanchez-Diaz E, Rouillard AP, Davies JA, et al (2017b) Observational Evidence for the Associated Formation of Blobs and Raining Inflows in the Solar Corona. *ApJ Letters*835(1):L7. <https://doi.org/10.3847/2041-8213/835/1/L7>, arXiv:1612.05487 [astro-ph.SR]

Schwadron NA, McComas DJ (2021) Switchbacks Explained: Super-Parker Fields—The Other Side of the Sub-Parker Spiral. *The Astrophysical Journal*909(1):95. <https://doi.org/10.3847/1538-4357/abd4e6>, arXiv:2102.03696 [astro-ph.SR]

Shebalin JV, Matthaeus WH, Montgomery D (1983) Anisotropy in mhd turbulence due to a mean magnetic field. *Journal of Plasma Physics* 29(3):525–547. <https://doi.org/10.1017/S0022377800000933>

Shi C, Velli M, Panasenco O, et al (2021) Alfvénic versus non-Alfvénic turbulence in the inner heliosphere as observed by Parker Solar Probe. *Astronomy and Astrophysics*650:A21. <https://doi.org/10.1051/0004-6361/202039818>, arXiv:2101.00830 [astro-ph.SR]

Shi C, Panasenco O, Velli M, et al (2022a) Patches of Magnetic Switchbacks and Their Origins. *The Astrophysical Journal*934(2):152. <https://doi.org/10.3847/1538-4357/ac7c11>, arXiv:2206.03807 [astro-ph.SR]

Shi C, Panasenco O, Velli M, et al (2022b) Patches of Magnetic Switchbacks and Their Origins. *The Astrophysical Journal*934(2):152. <https://doi.org/10.3847/1538-4357/ac7c11>, arXiv:2206.03807 [astro-ph.SR]

Shi C, Velli M, Toth G, et al (2024) Analytic Model and Magnetohydrodynamic Simulations of Three-dimensional Magnetic Switchbacks. *ApJ Letters*964(2):L28. <https://doi.org/10.3847/2041-8213/ad335a>, arXiv:2401.11334 [physics.space-ph]

Shoda M, Chandran BDG, Cranmer SR (2021) Turbulent Generation of Magnetic Switchbacks in the Alfvénic Solar Wind. *The Astrophysical Journal*915(1):52. <https://doi.org/10.3847/1538-4357/abfdcb>, arXiv:2101.09529 [astro-ph.SR]

Sioulas N, Huang Z, Velli M, et al (2022a) Magnetic Field Intermittency in the Solar Wind: Parker Solar Probe and SolO Observations Ranging from the Alfvén Region up to 1 AU. *The Astrophysical Journal*934(2):143. <https://doi.org/10.3847/1538-4357/ac7aa2>, arXiv:2206.00871 [astro-ph.SR]

Sioulas N, Velli M, Chhiber R, et al (2022b) Statistical Analysis of Intermittency and its Association with Proton Heating in the Near-Sun Environment. *The Astrophysical Journal*927(2):140. <https://doi.org/10.3847/1538-4357/ac4fc1>, arXiv:2201.10067 [astro-ph.SR]

Sioulas N, Velli M, Huang Z, et al (2023) On the Evolution of the Anisotropic Scaling of Magnetohydrodynamic Turbulence in the Inner Heliosphere. *The Astrophysical Journal*951(2):141. <https://doi.org/10.3847/1538-4357/acc658>, arXiv:2301.03896 [physics.space-ph]

Soni SL, Akhavan-Tafti M, Suen GHH, et al (2024) Switchback Patches Evolve into Microstreams via Magnetic Relaxation. *The Astrophysical Journal*977(2):264. <https://doi.org/10.3847/1538-4357/ad94da>,

arXiv:2402.13964 [astro-ph.SR]

Sonnerup BUO, Cahill JL. J. (1967) Magnetopause Structure and Attitude from Explorer 12 Observations. *Journal of Geophysical Research* 72:171. <https://doi.org/10.1029/JZ072i001p00171>

Sorriso-Valvo L, Carbone V, Veltri P, et al (1999) Intermittency in the solar wind turbulence through probability distribution functions of fluctuations. *Geophysical Research Letters* 26(13):1801–1804. <https://doi.org/https://doi.org/10.1029/1999GL900270>

Sorriso-Valvo L, Marino R, Foldes R, et al (2023) Helios 2 observations of solar wind turbulence decay in the inner heliosphere. *Astronomy and Astrophysics* 672:A13. <https://doi.org/10.1051/0004-6361/202244889>, arXiv:2302.09064 [physics.space-ph]

Squire J, Chandran BDG, Meyrand R (2020) In-situ Switchback Formation in the Expanding Solar Wind. *ApJ Letters* 891(1):L2. <https://doi.org/10.3847/2041-8213/ab74e1>, arXiv:2001.08422 [physics.space-ph]

Squire J, Johnston Z, Mallet A, et al (2022) On the properties of Alfvénic switchbacks in the expanding solar wind: The influence of the Parker spiral. *Physics of Plasmas* 29(11):112903. <https://doi.org/10.1063/5.0099924>, arXiv:2205.09455 [astro-ph.SR]

Suen GHH, Owen CJ, Verscharen D, et al (2023) Magnetic reconnection as an erosion mechanism for magnetic switchbacks. *Astronomy and Astrophysics* 675:A128. <https://doi.org/10.1051/0004-6361/202345922>, arXiv:2305.06035 [physics.space-ph]

Swisdak M, Rogers BN, Drake JF, et al (2003) Diamagnetic suppression of component magnetic reconnection at the magnetopause. *Journal of Geophysical Research (Space Physics)* 108(A5):1218. <https://doi.org/10.1029/2002JA009726>

Tatum PD, Malaspina DM, Chasapis A, et al (2024) The Independence of Magnetic Turbulent Power Spectra to the Presence of Switchbacks in the Inner Heliosphere. *The Astrophysical Journal* 973(2):156. <https://doi.org/10.3847/1538-4357/ad7115>, arXiv:2404.03075 [astro-ph.SR]

Telloni D, Zank GP, Stangalini M, et al (2022) Observation of a Magnetic Switchback in the Solar Corona. *ApJ Letters* 936(2):L25. <https://doi.org/10.3847/2041-8213/ac8104>, arXiv:2206.03090 [astro-ph.SR]

Tenerani A, Sioulas N, Matteini L, et al (2021) Evolution of Switchbacks in the Inner Heliosphere. *ApJ Letters* 919(2):L31. <https://doi.org/10.3847/2041-8213/ac2606>, arXiv:2109.06341 [astro-ph.SR]

Toth G, Velli M, van der Holst B (2023) Formation of Magnetic Switchbacks Observed by Parker Solar Probe. *arXiv e-prints* arXiv:2301.02572. <https://doi.org/10.48550/arXiv.2301.02572>, arXiv:2301.02572 [astro-ph.SR]

Toussaint J, Pariat E, Froment C, et al (2024) Propagation of untwisting solar jets from the low-beta corona into the super-Alfvénic wind: Testing a solar origin scenario for switchbacks. *Astronomy and Astrophysics* 692:A71. <https://doi.org/10.1051/0004-6361/202452019>, arXiv:2412.15930 [astro-ph.SR]

Tripathi D, Kasper J, Raouafi NE, et al (2026, this collection) Potential Solar Precursors to Magnetic Switchbacks. *SSRv*, in preparation, this issue

Tsurutani BT, Smith EJ (1979) Interplanetary discontinuities: Temporal variations and the radial gradient from 1 to 8.5 AU. *Journal of Geophysical Research* 84(A6):2773–2787. <https://doi.org/10.1029/JA084iA06p02773>

Tsurutani BT, Lakhina GS, Sen A, et al (2018) A Review of Alfvénic Turbulence in High-Speed Solar Wind Streams: Hints From Cometary Plasma Turbulence. *JGRA* 123(4):2458–2492. <https://doi.org/10.1002/2017JA024203>

Vasko IY, Alimov K, Phan TD, et al (2021) Kinetic-scale Current Sheets in the Solar Wind at 1 au: Properties and the Necessary Condition for Reconnection. *ApJ Letters* 923(1):L19. <https://doi.org/10.3847/2041-8213/ac3f30>

Velli M, Owens M (2026, this collection) Switchbacks, from Mariner to PSP. SSRv, in preparation, this issue

Velli M, Grappin R, Mangeney A (1989) Turbulent cascade of incompressible unidirectional Alfvén waves in the interplanetary medium. *Physical Review Letters* 63(17):1807–1810. <https://doi.org/10.1103/PhysRevLett.63.1807>, URL <https://link.aps.org/doi/10.1103/PhysRevLett.63.1807>, publisher: American Physical Society

Verniero JL, Larson DE, Livi R, et al (2020) Parker Solar Probe Observations of Proton Beams Simultaneous with Ion-scale Waves. *ApJS* 248(1):5. <https://doi.org/10.3847/1538-4365/ab86af>, [arXiv:2004.03009](https://arxiv.org/abs/2004.03009) [physics.space-ph]

Verniero JL, Chandran BDG, Larson DE, et al (2022) Strong perpendicular velocity-space diffusion in proton beams observed by parker solar probe. *The Astrophysical Journal* 924(2):112. <https://doi.org/10.3847/1538-4357/ac36d5>, URL <https://dx.doi.org/10.3847/1538-4357/ac36d5>

Verscharen D, Marsch E (2011) Apparent temperature anisotropies due to wave activity in the solar wind. *Annales Geophysicae* 29(5):909–917. <https://doi.org/10.5194/angeo-29-909-2011>, [arXiv:1106.5878](https://arxiv.org/abs/1106.5878) [physics.space-ph]

Verscharen D, Klein KG, Maruca BA (2019) The multi-scale nature of the solar wind. *Living Reviews in Solar Physics* 16(1):5. <https://doi.org/10.1007/s41116-019-0021-0>, [arXiv:1902.03448](https://arxiv.org/abs/1902.03448) [physics.space-ph]

Vo T, Agapitov OV, Choi KE, et al (2024) Enhanced Efficiency of Solar Wind Electron Interaction with Whistlers Caused by Switchback-related Magnetic Dips. *The Astrophysical Journal Letters* 970(2):L38. <https://doi.org/10.3847/2041-8213/ad614b>, URL <https://dx.doi.org/10.3847/2041-8213/ad614b>, publisher: The American Astronomical Society

Wang R, Vasko IY, Phan T, et al (2023) Solar wind current sheets: MVA inaccuracy and recommended single-spacecraft methodology. *arXiv e-prints* arXiv:2312.06043. <https://doi.org/10.48550/arXiv.2312.06043>, [arXiv:2312.06043](https://arxiv.org/abs/2312.06043) [physics.space-ph]

Wang YM, Sheeley JN. R., Walters JH, et al (1998) Origin of Streamer Material in the Outer Corona. *ApJ Letters* 498(2):L165–L168. <https://doi.org/10.1086/311321>

Wheatland MS, Litvinenko YE (2002) Understanding Solar Flare Waiting-Time Distributions. *Solar Physics* 211:255–274. <https://doi.org/10.1023/A:1022430308641>

Whittlesey PL, Larson DE, Kasper JC, et al (2020) The solar probe ANalyzers—electrons on the parker solar probe. *The Astrophysical Journal Supplement Series* 246(2):74. <https://doi.org/10.3847/1538-4365/ab7370>, URL <https://doi.org/10.3847%2F1538-4365%2Fab7370>

Wicks RT, Alexander RL, Stevens M, et al (2016) A Proton-cyclotron Wave Storm Generated by Unstable Proton Distribution Functions in the Solar Wind. *ApJ* 819(1):6. <https://doi.org/10.3847/0004-637X/819/1/6>

Woodham LD, Horbury TS, Matteini L, et al (2021) Enhanced proton parallel temperature inside patches of switchbacks in the inner heliosphere. *Astronomy and Astrophysics* 650:L1. <https://doi.org/10.1051/0004-6361/202039415>, [arXiv:2010.10379](https://arxiv.org/abs/2010.10379) [astro-ph.SR]

Woolley T, Matteini L, Horbury TS, et al (2020) Proton core behaviour inside magnetic field switchbacks. *Monthly Notices of the Royal Astronomical Society* 498(4):5524–5531. <https://doi.org/10.1093/mnras/staa2770>, [arXiv:2007.10906](https://arxiv.org/abs/2007.10906) [physics.space-ph]

Wu H, Tu C, Wang X, et al (2021) Large Amplitude Switchback Turbulence: Possible Magnetic Velocity Alignment Structures. *The Astrophysical Journal* 911(2):73. <https://doi.org/10.3847/1538-4357/abec6c>, [arXiv:2104.11876](https://arxiv.org/abs/2104.11876) [astro-ph.SR]

Wu H, Tu C, He J, et al (2023) Energy transfer of the solar wind turbulence based on Parker solar probe and other spacecraft observations. *Physics of Plasmas* 30(2):020501. <https://doi.org/10.1063/5.0137370>

org/10.1063/5.0121140, URL <https://doi.org/10.1063/5.0121140>, https://pubs.aip.org/aip/pop/article-pdf/doi/10.1063/5.0121140/16681271/020501_1_online.pdf

Wyper P, Squire J, Pariat E, et al (2026, this collection) Magnetic switchback formation: a review of proposed mechanisms. SSRv, in preparation, this issue

Wyper PF, DeVore CR, Antiochos SK, et al (2022) The Imprint of Intermittent Interchange Reconnection on the Solar Wind. ApJ Letters941(2):L29. <https://doi.org/10.3847/2041-8213/aca8ae>

Yamauchi Y, Suess ST, Sakurai T (2002) Relation between Pressure Balance Structures and polar plumes from Ulysses high latitude observations. Geophysical Research Letters29(10):1383. <https://doi.org/10.1029/2001GL013820>

Yamauchi Y, Suess ST, Steinberg JT, et al (2004) Differential velocity between solar wind protons and alpha particles in pressure balance structures. Journal of Geophysical Research (Space Physics) 109(A3):A03104. <https://doi.org/10.1029/2003JA010274>

Zank GP, Nakanotani M, Zhao LL, et al (2020) The Origin of Switchbacks in the Solar Corona: Linear Theory. The Astrophysical Journal903(1):1. <https://doi.org/10.3847/1538-4357/abb828>

Zank GP, Zhao LL, Adhikari L, et al (2022) Turbulence in the Sub-Alfvénic Solar Wind. ApJ Letters926(2):L16. <https://doi.org/10.3847/2041-8213/ac51da>, arXiv:2202.02563 [astro-ph.SR]